UNIVERSITÀ DEGLI STUDI DI PALERMO

Dottorato di Ricerca in Ingegneria Civile, Ambientale, dei Materiali
Dipartimento di Ingegneria Civile, Ambientale, Aerospaziale, dei Materiali (DICAM)
Settore Scientifico Disciplinare ICAR 02

Dam displacements monitoring by using GNSS and remote sensing techniques

IL DOTTORE
Ing. Claudia Pipitone

IL COORDINATORE
Ch.ma Prof.ssa Ing. Antonina Pirrotta

IL TUTOR
Ch.mo Prof. Ing. Goffredo La Loggia

CO TUTORS
Dr. Ing. Gino Dardanelli

Dr. Ing. Antonino Maltese

CICLO XXXI

ANNO CONSEGUIMENTO TITOLO 2019

Table of Contents

Acknowledgments

Firstly, I would like to acknowledge my Advisor Prof. Goffredo La Loggia. He allowed developing this research, with interesting suggestions and support to make relevant scientific discoveries in this field.

Then, I would like to thank Drs. Gino Dardanelli and Antonino Maltese for their contributions to this work. With their passionate participation and input, the research developed in these years was successfully conducted, with increasing motivation and passion for the topic developed.

A special thanks to Dr. Francesco Vuolo, for his supervision during my staying at the Boku University in Vienna and Prof. Jan-Peter Muller, for his precious suggestions aimed to improve the research developed at MSSL, UCL, London.

I am also grateful to the developer of the software SARProZ © (https://www.sarproz.com) used for the InSAR processing, Prof. D. Perissin, for his technical support.

Thanks to everyone who shared my stay abroad at Boku University, in particular, Luca and Hannah and at MSSL University: all “Imaging Group”, and in particular Jacqueline for helping and supporting me during that period. You all made these experiences very beautiful and all moments will be embedded in my mind and in my heart forever.

Claudia Pipitone

Many thanks to Gian Paolo, Davide and Katerina, who always helped and supported me during my stay in UK. I met beautiful people during this experience and because of you I felt home also far away from Italy.

Thanks to Donatella, Rosanna and all people from Geomatics Laboratory of DICAM, University of Palermo. You were part of my life, we shared lots of professional but also friendly moments that I will never forget. Thanks for your support, especially in the last period.

A special thanks to my family for their unconditional love, their support and encourage to all of my choices.

Finally, the most important acknowledge is for my husband, Vito, my best supporter since the beginning of this experience, and not only. You encouraged me and believed in my potentialities every single moment and you gave me the strength to take on every challenges. Every successful moment achieved in these years could not be possible without you.

Sommario

Il presente lavoro mira a valutare le potenzialità delle tecniche satellitari per il monitoraggio delle dighe. In particolare, l'attenzione è stata rivolta alle dighe di terra, poichè queste rappresentano la tipologia costruttiva più diffusa ed i modelli esistenti in letteratura sono in grado di descriverne gli spostamenti solo nell'ipotesi di conoscere accuratamente tutti parametri geotecnici e strutturali che caratterizzano la composizione della diga stessa.

Negli ultimi anni, è stato ampiamente dimostrato che le tecniche satellitari da remoto sono in grado di individuare con elevata accuratezza, il comportamento di grandi strutture (incluse le dighe), valutandone spostamenti e deformazioni.

In questo lavoro, è stato condotto il monitoraggio di una diga di terra (la diga Castello), ubicata nel sud Italia, utilizzando varie tecniche satellitari. In particolare, per la stima degli spostamenti della diga, sono stati utilizzate tecniche Global Navigation Satellite System (GNSS) ed interferometriche satellitari, mentre per la stima delle superfici e dei livelli di invaso, sono state messe a punto tecniche di classificazione di dati telerilevati e tecniche di Object-Based Image Analysis (OBIA).

Sono stati utilizzati dati GNSS acqusiti da una Continously Operating Reference Station (CORS) distante dal sito monitorato ed immagini telerilevate aventi differente risoluzione spaziale e radiometrica

(sia ottiche sia immagini Sinthetic Aperture Radar, SAR) acquisite in un ampio intervallo temporale (dal 2011 al 2016).

Gli spostamenti sono stati determinati utilizzando la tecnica differenziale GNSS (DGNSS), attraverso un approccio sperimentale basato sull'utilizzo di una CORS posta distante dal sito monitorato. Gli spostamenti reversibili ed irreversibili del coronamento della diga sono stati analizzati tramite tecnica Permanent Scatterers Interferometrica SAR (PS-InSAR) utilizzando differenti Multi-Baseline Construction Methods (MBC), in particolare lo star-graph ed il full-graph.

Dall'analisi degli spostamenti GNSS su un periodo di circa un anno (Aprile 2011 – Marzo 2012) si evince che solo la componente planimetrica possiede un'accuratezza idonea per il monitoraggio degli spostamenti della diga ($\approx$ 1–5 x 10^{-3} m). L'analisi del trend non lineare degli spostamenti evidenzia un range di variabilità pari a $\approx$ 2 mm/anno, mentre l'analisi del trend lineare evidenzia una velocità di spostamento ortogonale al coronamento pari a $\approx$ -1 mm/anno. Oltremodo, il confronto tra gli spostamenti GNSS e i livelli di invaso misurati evidenzia una relazione non lineare tra le variabili. In particolare la risposta della diga è legata alla variazione del livello idrico durante il periodo di svuotamento e riempimento dell'invaso. Parimenti, anche la temperatura dell'aria influenza gli spostamenti della diga. Si osservano, infatti, due massimi spostamenti, uno in corrispondenza della massima temperatura media giornaliera, l'altro al verificarsi del minimo livello di invaso; viceversa, lo spostamento minimo si ha in corrispondenza del valore minimo della temperatura media giornaliera, mentre il massimo livello di invaso veniva mantenuto costante per tutto il periodo primaverile.

L’utilizzo di differenti strategie per la stima degli spostamenti PS InSAR, evidenzia un’accuratezza migliore nel caso di connessioni ridondanti (full-graph). La componente irreversibile degli spostamenti è ottenuta attraverso la stima del trend lineare e mostra valori comparabili con quelli ottenuti tramite GNSS (~ -1 mm/anno). La componente reversibile degli spostamenti è interpretabile attraverso l’impiego di un modello polinomiale ($r^2 \approx 0.80$) sulla media mobile temporale.

Le tecniche di classificazione di immagini ottiche e radar consentono di stimare accuratamente ($r^2 > 0.95$) sia le superfici sia i livelli dell’invaso. Le tecniche OBIA implementate (edge e distance similarity indices), hanno consentito di stimare i livelli di invaso con una accuratezza pari a ≈ 2 m ($r^2 > 0.9$, dataset Sentinel-1A).

Sebbene l’applicazione della tecnica PS-InSAR necessiti ulteriori approfondimenti, l’utilizzo di un unico dataset (Sentinel-1A) consente sia la stima degli spostamenti del coronamento, sia dei livelli di invaso, e pertanto costituisce un elemento di innovazione di questo lavoro. I suddetti approfondimenti includono l’integrazione delle analisi PS effettuate su scene descending ed ascending e su un periodo di indagine più ampio.

Abstract

This work aims to evaluate the capability of satellite techniques for dams monitoring. In particular the attention is focused on earth dams, because they are the most common type and the existing models in literature are able to describe their displacements if mainly the structural and geotechnical parameters characterizing the dam composition are deeply evaluated.

During the last years, it has been demonstrated that remote sensing satellite technologies are able to detect the structural behaviour of strategic structures (including the dam response), evaluating both displacements and deformation with high accuracy.

In this work, the monitoring of an embankment dam (the Castello dam), located in southern Italy, has been carried out using different satellite techniques. In particular, Global Navigation Satellite System (GNSS) and Synthetic Aperture Radar Interferometry (InSAR) have been used for the detection of dam displacements, while classification technique and Object-Based Image Analysis (OBIA)have been involved for the estimation of the reservoir surface and levels.

GNSS data from a Continuously Operating Reference Station (CORS) far away from the monitored site and remote sensing images with different spatial and radiometric resolution (optical and Synthetic Aperture Radar, SAR, images) and temporal coverage (from 2011 to 2016) have been used.

The displacements by using the Differential GNSS (DGNSS) technique have been retrieved employing an innovative approach, based on the use of a CORS far away from the monitored site. The reversible and irreversible displacements of the dam have been analysed *via* Permanent Scatterers InSAR (PS-InSAR), using different Multi-Baseline Construction Methods (MBC), in particular, the star-graph and the full-graph.

From the analysis of the GNSS displacements over ~1 year (April 2011 – March 2012), only the planimetric component reaches a suitable accuracy for monitoring the dam displacements (≈ 1–5 x 10^{-3} m). The non-linear trend shows a variability range of ≈ 2 mm y^{-1}, while the linear trend highlights an estimated velocity orthogonal to the dam of ≈ -1 mm y^{-1}. The comparison between the GNSS displacements and the measured water levels shows a non-linear relation between the variables. In particular, the dam response is related to the water levels during the emptying and filling periods. Also, the air temperature influences the dam displacements. Indeed, two maximum displacements have been recorded, the first corresponding to the maximum daily averaged air temperature, the other to the minimum water level; also, the minimum displacement corresponds to the minimum daily averaged air temperature, while the maximum water level was constant in the springtime.

The use of different strategies for PS-InSAR analysis, highlights higher accuracy when more redundant connection are used (full-graph). The irreversible displacements are evaluated with a linear trend estimation and the results are comparable to those obtained *via* GNSS (~

-1 mm y^{-1}). Analysing the reversible component of displacements, the best fitting model has been obtained superimposing a polynomial interpolating curve ($r^2 \approx 0.80$) on the temporal moving average of displacements.

The classification techniques applied on both optical and SAR images allows estimating the water surface and levels with high accuracy ($r^2 > 0.95$). The implanted OBIA techniques (edge and distance similarity indices) allowed estimating the water levels with accuracy of ≈ 2 m, ($r^2 >$ 0.90, with Sentinel-1A data).

Although the application of PS-InSAR needs more deep analyses, the use of the same dataset (Sentinel-1A) for both dam displacements and water levels evaluation, represents an innovative approach of this work. Further studies will include the analysis of PS on both ascending and descending orbits over a wider time-span.

List of Figures

List of Tables

Introduction

The monitoring and the evaluation of structural behaviour of civil infrastructures and strategic structures, like dams, has become a topic of a great interest because of their role in the society. By using an efficient control system of the dams behaviour, analysing all environmental and physical factors involved in the deformation process, it might be possible to ensure their stability and efficiency over time. Statistical methods and different approaches are used to analyse the correlation between the deformations of dams, made of concrete or embankment dams, and the environmental variables, such as water levels, air temperature, wind speed. Also the instrumentations involved could be various, depending on the parameters to be monitored and the time frequency, thus the choice of suitable sensors to be involved during the monitoring process become the most important to detect the displacements of a dam, establishing the short or long term deformation process of the structure (Scaioni et al., 2018).

During the last years, it has been demonstrate that the satellite technologies are able to detect the dams response in terms of deformations, but not only, with high accuracy, with the advantage to be used even remotely. The availability of historical data allows the

interpretation of the actual behaviour of the structure, according to the past analyses and environmental changes.

In this work, the monitoring of an embankment dam has been carried out using Global Navigation Satellite System (GNSS) for the displacements estimation and remote sensing for the detection of dam displacements and water levels of reservoir. In particular, for the estimation of dam displacements the Interferometric Synthetic Aperture Radar (InSAR) technique has been adopted, analysing within the scenes, the dam itself and the surrounding area, while the water levels have been retrieved using both optical and Synthetic Aperture Radar (SAR) images, characterized by different spatial resolutions.

The study has been conducted using different techniques and different approaches to test the capability of satellite technologies for dam monitoring in this case study. Both GNSS and remote sensing were able to show the behaviour of the embankment dam and the comparison between the results highlighted the agreement between GNSS and InSAR displacements and a relationship between the displacements and the water levels fluctuations.

In particular the analysis is focused on the Castello dam on Magazzolo reservoir, that is an embankment dam located in south Italy, ~30 km far away from the main city of Agrigento, Sicily (37°34'51" N, 13°24'48" E, World Geodetic System 1984, WGS84). The main composition of the dam is made of coarse-grained homogeneous alluvium from the valley and limestone and a seal coat of bituminous conglomerate. The structure is also characterized by a stable left bank on a stone plinth made of coarse-grained material too.

The GNSS time series of displacements refers, preliminary, to three different sections on the top of the dam on which three receivers have been located and then, specifically, to one of those, located in the middle section. The displacements has been evaluated using the Differential GNSS (DGNSS) technique using a single-baseline connection, involving as reference station the Continuously Operating Reference Station (CORS) of Agrigento (37°19'13" N, 13°36'04" E) of UNIPA CORS network. In the same period, the dataset to retrieve the water surface and water level of the reservoir has been collected. For this purpose, both optical and SAR images has been used. The optical dataset includes Landsat 5 (LS5) Thematic Mapper (TM), Landsat 7 (LS7) Enhanced Thematic Mapper Plus (ETM+) with the Scan Line Corrector turned off (SLC-Off), Landsat 8 Operational Land Imager (OLI) and Thermal Infrared Sensor (TIRS) and the Advanced Spaceborne Thermal Emission and Reflection Radiometer (ASTER) at different geometric resolutions. The SAR dataset includes TerraSAR-X (TSX) and Cosmo-SkyMed (CSK) at higher spatial resolutions. The images have been processed using two different strategies based the first on the traditional unsupervised classification method and the other on an innovative method consisting on the overlapping between the radiometric calibrated image and the contour lines extracted from the dam project and the visual interpretation. In the first case, also post-classification methods have been applied to solve problems within the scenes connected to the different spatial resolutions, different acquisitions, georeferencing problems and the influence of wind speed on SAR images or clouds and shadows on optical images. The techniques involved were the

segmentation image and the classes clump, by using ENVI-IDL software. The latter technique adds spatial coherency to the classified areas affected by speckle or holes within the scenes, involving a kernel of a specific size (Harris Geospatial product documentation).The results in terms of water surface have been converted into water levels using the specific relationship between the storage, the surface and the levels for the reservoir.

Using the same dataset, two innovative techniques have been applied for the detection of water surface and levels of reservoir involving the object-based methods. The first called STEP, implemented within a Geographic Information System (GIS) software that compares classified images with reference objects (contour lines in this case) using the Shape (S), the Theme (T), the Edge (E) and the Position (P) similarity metrics. The other technique compare the same reference objects with the classified image through the extracted nodes from the vector file, using the average distance of a shoreline with the contour lines.

The two object-based images have been also applied on a different SAR dataset, including the Sentinel-1A (S-1A) images acquired during the period October 2014-December 2016 in Ascending and Descending tracks, Single Look Complex (SLC) format and dual polarization (VV-VH). The same dataset has been used for the InSAR analysis to evaluate the displacements of the dam. Different techniques have been analysed also in this case, based on the basic concept of the standard Permanent Scatterers (PS) method, originally introduced in 2001 able to evaluate ground motions, building stability but also dam deformations. The method extracts all information related to distributed natural targets

having high reflectivity, especially located in urban areas, over time using a stack of SAR images.

Considering the area surround the dam, mainly vegetated, many innovations have been applied on the standard procedure, as using multi-baseline construction methods between the images or using the spatial coherence as weight during the phase information processing.

The results by using different sensors and applying several methods for the estimation of dam displacements and the water surface and levels of the reservoir have shown the capability of satellite technology for dam monitoring. Indeed, by using GNSS the trend of the displacements has been found after applying a temporal filter of two-month moving average. The time series of the displacements orthogonal to the dam during the period 2011-2012 highlighted a non-linear behaviour of the dam, probably due to the water levels fluctuations acting on it. The estimated velocity during one year is approximately -1 mm y^{-1}, while the relationship between the estimated GNSS displacements and the water levels from measurements in situ and remote sensing results showed an hysteresis-kind loop during the emptying and filling periods of the reservoir. Also it was verified the influence of the measured air temperature, on the displacements. The behaviour is in agreement with other dam deformations related to seasonal temperature and hydrostatic pressure fluctuations (Milillo et al., 2016). Also other studies have found a relation between displacements and water height and temperature for both concrete and earth-dams analysed (Galan-Martin et al., 2013; Behr et al., 1998; Radhakrishnan, 2014). The results of these researches are discussed below.

Comparing the results from remote sensing many limitations occurred by using LS7 ETM+ SLC-Off images and SAR images with the highest spatial resolutions. The results in terms of statistical indicators showed comparable results by using both the classification and the visual matching methods, but in the first case the available dataset was drastically reduced after removing lots of corrupted images. The results of the classification method on these images are considered not suitable for the analysis, due to the failure of the identification of the water class within the scene. Indeed, after applying the classification method on these images, due to the missing scan lines within the scene, the water class was not correctly identified, thus the images were removed from the analysis. More information about the final products of LS7 ETM+ SLC-Off after classification will be discussed below, in the specific section. Comparing the results from the object-based analysis, best results have been found using the average distance between the reference objects and the nodes extracted from the vectorized image after classification. Using the STEP analysis, it has been found that the Edge similarity index is more suitable to identify the closest contour lines to the boundary of the classified image.

Finally, the InSAR analysis points out the capability to retrieve both the linear and non-linear terms of the displacements, due to external factors but also to the composition of the dam itself. The different results are in agreement with those found with GNSS technique during a different period.

Thesis structure

The thesis is organized into 4 chapters: starting from introducing the research and the main objectives obtained, the following paragraphs describe the main steps of the research.

Chapter 1-Theoretical Background – This chapter aims to illustrate the main relevant studies in literature describing the dam monitoring. The chapter is divided into two main sections regarding the dam displacements monitoring (using satellite techniques) and the water surface and levels monitoring *via* remote sensing.

Chapter 2-Materials – This chapter describes the study area, an embankment dam (Castello dam) located in Sicily (Italy), monitored *via* GNSS and remote sensing from 2011. Also the main characteristics of instruments and satellite imagery involved for dam monitoring have been described.

In Chapter 3-Methods – In this chapter the methodologies involved for the analyses have been reported, distinguishing the different techniques involved and the different strategies for the displacements and water levels estimation.

In Chapter 4- Results and Discussion – This chapter focuses on the analysis and description of the main results obtained from the research.

Advantages and limits of the different techniques involved are also discussed.

In Chapter 5- Conclusions – The chapter summarizes the main results and points out some recommendations for further works and future developments in the research.

Chapter 1

Theoretical Background

1.1 Overview

The monitoring and the evaluation of complex behaviour of strategic structures, like dams, has become a topic of a great interest because of their role in the society. Indeed, these structures are generally used for different purposes, as water supply, agricultural irrigation, electricity generation and the potential damages affecting the dams should be constantly and continuously under control avoiding any deficiency that could compromise the human life safety. The analysis and the evaluation of the deformations for both concrete and earthen dams represent a complex process because of the parameters involved. Indeed, it is known that the deformations vary according to the type of structure (Scaioni et

al., 2018), and generally, the concrete dams have a different behaviour than embankment dams. In the first case, the dam behaviour is strictly related to the hydrostatic water pressure and the air temperature variations and many models are well described in literature (Carosio and Dupraz, 1993; De Sortis and Paoliani, 2007; Barzaghi et al., 2012). The embankment dams are generally characterized by more permanent deformations, due to the material composition of the dam, the water loads, and generally the main critical movements are recorded in the direction perpendicular to the dam crest in the middle section. These loads can be different over time and also the response of a dam could change; thus the instrumentations involved in the monitoring process need to be adequate in order to rectify any potential structural deficiency. From the analysis of results in terms of deformations, the further important step is the understanding of the mechanism influencing the deformation, determining the relationship between the parameters involved and the deformations.

The International Commission on Large Dams (ICOLD) collected information about large dams in the world, defined as structures with a height of 15 m or more, but also between 5 and 15 m enclosing more than 3,000,000 m^3 of water (ICOLD Constitution Statuts). Many statistics have been also calculated based on the available data, even if some of them are missing.

The number of dams collected by the institution based on these data are reported as follow, differentiated for continents (Table 1.1).

Table 1 1 Large dams globally distributed in the world (modified from ICOLD database)

Continents	Number of large dams
Europe	6611
South of America	1825
North of America	11076
Africa	2167
Asia	36009
Australia and Oceania	663
Antarctica	-

Figure 1.1 shows the main countries, in the continents, with the largest number of large dams, based on the available ICOLD database. As shown in this figure, the highest number of large dams is located in China (23841), followed by the United States of America (9265). In Europe the main country is Spain with 1063 large dams, while in Italy, 541 large dams are recorded within the database.

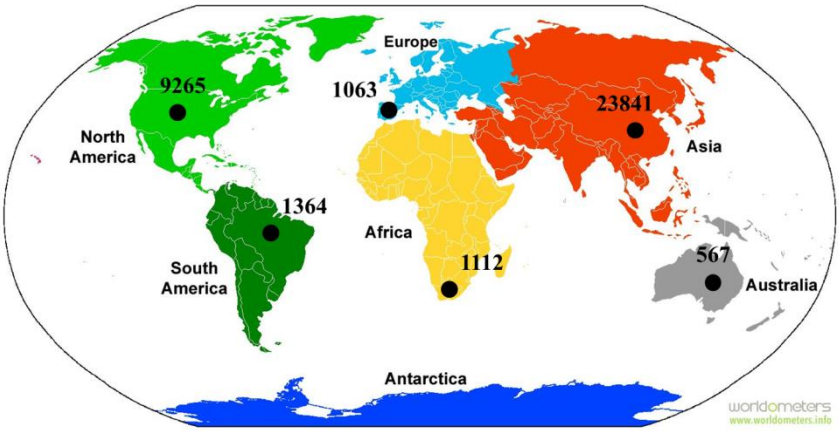

Figure 1. 1 Distribution of large dams for continents. The numbers identify the main country in the continent with the highest number of large dams (based on the ICOLD database)

The different dams type are described in Figure 1.2 (ICOLD, World Register of Dams). 65 % of the dams reported in the database are earth dams, corresponding to the oldest type, followed by rockfill dams.

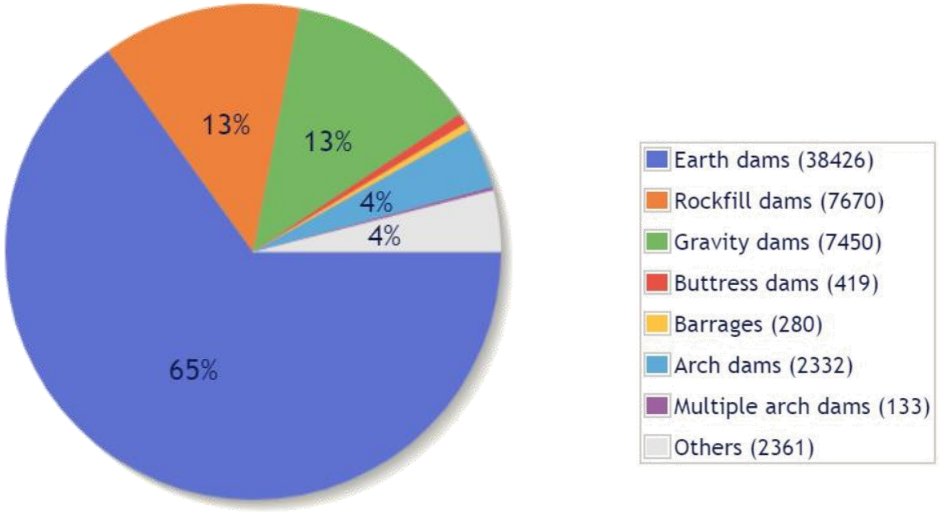

Figure 1. 2 Worldwide dams classification by type

The interpretation of the deformations of a dam requires a deep analysis of the results retrieved from field measurements (e.g. using pendulums, inclinometers, piezometers, traditional geodetic survey) and estimates from application of models and Information Technology (IT). The type of instrumentation installed its distribution along the dam must consider the characteristics of the geological site and the dam itself, and also the environmental effects which cause changes in the structure. Traditionally, the instrumentation are installed close to the bridges, if existing, or near the river gate and the river end, however the *in situ* measurements have decreased during the last decades (Duan and Bastiaanssen, 2013). The loss of *in situ* measurements are verified for the developing countries (Zhang et al., 2006; Vörösmarty et al.,1999; Ye et al., 2017; Gao et al., 2012; Solander et al., 2016; Albright et al., 2011, Cretaux et al., 2015), especially for a large part of Africa and Arctic where measurements are not existing or sparsely recorded (Alsdorf et al., 2007). In other developed countries, as well, the information about water reservoirs are recorded but they are not even distributed or freely available. The motivations of the lack of data are due to political or national legislation conditions (Magome et al., 2003; Ni et al., 2017; Busker et al., 2018, Avisse et al., 2017), but also economic (Mustafa and Noori, 2013); indeed the installation of the instrumentation requires much time and effort. Many countries, are also not interested in sharing information about water reservoirs information for scientific purposes (Famiglietti et al., 2015; Alsdorf et al., 2007), because sensitive data.

In Italy, the regulation of water reservoir resources is managed by The Ministry of Infrastructures and Transport and other institutions (*http://www.registroitalianodighe.it*). In particular, in southern-Italy, specifically in Sicily, where the study area is located, the management of water reservoirs is guaranteed by the Water Observatory (*Osservatorio delle Acque, https://www. osservatorioacque.it*). Information available on the website (recorded each month) are related to the capacity (millions of cubic meters) of the monitored reservoirs since 2010, . Unfortunately, there are also other reservoirs located in the same region, not reported on the website (*e.g.* in October 2018).

The list and the graphic representation of the dams distributed in Sicily are reported in Table 1.2 and Figure 1.3 respectively. They both refer to the available data on the website recorded in October 2018.

Table 1 2 List of dams located in Sicily (available at https://www. osservatorioacque.it, October 2018).

Available online	Not available online
Scanzano	Fiumara Grande
Piana degli Albanesi	Furore
Poma	Gammauta
Arancio	Gibbesi
Nicoletti	Guadalami
S. Rosalia	Licodia Eubea
Trinità	Monte
Ogliastro (Don Sturzo)	Mulinello
Rubino	Paceco (Baiata)

Available online	Not available online
Comunelli	Ponte Barca
Cimia	Ponte Diddino
Disueri	Sciaguana
Ancipa	Vasca Ogliastro
Pozzillo	Villa Rosa
Fanaco	Zaffarana
Castello	
Garcia	
Prizzi	
Olivo	
Leone	
S. Giovanni	
Gorgo Lago	
Rosamarina	
Lentini	

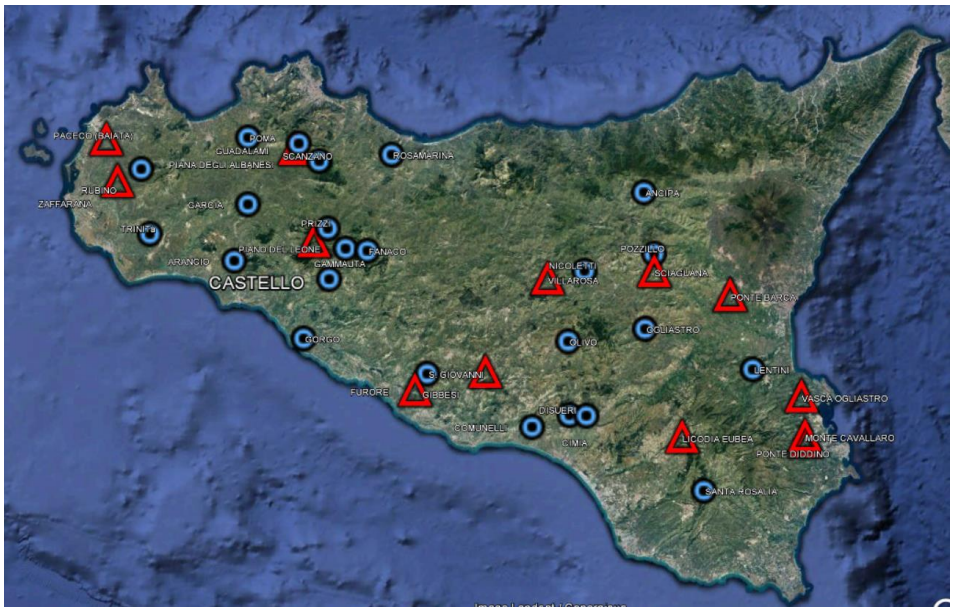

Figure 1. 3 Overview of reservoirs in Sicily. Blue icons identify the available reservoir data (available data on the website: https://www.osservatoriodelleacque.it*, October 2018), the red ones identify the reservoirs data not available for the same month, superimposed on Google Earth image.*

The information involved for this research are referred to one of the monitored dams (Castello dam, Agrigento), and aims to validate the strategies involved for the monitoring purposes. Then, the methodology could be easily applied on unmonitored reservoirs located elsewhere in the world where data are not available.

Other studies involved the knowledge of existing measured data to verify the correctness of the monitoring strategy, e.g. *via* InSAR (Lier et al., 2015). Results shown a comparable accuracy with traditional measurements.

The models involved in the physical interpretation of dam deformation process could be various, depending on the parameters used. Generally, analysing the time series of displacements, the main models involved are the descriptive models, in which the forces generating the effects are not considered and the Cause-Response models (statistical models), in which the relationship between the causative forces and the deformations is investigated. Other predictive models are also based on the time series analysis. The main are the smoothing models, including the simple mean, the moving average and the exponential smoothing, the Auto-Regressive Integrated Moving Average (ARIMA) models, mainly used for random process and time series decomposition, separating the different terms of the time series (linear, cyclic, season and random) (Alevizakou and Pantazis, 2017).

Recently a study has been performed on the evaluation of dam horizontal displacements based on three methods: the multi-regression method, the Seasonal ARIMA (SARIMA) model and the back propagation neural network (BPNN) (Zou et al., 2018). The parameters involved for this study were the horizontal displacements of the rock-fill dam, time, water level and air temperature. All models were able to provide the deformation trend of the dam with different accuracies over a long time. They provide better results for short-time provisional behaviour (few months) involving the multi-regression and SARIMA models.

The water level and horizontal and vertical time series have been also investigated for a concrete dam to establish a relationship between water loads and dam deformation (Pytharouli and Stiros, 2005). In this case, the geodetic data referred to six control stations on the crest and to reference stations close to the abutments. recorded for more than 30 years, since the first filling of the reservoir has been analysed. In particular, both horizontal and vertical displacements have been detected, by using a high precision theodolite and the spirit levelling, respectively and measurements of water level and temperature have been collected and statistically analysed.

The time series have been analysed using three different models aiming to detect the periodicity and the dominant periods of dam deformation. The three models were the Discrete Fourier Transformation (DFT), the Lomb normalized periodogram analysis and a trigonometric/polynomial fitting. Apparently there was not an evident linear correlation between the hydraulic load and the deformations, but all models revealed a causative relation, because of the 12 months dominant period for both water level and deformation time series, corresponding to the hydrological cycle.

The same authors analysed the long-term vertical component of displacements of an earth-fill dam using an innovative statistical approach based on the cross-correlation analysis (Pytharouli and Stiros, 2009). The approach revealed important results for Kremasta dam (Greece), but can be involved for any earth-fill dam without limitations.

Dam monitoring need to include the responsible causes of deformation process, analysing the relations with external loads using different approaches (Chrzanowski et al., 2011). Indeed, the deformations could be generally due to the ordinary action of hydrostatic pressure of reservoir or air/water temperatures (Oro et al., 2016) or could be also generated by extraordinary events, as earthquake (Siyahi and Arslan, 2008).

Scaioni et al. (2018) describing different technologies to be involved in the deformation process monitoring, discussed two different components of deformations affecting both concrete and earth dams: the long term and permanent deformations and the other components characterized by cyclic behaviour generally caused by external forces. Therefore become necessary the knowledge of weather parameters and reservoir water levels.

Recently, radar images and interferometry have been used as complementary techniques to analyse the dynamic deformation process of a concrete dam in Basilicata (Italy) (Milillo et al., 2016). The time series obtained from interferometry analysis has been integrated to the statistical analysis performed with hydrostatic-seasonal-temporal (HST) and hydrostatic-temperature-temporal (HTT) models to determine the non-linear dam deformations. The two deterministic models, suitable for elastic structures, are able to determine the displacements orthogonal to the dam. The models consider the aging term (time), the reservoir water level and the recorded temperature for the estimation of dam

displacements. Different results have been obtained for the aging term interpretation. Indeed, as reported by the authors, this term represents the most important and irreversible component of deformations, sensitive to the structure stability. The models involved have been used and validated also in different studies (De Sortis and Paoliani, 2007; Barzaghi et al., 2012).

In particular, De Sortis and Paoliani (2007) adopted the seasonal model, including three different terms for the dam deformation evaluation. The three terms were represented by the harmonic component, related to periodic displacements of the dam mainly caused by thermal expansion; the influence of hydrostatic pressure on the dam and a linear trend caused by non-reversible deformations (aging term).

Barzaghi et al., (2012), proposed a model based on De Sortis and Paoliani model, removing the term related to the hydrostatic pressure because no relevant changing water levels were detected on the analysed concrete dam. Also the period of oscillations is not fixed to one year as in the previous case, but it is estimated with Fast Fourier transform (FFT) model.

The use of Finite Element Model (FEM) is able to determine deterministic models for the dam deformation estimation, based on the knowledge of physical and mechanical properties of materials finning the dam.

Specifically used for embankment dams, FEM is able to determine the displacements and the stresses of a structure due to the external loads or changing boundary conditions. The geotechnical parameters depending on the composition of the dam itself need to be determined using, for example, laboratory test or the parameters estimated with the hyperbolic non-linear models; then the FEM analysis could be used to confirm the expecting behaviour (Szostak-Chrzanowski and Massiera, 2004).

Szostak-Chrzanowski (2006) adopted the model to analyse the behaviour of large earth dams, verifying the geotechnical parameters for all conditions. The results from modelled and measured deformations revealed that the model works correctly and could be involved for future developments. The integration between geodetic and geotechnical measurements has been also tested to determine the displacements of Mactaquac dam (Chrzanowski et al., 1989), according to the method developed by Chen (1983).

This method can be also used as support for geodetic survey, indeed, many studies were focused on the integrated use of geotechnical instrumentation and FEM analysis, accelerometers and geodetic systems including multi-sensors as total stations and prisms, Global Positioning System (GPS) receivers, InSAR.

Gikas and Sakellariou (2008) in their work compared the results from the geodetic campaign and the numerical modelling, to detect the

behaviour of an earth dam in Greece for over 30 years. The measured data were those from precise levelling and extensometers, since the first phases of construction of the dam. The comparison between results from measured data and FEM shown a good agreement between the tested techniques.

1.2 Dam displacements monitoring *via* GNSS and integrated systems

The use of GNSS for dam displacements monitoring allows the determination of three-dimensional position of one (or more) specifics points located on the monitored site, with high accuracy, comparable with that of other surveying approaches (Scaioni et al., 2018). The coordinates are estimated in the International Terrestrial Reference Frame (ITRF), at the recent epoch, the most recent is ITRF2014 (Altamimi et al., 2017). Then, it is possible the conversion of global coordinates into a local reference system.

The monitoring system, firstly used in 1995 for an arch concrete dam monitoring in California (Behr et al., 1998) only requires the interpretation of the data processing after designing the acquisition network. One of the first studies, involving the GNSS technique but also robotic total stations, for the analysis of deformation of three earth dams has been developed by Whitaker et al. (1998).

Recent studies (Montillet et al., 2016) demonstrated the capability of GPS system for real time and post-processing monitoring of earth dams

in the United States of America (USA), with different levels of accuracy. The real time kinematic (RTK) monitoring is able to provide an early-warning monitoring system for these structures with centimetre accuracy, while using the post-processing method with daily GNSS acquisitions (24 h) the achievable accuracy is sub-centimetre, comparable with that required for long-term deformations.

Using master reference stations on stable areas and control points on the site to be monitored, the visibility between the instruments is not necessary, as also the presence of an operator on the field. The estimation of the coordinates of the control points derived from the processing of the baseline connecting the receivers.

The GNSS antennas of the reference stations need to be fixed on forced-centering equipment to guarantee their position over time during the survey. Nowadays also CORS are involved for this purpose. Then, dual-frequency receivers with L1 and L2 carrier phase measurements need to be used to estimate and reduce (by implemented algorithms) the atmospheric delays. Then, results, in terms of deformations and, in particular, displacements, are statistically analysed involving different strategies, depending on the specific test (Koch, 1999; Sacerdote et al., 2010).

Rutledge et al. (2006) described the interaction between the GPS system and inverted pendulums installed on a concrete dam, located in northwest Montana. Four GPS receivers were located on the dam crest in the same positions occupied by gravity plumb-lines, to evaluate the

horizontal displacements obtained by the different instruments. GPS reference stations were installed on the ground on stable positions. Three years of data have been recorded and from results a strong linear correlation between the GPS and plumb-lines measurements exists. The comparison between the two techniques in an integrated monitoring system allows demonstrating the capability of GPS system for long-term dams monitoring, indeed, the GPS was able to detect the same deformations obtained by the plumb-lines, with high accuracy and precision. Indeed, analysing the performances of GPS characteristics the authors found a small bias of 0.25 mm between GPS and plumb-lines system.

The comparison between different measurements (GPS and inverted pendulum) has been also discussed by Bond et al. (2011) for a concrete dam in Canada over 5 months. Six receivers have been used for this purpose, located on the dam and two reference stations have been established on the ground, close to the structure. In this case, many differences have been found between the two measurements, probably due to the possible movement of GPS stations or inverted pendulums, or the different influence of thermal effects on measurements. Indeed, the different location of GPS antennas and inverted pendulums determines differences in the measurements probably due to the different thermal warming of the structure.

The Mornos dam, in Greece, has been analysed using different and independent analysis, involving a geodetic control network and a numerical model, for the evaluations of deformations from the

construction to the operational life (Gikas and Sakellariou, 2008). In particular, the geodetic network consist of 53 control station for the monitoring of the dam itself and the surrounding area and it was monitored, since the first year of its construction by using the theodolite, the Electronic Distance Measurement (EDM), the Total Station and later, the GPS. The results highlighted higher movements in the upstream-downstream direction, identified in the middle section of the dam and in the terminal part of the structure. From the numerical model, the results agree with those from geodetic survey, exploiting, also in this case, the highest horizontal displacements in the orthogonal direction to the dam.

The monitoring strategy adopted for the Arenoso reservoir (embankment dam) considers the analysis and the comparison between the settlements and the horizontal displacements retrieved from high precision geodetic monitoring system and numerical model (FEM) (Acosta et al., 2018). The vertical and the horizontal displacements are carried out using the high-precision levelling and GNSS, respectively. The measurements are not continuously recorded over time, but many fields surveys have been made during the monitoring. Both measurements showed the maxima values of displacements in a critical area, with a similar trend in the downstream direction. The FEM analysis involved for the materials properties the general information for an embankment dam and not the real values from laboratory tests or previous studies, also the structure is simplified without considering the real distribution of material composition. Thus the comparison shows a similar pattern but the differences between the two methods are high.

The Differential GPS (DGPS) technique for real time monitoring is also suitable for predicting absolute deformations of dams, with a millimetre accuracy (Galan-Martin et al., 2013). The monitoring of La Acena dam, Spain, using DGPS receivers, precise angular collimation and direct pendulums systems, showed comparable results using the different techniques, when the data are transmitted without discontinuity, depending on the GPRS System communication. The more relevant displacements are those in the cross-section on the dam crest with an annual cycle depending on the water loads and temperatures actions.

An accurate full monitoring system need to be developed in case of potential damages from earthquakes. This is the case of Sermo Dam, Turkey, that is one of the large dams, located in Java Islands (Tarsisius Aris et al., 2012). Lots of strategic structures as dams are not well maintained in Turkey. Thus, the knowledge of deformations over time could provide useful information about the dam safety and unexpected behaviours. The monitoring system involved for this study included multi-sensors, as 3D robotic total station, GNSS CORS, automatic recording of the reservoir water level and digital IP camera. The preliminary results showed the capability of the GNSS monitoring for detecting with high precision stable areas for the reference station located on a tower, close to the structure and the back sight station, involved for the detection of displacements of both the displacements of the dam and the surrounding area.

The relationship between the displacements and water loads changing over time, for both concrete and earth dams has been investigated; also, for embankment dams, this relation can change because of the weight of the dam itself and the composition of the materials. The main dam displacements are generally located on the top of the dam, in the middle section, along the direction orthogonal to the dam. Several studies highlighted these results for both concrete dams (Behr et al., 1998; Yigit et al., 2016; Kalkan, 2014; Yavasoglu et al., 2018; Radhakrishnan, 2014) and earth-filled and embankment dams (Tasci, 2008; Sousa et al., 2016; Ruiz-Armenteros et al., 2018). Based on these results only the horizontal component of displacements will be discussed within the dissertation.

The first monitoring using the GPS was assessed for the Pacoima dam, California in 1995 (Behr et al., 1998). At that time, the satellite technique was considered as an alternative to the traditional instruments adopted for the purpose, although the limitation of the proposed method at that time. It was the first experience that highlighted the capability of GPS monitoring for this kind of structures. Also, the recorded displacements in the middle section were strongly correlated to the temperature and a sinusoidal behaviour has been found and the residual displacements, after removing the annual component are able to describe the behaviour of the dam under different water loads.

GPS receivers in static survey have been used for the Altynkaya dam monitoring, Turkey (Tasci, 2008). The monitoring was able to detect the

deformations of the rock fill dam crest, due to the water loads. The effects of hydrostatic pressure on the earth dams are permanent deformations along the direction orthogonal to the dam, in the middle section. A relation between the water levels and displacements, in the hydrological periods have been found. In particular, it has been found that during the emptying period, the deformation of the dam was to downstream, otherwise, during the filling period, to upstream. In the middle section the main movements have been found, but only the planimetric components have been evaluated due to the lower accuracy of the vertical component.

The relation between the horizontal displacements of a concrete dam and the water level and dam body temperature were examined for Ermenek dam, Turkey (Yigit et al., 2016). The variables have been investigated during the first filling of the reservoir, involving geodetic instrumentation. The radial movements, more relevant than the tangential, have shown an increasing linear trend and a sinusoidal trend, caused by linear water levels changes and concrete temperature changes, respectively, mainly in the middle section. On the contrary, no relationships have been found between the tangential displacements and the water levels changes.

Considering the importance of monitoring the main factors influencing the dam behaviour and the accuracy to be achieved (±5-10 mm for horizontal displacements and ±2 mm for vertical displacements for concrete dams and ±20-30 mm for horizontal displacements and ±10

mm for vertical displacements for rock fill dams), traditional geodetic methods and GNSS have been used for deformation monitoring of Ataturk dam, Turkey (Kalkan, 2014). Comparing the results between different methods, a comparable positional accuracy has been found between the different techniques, generally higher than ±10 mm. The radial displacements represent the main horizontal component of displacements, but the relation between the latter and the water levels is not really clear from the study. Further studies, involving terrestrial and GNSS measurements over a larger period demonstrated that maxima horizontal displacements have been reached in the middle section of the dam crest, along the upstream-downstream direction (Yavasoglu et al., 2018).

The Koyna dam is a large concrete dam monitored via GPS technique, in which the effects of reservoir water levels changes have been estimated to better understand the dam safety (Radhakrishnan, 2014). The deformation referred to one receiver located on the top of the dam, continuously operating (24h), close to a coordimeter used for the validation data. Three different periods have been considered for the analysis, according to different emptying and filling of reservoir water level, over a hydrological period of one year. Indeed, the water level changes are considered the main cause of deformation of this structure, followed by the seasonal temperature changes. The results have shown an elastic behaviour of the structure. During the refilling period (May-September) an inclination of the body dam was observed in the downstream direction, from September to December with small decrease

of reservoir water levels the structure sprung back, finally, during the emptying period (December-May) the deformations of the dam are mainly in the upstream direction.

The analysis of different integrated systems combined with GNSS highlighted the high capabilities of the latter for structural monitoring in terms of deformations. Also many limitations, related to the use of the GNSS in specific unsuitable sites (e.g. urban areas or valleys) could be easily overcome for example by using pseudolites (Yang et al., 2010) or new sensors as discussed below.

1.3 Dam displacements monitoring *via* InSAR techniques

During the last decades, InSAR technique has been used for structure deformation monitoring, since the monitoring is essentially remote and a direct contact with the structure is not required. The accuracy of the technique is also comparable with other traditional techniques (sub-centimetre to millimetre accuracy) and the results are able to show unexpected changes in the operational life of the structure. Several techniques have been implemented for structures monitoring, such as dams, and most of the results have been compared and validated by using integrated monitoring systems. This approach is really useful to provide provisional models of the long term behaviour of these structures.

For example, recently, the InSAR technique has been involved for the analysis of the destabilization process of the Mosul dam, Iraq (Milillo et al., 2016; Milillo et al., 2017), using high resolution images from

COSMO-SkyMed and Sentinel-1A satellites. The aim of this study was focused on the realization of the first cumulative deformation map of the dam using together multi SAR-sensors. In the study of 2017, the comparison between InSAR results and numerical modelling has been also analysed, despite future improvements need to be assessed.

Different approaches can be involved for interferometry application, based on the use of terrestrial acquisitions, *via* Ground-Based InSAR (GB-InSAR) technique, or satellite acquisitions, involving one pair of images (Differential InSAR (DInSAR) technique) or a multi-temporal approach using the Permanent Scatterers (PS) technique.

All InSAR techniques involve the same concepts for structure of land monitoring, using different sensors (on the ground or satellites) and they are based on SAR principles described by Ferretti et al., (2007). Indeed, they exploit the content of a radar signal emitted and received by the sensor, including information about the phase, related to the acquired geometric information and the amplitude of the signal. Then, using the interferometry, the phase content is investigated using different algorithms, and the difference between the corresponding pixels of two coherent SAR images allows determining the displacements measurements of structures or land with sub-millimetre precision.

The capability of InSAR techniques have been tested on different type of structures, as buildings, bridges and dams (Sousa et al., 2014; Lazecky et al., 2015). The studies involved the latter are the most important to the aim of this research.

The GB-InSAR is a powerful instrument to determine the structure deformations but requires the installation of a GB-SAR sensor on the ground, generally located in front of the monitored site, for the data acquisition. Several studies focused on the application of GB-InSAR technique for dam monitoring (Alba et al., 2008; Luzi et al; 2010; Nico et al., 2015; Talich, 2016; Qiu et al., 2016; Di Pasquale et al., 2018).

Scaioni et al. (2018) discussed the main advantages and limits by using the GB-InSAR technique. As reported by the authors, this technique can be involved in an integrated monitoring system as complementary to the other techniques involved. Indeed, it offers lots of advantages allowing achieving high precisions of measurements (millimetre to sub-millimetre), especially on dams. The use of the GB-InSAR provides high temporal resolution (minutes to seconds) and spatial resolution depending on the distance between the sensor and the dam, operating continuously over time (day and night) under all weather conditions. Also, it doesn't require the installation of any sensors on the dam, but at a distance from it. The latter represents also a limitation of the method because of the materialization costs to install the sensor, but other limitations can influence the performances of the method. For example, the GB-SAR measurements require the correct estimation of the phase ambiguity, the correct position of the sensor need to be correctly investigated before its installation, depending on the expecting behaviour of the dam. Indeed, the displacements perpendicular to the Line of Sight (LOS) of the sensor cannot be recorded, but the main disadvantage is represented by the estimation of the atmospheric delay.

The influence is higher when the distance between the sensor and the structure is high and the structure is large. Qiu et al. (2016) proposed an innovative approach for atmospheric contribute determination that should be removed by using the PS-InSAR analysis.

The use of DInSAR, developed during the last decade, has been widely used for dam monitoring, especially earth and embankment dams, achieving good results in terms of ground deformations. The analysis of single pairs of images or multi images approaches, e.g. by using Small Baseline Subset (SBAS) technique, reveals the capability of these techniques to obtain precise results (Corsetti et al., 2018).

The principle of DInSAR technique is based on the evaluation of the interferometric phase, as difference between the phase of two acquisition of the points on the ground from the same sensor at a different position, related to the difference between the two acquisitions.

A comparison between the results obtained from in situ monitoring systems and DInSAR technique for La Pedrera dam, Spain, showed the capability of the latter to provide a complementary method for displacements evaluation (Tomas et al., 2013). Involving an advanced DInSAR technique, so called Coherent Pixel Technique (CPT), the method was able to detect both the linear and non-linear deformations components of the dam, involving three different datasets. From the results a similar behaviour has been detected in the mid-section of the dam, exploiting the largest displacements over 15 years.

The same technique (CPT) was conveniently used for the Conza dam monitoring, Italy (Di Martire et al., 2014). Also, in this case, the use of existing monitoring system was useful to compare the results and validate the use of the DInSAR for precise monitoring of infrastructures and structures, especially dams. The comparison between the results obtained from extensometers located on the dam and those from DInSAR technique revealed a strong agreement. Also in this case, the largest deformations occur in the central section of the structure, because this is the mainly stressed section.

The Advanced-DInSAR technique has been successfully used for monitoring the structural health of three dams:, using both high and low resolution images depending on the objective of the studies. In particular, for Three Gorges dam, results are comparable for both ascending and descending data, but the interpretation of 3D displacements was not possible because of the missing merging of the processed data for ascending and descending orbits. From the analysis of Plover Cove dam a high correlation between non-linear displacements and water level fluctuations was found. Finally, for San Liberato dam, no permanent deformation have been found during the analysed period (Mazzanti et al., 2015).

The combined use of GNSS and InSAR techniques for dam monitoring has been evaluated by Shimizu (2015) for a rockfill dam in Japan. The comparison between the results highlighted an high

correlation between the two techniques, exploiting both ascending and descending orbits tracks.

Also the results were confirmed by another study involving GNSS measurements and SAR displacements evaluated *via* PS and SBAS techniques over a large area including several permanent stations (Armas et al., 2016). The comparison has been set between the data acquisition from GNSS receivers located on the ground and PS identified close to the GNSS positions. From the comparison the two techniques can be considered complementary and a strong correlation has been found, after converting the 3D GNSS displacements into LOS direction.

Previous results highlighted the promising capability of the discussed InSAR technique for structures monitoring, but many limits can influence their performances, as the temporal or spatial decorrelation (Hanssen, 2001), the unwrapping of the phase (Ghiglia and Pritt, 1998) for DInSAR technique and the atmospheric effects (Zebker et al., 1997). Some of these problems can be solved using a different approach, based on multi-temporal InSAR analysis. The method was originally developed by Ferretti et al. (2001) and it is known as PS-InSAR technique.

The PS technique involves multiple SAR images over the same area, identifying within the scenes natural targets with high backscattered signal over time, not influenced by decorrelation. Also the interferometric phase is evaluated using the normal and temporal baselines between the images (Crosetto et al., 2016).

Roque et al. (2015) applied the InSAR technique on three different dams, two earth dams, Alamos I and II, and a concrete one, the Alqueva dam, in Portugal. Results from PS-InSAR technique have been compared with those of geodetic measurements. For the earth dams, a discrepancy of few mm/y has been found, probably due to the small number of images involved for the analysis. For the concrete dam, analysing two years of data, the results agree with geodetic measurements, later, also in this case there is a discrepancy between the two datasets.

A study involved the analysis of C-band images, as ERS, Envisat and recently Sentinel-1 images, demonstrated the capability of these data for continuous dam deformations monitoring (Sousa et al., 2016). In this study, six dams (both made up of concrete and loose materials) have been monitored using multi-temporal InSAR techniques (PS-InSAR and SBAS). For each case study, the techniques were able to detect the deformation trend of the structures with changing number of images involved. The behaviour of the analysed dam is obviously different and depends on the materials of the dam and the loads acting on it. However, the use of C-band images allows determining high-intensity stable points (PS) on the structure highly coherent.

Another study involving the multi-temporal approach *via* PS-InSAR technique exploited the availability of C-band (ERS, Envisat and Sentinel images) for La Vinuela dam monitoring (Spain) (Ruiz-Armenteros et al., 2018). In this case, not only different data has been used for the earth-filled dam, but also different algorithms have been implemented, to

estimate the LOS trend deformation since the initial period of monitoring. The use of recent data (Sentinel-1) was able to confirm the deformation pattern recorded on the top of the dam, in the central part, along the orthogonal direction to the dam). The orthogonal movements are related to the water levels fluctuations.

The non-linear deformations of Petrusillo dam located in a rural area, have been evaluated using another approach, called Quasi-PS (QPS) method (Perissin et al., 2007), involving the X-band Cosmo-Skymed SAR images characterized by short repeat pass (Milillo et al., 2015). The QPS technique differs from traditional PS-InSAR technique mainly for two aspects (Wang et al., 2011): the first is the graph connecting the available dataset (spatial and temporal baselines), the other is the selection of PS within the scene. The graph connection involved for the QPS analysis, in this case, is based on the minimum spanning tree (MST) method, maximizing the coherence of the generated interferograms, while usually for PS-InSAR analysis the common graph connecting the images is the star graph, characterized by single baselines connecting the master acquisition and the slaves images. Also, using the PS-InSAR technique, the PS are determined after selecting a threshold for a specific parameter (Amplitude Stability Index, ASI), while, using the QPS technique, the coherence of each interferogram is used as weight for the estimation of target displacements and heights. The application of both PS and QPS techniques revealed the capability of the latter for landslide monitoring in extra-urban areas where the application of PS fails. Also the QPS technique over short repeat-pass interferometry was able to

detect the non-linear movements of the dam, caused by the temperature and the hydrostatic pressure.

The combination of PS and QPS InSAR have been also involved for Three Gorges dam monitoring, located in the town of San Douping, 40 km from Yichang, Hubei Province (Wang et al., 2011). The dam deformations caused by changing temperature and water levels of Yangtze River (Zhongbao Island) and the surrounding area deformations have been evaluated using the two complementary techniques, with satisfactory results. Indeed, the QPS technique was helpful when decorrelated signals occurred over extra-urban areas, increasing the availability of selected points on the monitored site.

Also, the determination of both dam deformations (irreversible component) and the seasonal deformations (reversible component, mainly due to external forces) has been retrieved by Lazecky et al. (2015) for different case studies: Three Gorges dam (China), Plover Cove dam (Hong Kong) and Charvak dam (Uzbekistan). In particular, the techniques were able to evaluate the influence of different forces acting on the dams (e.g., water loads) and consequently both components of displacements (linear and non-linear movements).

The application of standard procedures for the linear displacements trend and non-linear models for seasonal movements has been also discussed by Bakon et al. (2014) for Plover Cove dam and a building, located in Hong Kong. The possibility of separating the two components

of displacements, using TerraSAR-X data, is, indeed, the main goal of the work, when non-linear movements characterize the behaviour of dams or the land.

Recently, PS-InSAR and SBAS techniques have been involved to detect both linear and nonlinear ground displacements in the mining structures after the collapse of the tailings of Fundao dam, Brasil (Mura et al., 2018). Results from the InSAR analysis are in agreement with those found by geodetic survey. Several traditional and innovative techniques have been involved for dam monitoring (total station/prisms, levelling, GNSS, optical fibre sensors, piezometers, inclinometers, GB-SAR). However, results referred to specific monitored points, without considering the overall deformation of the dam body. Thus the InSAR techniques were helpful and complementary to the other techniques to detect the overall deformation process of the structure. Also, the comparison between the two InSAR techniques involved, showed not relevant differences, demonstrating the high potentiality of short-repeat pass SAR acquisition for structure monitoring.

However, many limits occurred also for dam monitoring using the PS-InSAR technique, summarized in Sousa et al. (2015). Indeed, the deformation accuracy depends on the orientation of the structure related to the LOS of sensor, the resolution of SAR images used for the monitoring and the wavelength. Also, the determination of vertical and planimetric components requires the acquisition of SAR images in both ascending and descending tracks and their combination.

1.4 Reservoir water surface and levels estimation *via* remote sensing

The analysis of water surface and levels from satellite aims to perform the full design monitoring system for Castello dam. Many techniques are available for water storage- surface and level detection, involving different SAR and optical imagery.

The water levels investigated to determine the causative relationship with dam deformation can be directly estimated through Satellite Radar Altimetry (SRA) and Satellite Laser Altimetry (SLA) or can be evaluated using the elevation-storage-surface curve, from the surface determination.

The main instruments and algorithms involved for the water levels and water surface estimation are summarized below (Gao, 2015).

It was also found that satellite data combined with in situ data are able to describe earth and water surface behaviour, with limited costs (Klemas and Pieterse, 2015). The potentialities of the satellite techniques have been discussed by several authors in terms of cost-effectiveness, time consuming and easier elaboration of acquired data. Also data are available for a large period and time series can be easily estimated and analysed (Peng et al., 2006; Singh et al., 2015). The direct estimation is provided by spaceborne radar altimeters (from GEOSAT, 1985-1989 to Jason-CS, 2017) or the Geoscience Laser Altimeter System (GLAS) on the Ice Cloud and Land Elevation Satellite (ICESat).

SRA represents an important technology for monitoring water levels, but issues can be revealed when rivers, narrow reservoirs, and small lakes are examined (Xue et al., 2018). The authors in their study presented an approach to detect stable inland lake levels from Cryosat-2 SAR interferometer waveforms.

The reservoir water surface estimation is based on the use of visible and infrared bands, involving different approaches, depending on the image resolutions and the level of accuracy. The main algorithms are the threshold-based approaches, classification-based approaches (supervised or unsupervised, depending or not from the subjectivity of the operator), and the multiple-step hybrid approaches.

Using the first method, a threshold is selected for the single band properties or the spectral water index involved, as the Normalized Difference Water Index (NDWI). The threshold is able to separate water from the land.

As discussed by Jiang et al. (2014), many limits occur by using the threshold-based approach. Indeed, generally, the technique is not able to identify mixed water pixels, the noise within images can influence the accuracy of the method and also the threshold values need to be changed according to the image acquisitions. Thus, the authors proposed an automated based on the combination of water index (WI) and image processing techniques. The multiple step approach improved the performance of the traditional technique.

The supervised classification requires the selection of pixels detected as water, then using statistical parameters other pixels with statistical similarity are associated to the same class, with high accuracy. On the contrary, the use of unsupervised classification doesn't require any preliminary selection of pixels belonging to the same class. The latter method can be also automatized.

The last technique requires the application of several approach using multiple steps, adding some innovations to the traditional methods.

Object-based image analysis (OBIA) involves multiple bands for multi-resolution segmentation and classification. Kaplan and Avdan (2017) compared results from NDWI, supervised and unsupervised classification and OBIA classification. Also a new approach has been developed based on the combined use of OBIA classification and NDWI analysis for image at 10 m resolution (Sentinel-2).

Chapter 2

Materials

2.1 Castello dam monitoring

The study area is the Castello dam (Figure 2.1), an embankment dam located in south Italy ~30 km away from Agrigento (37°34’51”N, 13°24’48”E, WGS84) and it represents one of the main reservoirs in the western part of Sicily (Figure 2.2).

The embankment dam is made up of a coarse-grained homogeneous alluvium from the valley and limestone, with a seal coat of bituminous conglomerate.

Figure 2. 1 Geographic location of Castello dam, Sicily, south-Italy. (Pipitone et al., 2018, Remote Sensing)

Figure 2. 2 Satellite view of Castello dam (from Google Earth). (Pipitone et al., 2018, Remote Sensing)

The seal coat stands on a reinforced concrete structure with a thickness of 80 cm fitted below the bulkhead in reinforced concrete. This structure is crossed by an inspection tunnel in which a piping drainage system is installed.

The foundation soils consist of alluvial materials with variable. The main structure consists of two segments, of 165.00 m length and 317.00 m respectively; connected by an arc of a circle developing for 309.80 m, with a radius of 268.08 m and concavity facing valley.

The vertical cross section of maximum height has a trapezoidal shape, characterized by 9.00 m width on the top and approximately 214.00 m at the base (Figure 2.3); the side of the valley, covered with turf of vegetable soil, is constituted by a broken line interrupted by two quays with 2.50 m width and an elevation between 284.00 and 272.00 m a.g.l.

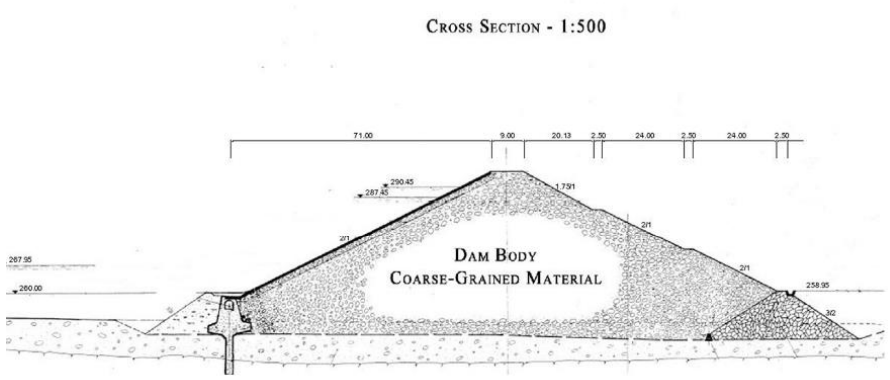

Figure 2. 3 Vertical cross section of Castello dam (documentation from the dam project, available from Regione Siciliana – Assessorato Agricoltura e Foreste – Ente di Sviluppo Agricolo Palermo. Servizio Bonifica ed Infrastrutture, Dardanelli et al., 2014)

The reservoir is used for civilian use and irrigation (*Dipartimento Regionale dell'Acqua e dei Rifiuti – Assessorato Regionale dell'Energia e dei Servizi di Pubblica Utilità*). The supervisors of the structure periodically carry out topographical surveys (excluding GNSS) according to the Italian legislation. Indeed, the law requires the installation of two group of monuments on the dam: the references, or control benchmarks, away from the structure or near the area where movements need to be investigated, and deformation monuments describing the movements of the structure (Figure 2.4).

The movements of the dam are evaluated by surveying with total station and digital level, with bi-monthly frequency or less, while the rotations of the surface is monitored by using clinometers with weekly frequency; also for the dam settlements and the evaluation of the deformations on the top of the dam settlement gauges were used, with bi-monthly frequency. Spirit levelling was also used to evaluate the vertical component of displacements of tunnels with bimonthly frequency.

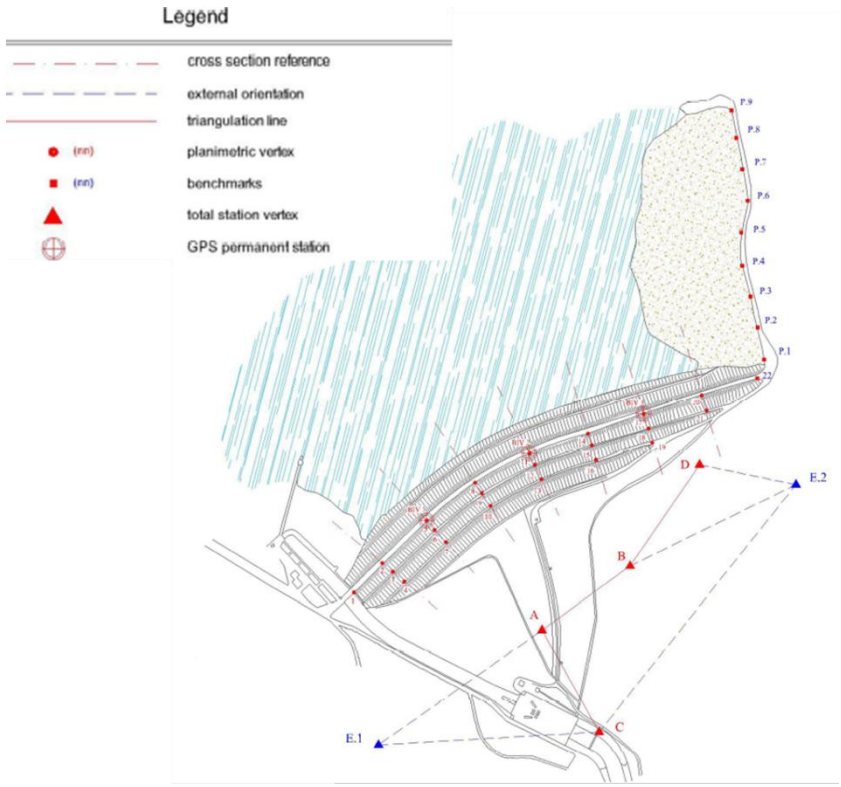

Figure 2. 4 Main instruments installed on the embankment dam (modified image from Dardanelli et al., 2014)

2.2 Dam displacements monitoring

2.2.1 GNSS data

To evaluate the dam displacements *via* GNSS, three receivers have been located on the top of the dam, one in the middle section and the others on the left and right sides respectively. A CORS, named AGRI far away from the monitored site (~30 km) has been also used as master reference station, with single baselines connecting the reference station and the receivers on the dam (Figure 2.5). Data for the reference

permanent station of UNIPA CORS network were retrieved from NetGEO website (http://www.netgeo.it). The innovative strategy allows reducing the costs of materialization and data management and also reducing the possibility to be influenced by the dam behaviour. The use of CORS became helpful for the building of the dam monitoring system in the past years (Drummond, 2010; Jiang et al., 2012) and it is, nowadays, an efficient approach for the analysis of strategic structures.

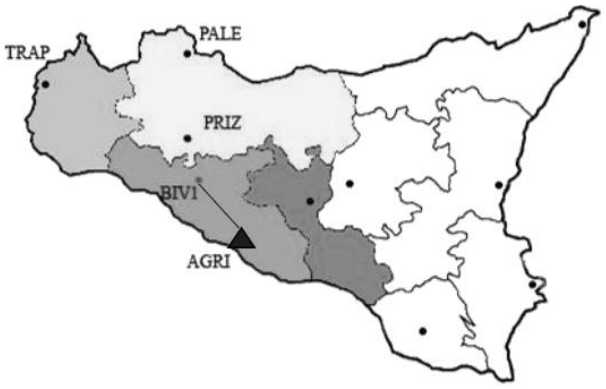

Figure 2. 5 Qualitative representation of baseline connection between CORS of AGRI and one of the receivers.

The three GNSS receivers have been located on stainless steel pillars provided by Topcon and fixed to the ground by using steel plates on concrete reinforce (Figure 2.6). In particular, two Topcon GB-500 receivers have been used with two Topcon PG-A1 antennas, and one Topcon NET-G3A receiver with Topcon G3-A1 antenna.

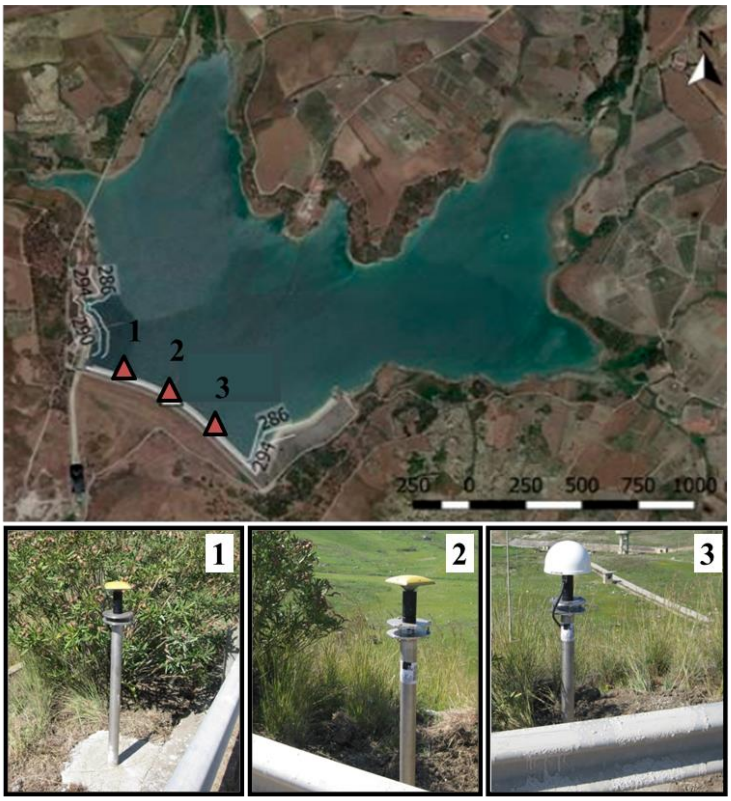

Figure 2. 6 GNSS receivers located on the dam crest

The time series has been obtained over time during the monitoring period and results refer to the Modified Julian Day, (MJD), the corresponding reference time from the analysis with Network Deformation Analysis (NDA) software.

The first day of acquisition was 08 April 2011, corresponding to the MJD 55659; the monitoring continued until 13 May 2013. During this period many data were missing due to the failure of acquisition.

2.2.2 Sentinel-1A TOPSAR data

Sentinel 1-A dataset has been used for both dam displacements monitoring *via* InSAR technique and water levels detection using the OBIA. The dataset has been provided free by Copernicus Open Access Hub (https://scihub.copernicus.eu/dhus/#/home) and acquired since October 2014. Figure 2.7 shows the availability of Sentinel-1 data. As reported in this figure, the study area and, generally, Italy, are completely covered by sensor acquisitions, recording a high number of observations (> 500) in both ascending and descending orbits. Indeed, ascending and descending passes provide at least two acquisitions for each area within 12 days.

The dataset used for the analysis has been acquired in Interferometric Wide (IW) Swath mode, with Terrain Observation by Progressive Scan (TOPSAR) and dual polarization VV-VH. It is characterized by 250 km swath width and 5m x 20 m ground resolution. Also the IW acquisitions, using the TOPSAR mode captures three sub-swaths (named IW1, IW2, IW3, from the closest to the sensor, respectively and contains one image for each sub-swath, depending also on the polarization (3 images for single polarization and 6 images for dual polarization) to be processed separately.

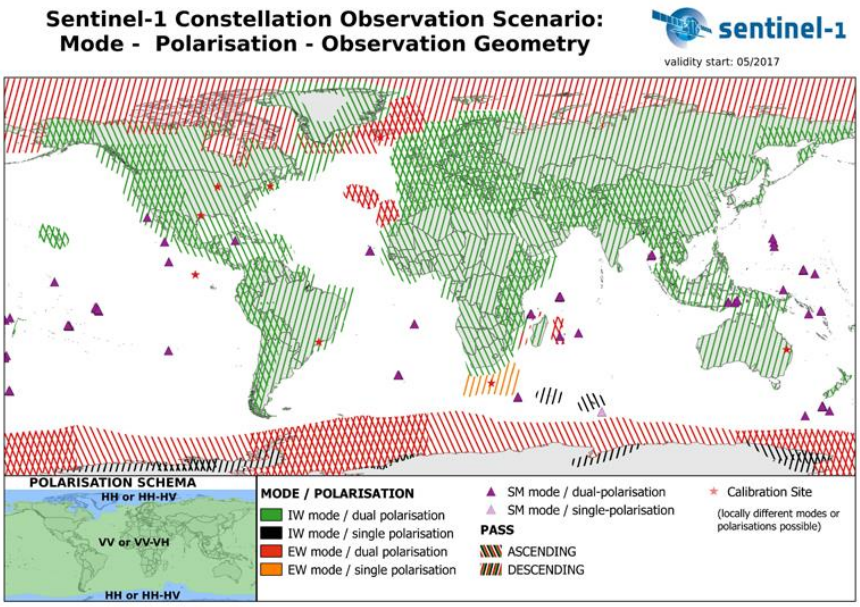

Figure 2. 7 Sentinel 1 Data scenario (https://media.asf.alaska.edu/uploads/sentinel/s1-constellation-mode-polarization-observation-geometry-800.png)

TOPSAR mode acquisition allows synchronising each burst ensuring the alignment of interferometric pairs of images.

The dataset includes 20 Sentinel TOPSAR S-1A images, in VV polarization acquired over a year (January 2015-January 2016) able to describe both an emptying and a filling periods of the reservoir (Figure 2.8). The images have been acquired in SLC format in ascending looking right track (track 117).

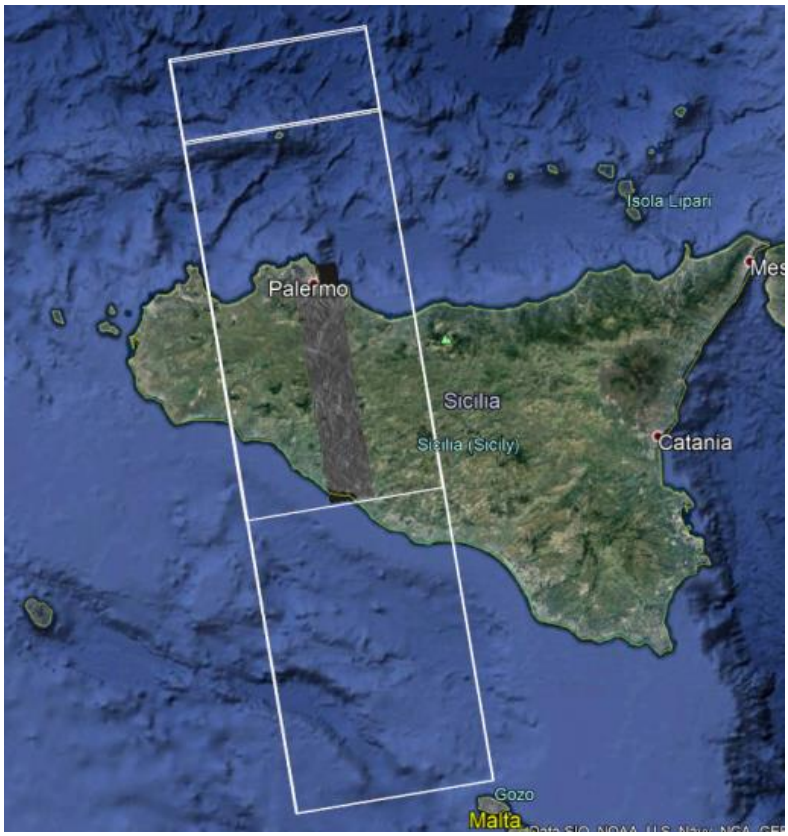

Figure 2. 8 View of ascending track 117 (white boxes) from IW2 of the S-1A dataset covering the study area in Sicily (Italy) (image available from Google Earth Professional).

Other 7 images TOPSAR S-1A images have been involved in a preliminary analysis, acquired from 28 June 2016 to 20 September 2016. The images have been acquired in SLC format in ascending looking right track.

The Digital Elevation Model (DEM) used for the InSAR analysis has been automatically downloaded from United States Geological Survey (USGS) site (https://dds.cr.usgs.gov/srtm/version2_1/SRTM3/).

The software involved for the processing is SARPROZ © (Perissin 2009-2017), available at https://www.sarproz.com) allowing an advanced multi-temporal InSAR analysis.

The same dataset has been also used for the water surface and level estimation using the OBIA. Preliminary the dataset has been processed using the open source toolbox online from European Spatial Agency (ESA), called Sentinel Application Platform (SNAP).

2.3 Water surface and level estimation

2.3.1 Optical data

Optical data were used for the water surface and levels estimation only. The dataset includes 7 Landsat 5 (LS) TM, 9 Landsat 8 (LS 8), 26 Landsat 7 (LS7) Enhanced Thematic Mapper Plus (ETM+) Scan Line Corrector-Off (SLC-Off) and 8 ASTER images. All images have been downloaded from USGS EarthExplorer website (https://earthexplorer.usgs.gov). They are all characterized by acquisitions during the day and cloud cover less than 20%.

LS7 images are characterized by missing scan lines within the scenes due to the failure of SLC from 31 May 2003. The width of the gaps is changing with the position of the area within the scene. Indeed, the gaps size is minimum towards the centre and maximum on the boundaries of the images.

Both LS7 and LS8 images are characterized by a panchromatic (PAN) band with higher spatial resolution (15 m) than the multispectral (MS) bands (30 m) and thermal infrared (TIR) bands. Only MS and PAN

bands have been used for the analysis (Visible, V, Near InfraRed, NIR and Short Wave InfraRed, SWIR).

LS5 images are characterized by MS bands with 30 m resolution, except for two images provided by ESA resampled at 60 m.

ASTER images are characterized by three bands in Visible Near Infrared (VNIR), five bands in TIR and six bands in SWIR. In this study only VNIR bands have been used, characterized by 15 m resolution.

Figure 2.9 shows 4 different optical images with a pseudo-colour representation.

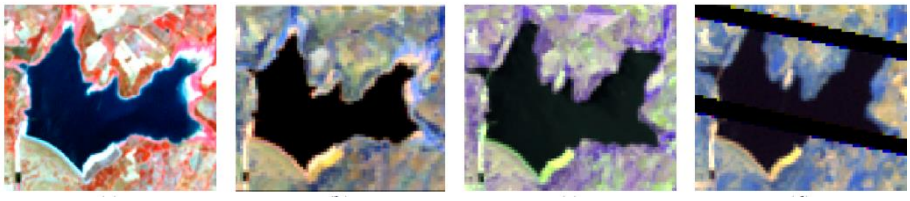

Figure 2. 9 Pseudo-colour visualization for ASTER image (on the left panel, VNIR bands), LS5 image (central-left panel), LS8 image (central-right panel) and LS7 ETM+ SLC-Off (right panel). Landsat images are shown using the SWIR1, 2 and NIR bands) (Pipitone et al., 2018, Remote Sensing).

2.3.2 TerraSAR-X and Cosmo- SkyMed data

Cosmo-SkyMed images used in this research were acquired within "Integrating radar images and hydrological modeling to quantify urban floods" funded by ESA (proposal Id: 31609—G. Ciraolo principal investigator). The utilization of TSX archive for scientific use has been granted with the proposal "Integrating RADAR images and flooding

hydrological modeling" (proposal code: HYD3110—A. Maltese principal investigator) funded by German Aerospace Center (DLR)).

These images have been used for the water surface and levels estimation, based on different remote sensing approaches.

6 Cosmo-SkyMed (CSK) and 2 TerraSAR-X (TSX) images have been acquired in the period January 2011 – October 2012 in single polarization (HH). The TSX images are characterized by two different acquisition modes, ScanSAR and Stripmap.

The main characteristics of the images are reported in Table 2.1 (for CSK images) and 2.2 (for TSX images).

Table 2. 1 Main characteristics of CSK images (Pipitone et al., 2018, Remote Sensing)

Cosmo-SkyMed					
Date (dd/mm/yyyy)	Acquisition Time (UTC)	Look Direction (°CW from N)	Orbit Direction	Far Incidence Angle (°)	Near Incidence Angle (°)
08/09/2011	17:15	≈11.17	Descending	≈28.28	≈24.90
08/02/2012	04:54	≈169.36	Ascending	≈33.85	≈30.78
15/02/2012	17:13	≈11.17	Descending	≈28.29	≈24.91
23/06/2012	04:53	≈169.52	Ascending	≈35.45	≈32.43
10/09/2012	17:11	≈11.18	Descending	≈28.28	≈24.90
13/10/2012	04:52	≈169.51	Ascending	≈35.45	≈32.44

Table 2. 2 Main characteristics of TSX images (Pipitone et al., 2018, Remote Sensing)

TerraSAR-X						
Date (dd/mm/yyyy)	Acquisition Time (UTC)	Look Direction (°CW from N)	Orbit Direction	Far Incidence Angle (°)	Near Incidence Angle (°)	Acquisition Mode
22/01/2011	16:57	≈ (169.78–169.54)	Ascending	≈34.56	≈31.76	Stripmap
15/03/2012	16:57	" "	Ascending	≈40.40	≈31.76	Scansar

The original resolution of the images was 2.50 m for CSK images, 1.25 for TSX acquired in Stripmap mode and 8.25 for TSX acquired in ScanSAR mode. The only grey-scale band has been involved in the processing for both CSK and TSX images.

2.4 Auxiliary data

The estimation of dam displacements and reservoir water levels requires the knowledge or the acquisition of auxiliary data, as the DEM around the study area or satellite specific parameters. For this purpose different types of data have been involved.

For the dam displacements estimation *via* GNSS ancillary data was involved, mandatory for high accuracy analysis. In particular, the ocean tide loading for the corrections based on Schwiderski model (Schwiderski, 1980) were downloaded from the provider on the website (http://holt.oso.chalmers.se/loading/), the Earth's rotation parameters (EOP) relative to the ground, provided weekly by the International GNSS Service (IGS), and the ephemerides relative to the sun and the moon provided by Jet Propulsion Laboratory (JPL) have been automatically downloaded by NDA software during the data processing.

For the dam displacements estimation *via* InSAR technique the DEM was required for the preliminary geocoding of the images and the estimation of the height. The DEM has been automatically downloaded from USGS site (https://dds.cr.usgs.gov/srtm/version2_1/SRTM3/).

For the estimation of the water surface and levels *via* OBIA the contour lines have been obtained from the dam building project

(*Assessorato Regionale dell'Energia e dei Servizi di Pubblica Utilità – Dipartimento Regionale dell'Acqua e dei Rifiuti*) (1:2000) and the DTM from *"Regione Siciliana, Assessorato Territorio e Ambiente Dipartimento Urbanistica" (Elemento di proprietà della Regione siciliana ceduto in data 16/02/2018 al n. 2018-B-1977).*

Chapter 3

Methods

3.1 Dam displacements evaluation

According to Milillo et al. (2016), the evaluation of the dam displacements, using both GNSS and InSAR techniques, aims to determine the irreversible component of displacements, known in literature as structural “aging” and the periodic component, mainly due to the external loads (e.g. water levels, temperatures). The irreversible component of displacements represents the most dangerous term and generally it is described as a linear term. This is accepted in literature for concrete dams. Indeed, the behaviour of concrete dams is considered known, because of the material characteristics involved, while the deformation process of embankment dams is generally different and

depends on the type of structure and filling materials. For both concrete and earth dams the deformations are distinguished into permanent and long term deformations (Scaioni et al., 2018) the most representative displacements are generally detected during the first period of activity, in particular during the construction and the first filling of the reservoir. The other deformations over time are mainly caused by external loads (e.g. hydrological, thermal) or unexpected causes (as earthquakes).

In this work, only the planimetric components of displacements has been evaluated using GNSS. The vertical component has not been analysed because the vertical accuracy, by using GNSS receivers, is worse than the planimetric one. As a consequence, the displacements time series is more scattered and also the precision of GNSS is one order of magnitude less than traditional geodetic techniques (e.g. spirit levelling). This was also experimented by several authors in the past. One of these studies highlighted the capability of GNSS networks to detect horizontal displacements, according to the precision of optical measurements, while the precision for the detection of the vertical component is not comparable with that of precise levelling (Liu, 2010).

The technique used for the displacements time series estimation *via* GNSS is innovative because it involves the use of a CORS far away from the monitored site as master reference station. Indeed, usually, the master reference station is located close to the monitored site in a stable area (Tarsisius Aris, et al., 2012). Results from the GNSS analysis have been considered for the comparison with InSAR technique.

3.1.1 GNSS data processing

The processing of GNSS data has been performed using NDA Professional software, applying simplified models for the ionospheric and tropospheric corrections, which have an impact on the time series. In particular, the Saastamoinen model (Saastamoinen, 1972) has been applied for the tropospheric corrections, involving the Neill mapping function (Niell, 1996). The latter is based on the Herring model mapping function (Herring, 1992), involving another additional term, which considers that the elevation depends only on geographical parameters.

The Klobuchar model (Klobuchar, 1996) has been used for the ionospheric correction and involves the parameters of Centre for Orbit Determination in Europe (CODE) of the Astronomical Observatory of the University of Bern. Within the software, the ocean loading corrections are also implemented, based on Schwiderski's model (Schwiderski, 1980).

Originally three receivers have been located on the top of the dam, in different positions: in the middle section and on the left and right sides, but even close to the central part. An unconventional approach has been used identifying the master reference station far away from the monitored site, reducing the materialization costs and excluding any influence by the dam deformation or the reservoir emptying-filling cycle (Dardanelli et al., 2014). Indeed, in literature the time series of displacements by using DGNSS is generally monitored employing a base station close to the structure (<≈1 km) (e.g., Tarsisius Aris et al., 2012).

In this study the CORS of Agrigento (AGRI) at ~30 km, was used as base station. Because of the length of the baseline (more than 15 km) the

zenith troposphere estimation, affecting the baseline coordinates estimation, was enabled on both reference and rover stations.

The AGRI CORS has been selected after preliminary studies which involved the analysis of four different CORS located many kilometres away from the monitored site (Dardanelli et al., 2014). From this study, best results have been found using the AGRI reference station.

Double-differenced observation data coming from the wide-lane and ionospheric-free frequency combination were used. Also the errors related to the satellite orbits have been corrected using the precise ephemeris. The correction of the antenna phase centre position, changing with GNSS satellites frequency and elevation, has been set using the parameters provided by the IGS. The Least-Squares Ambiguity De-correlation Adjustment (LAMBDA) method was also used to fix the phase ambiguity (Teunissen, 1995). The integer ambiguity resolution represents the way to find a rapid GNSS solution with high accuracy.

The Wide-lane observables were used for the wide-lane ambiguity estimation; then, the ionosperic-free observables for the remaining narrow-lane ambiguity estimation.

Other parameters involved in the processing are summarized in the table below:

Table 3. 1 Main parameters involved in GNSS analysis

Rate	**30 sec**
Cut-off angle	10°
Constellations	GPS-GLONASS
Frequency of receivers	Double

The results in terms of coordinates (X, Y, Z) have been originally computed in the International GNSS Service frame, epoch 2008.0 (IGS08).

The terrestrial reference frame provides a set of coordinates of many points located on the Earth's surface, giving a world spatial reference system co-rotating with the Earth in its diurnal motion in space. Then, the coordinates have been transformed to a local plane reference system, using as the origin of the for the local system a ground point (Pi) as illustrated in Figure 3.1 (Hofmann-Wellenhof et al., 1992).

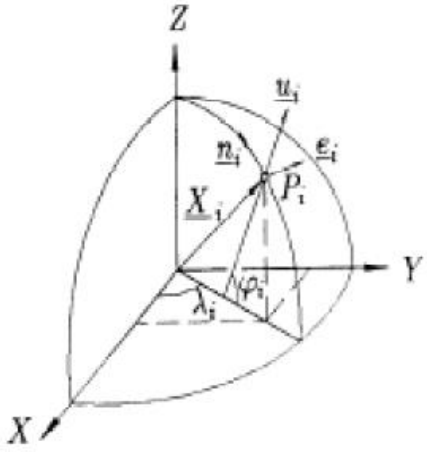

Figure 3. 1 Transformation of coordinates from the geocentric system to the local one (Hofmann-Wellenhof et al., 1992)

The coordinates of the points in this Cartesian reference system, are provided by using the roto-translation matrix and the horizontal plane tangent in the point with local coordinates (Hofmann-Wellenhof et al., 1992).

$$\begin{bmatrix} E \\ N \\ u \end{bmatrix}_P = \begin{bmatrix} -sin\lambda_0 & cos\lambda_0 & 0 \\ -sin\varphi_0 cos\lambda_0 & -sin\varphi_0 sin\lambda_0 & cos\varphi_0 \\ cos\varphi_0 cos\lambda_0 & cos\varphi_0 sin\lambda_0 & sin\varphi_0 \end{bmatrix} \begin{bmatrix} X_P - X_0 \\ Y_P - Y_0 \\ Z_P - Z_0 \end{bmatrix} \quad \text{(Eq. 3.1)}$$

Where:

- λ_0, φ_0 are the longitude and the latitude of the origin, respectively;

- the terms indicated with 0 as subscript refer to the origin coordinates;

- the terms indicated with "P" as subscript refer to the points coordinates to be determined.

Once obtained the coordinates in the local system (E, N, u), results have been statistically analysed, removing all outliers and the residual noises. Considering that the more relevant displacements are detected in the central part of the dams, because of the main stresses acting on it, a linear trend and a simple moving average (SMA) have been applied on the data time series of the receiver located in the middle section. The time span of the SMA was chosen by testing different values (~1 week, ~2 weeks, ~1 month and ~2 months). The application of SMA allows the estimation of the medium-long term displacements, when the behaviour is mainly scattered and not directly represented by simple or polynomial regression analysis. The main process to be assessed for the GNSS analysis are summarized in Figure 3.2.

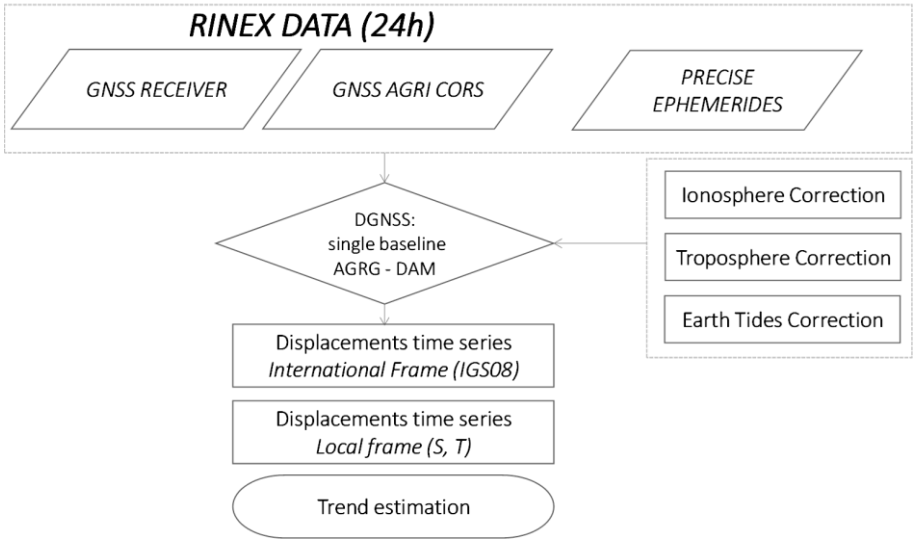

Figure 3. 2 Flowchart of the main steps involved for GNSS analysis

According to the existing models able to describe the behaviour of concrete dams (Carosio and Dupraz, 1993; De Sortis and Paoliani, 2007; Barzaghi et al., 2012), different analyses have been performed on the displacements time series of the embankment dam. The aim is the analysis of the influence, if any, of external factors in the deformation processing. The analysis started from testing four different existing models involving physical parameters, as water loads, temperature, but also sinusoidal models, already tested on concrete dams. The displacements (*d*) obtained are those on the top of the dam, along upstream-downstream direction expressed in millimetres.

The first experimental model is based on the use of water temperature and water level of the monitored reservoir. The equation of the model is the following:

$$d = a\ t + b\ \theta_{m,w} + c\ H + e \qquad \text{(Eq. 3.2)}$$

Where:

- t is the time (days);
- $\theta_{m,w}$ is the averaged water temperature;
- H is the water level (m);
- a, b, c, e are the model parameters, to be calibrated.

The second method involving physical parameters, was already tested on gravity arch dams (Carosio and Dupraz, 1993). In this case, the air temperature (θ_P) measured in correspondence of the dam was considered. The equation of the model is the following:

$$d = a\,H^3 + b\,\theta_P + c \qquad \text{(Eq. 3.3)}$$

In 2007, De Sortis and Paoliani proposed a new model for concrete dams involving the influence of hydrostatic pressure, thermal and time effects. These loads cause different effects on the dam, that can be separated into reversible (sinusoidal term) and irreversible (linear term) components. The equation of the model is:

$$d = a\,t + b + c\sin\left(\frac{2\pi t}{T}\right) + e\cos\left(\frac{2\pi t}{T}\right) + f\,H + g\,H^2 \qquad \text{(Eq. 3.4)}$$

Where:

- T is the annual period of the sinusoidal function.

The displacements over time are in millimetres and the parameters a, b, c, e, f, g are estimated using the least squares method. The last model involved for the analysis of Castello dam behaviour was implemented by Barzaghi et al. (2012), and it is based on De Sortis and Paoliani model. The difference consists in removing the contribute of the water level, not really relevant in the case studied by the authors, and considering a generic period in the equation different from one year, to be properly estimated. The equation of the model proposed by the authors is:

$$d = a\,t + b + \sum_{k=1}^{n} A_k\cos\left(\frac{k\pi t}{T}\right) + \sum_{k=1}^{n} B_k\sin\left(\frac{k\pi t}{T}\right) \qquad \text{(Eq. 3.5)}$$

The equation was then modified for the dam analysed by the authors, considering the frequency of the structure itself estimated *via* Fast Fourier Transform (FFT) method:

$$d = a\,t + b + A\cos\left(\frac{2\pi t}{T}\right) + B\sin\left(\frac{2\pi t}{T}\right) + C\cos\left(\frac{4\pi t}{T}\right) + D\sin\left(\frac{4\pi t}{T}\right) \quad \text{(Eq. 3.6)}$$

The proposed methods, based on different factors (time, water loads, temperature) applied on concrete dams have been tested on the embankment dam to better understand the deformation process of the structure. Indeed, as discussed in the previous paragraphs, there are no existing models describing the earth dam behaviour, since every structure is different from the other.

3.1.2 InSAR data processing

The InSAR technique has been tested on Sentinel-1A images acquired in both ascending and descending orbits for the evaluation of Castello dam displacements. The images acquired since October 2014 are characterized by temporal acquisition of 12 days, but in this study only one year of data have been analysed covering the emptying and filling periods of the reservoir. The analysis has been performed with SARProZ software and required only the acquisition of the images in SLC format. The analysis refers to the embankment dam and the surrounding area and aims to determine the planimetric displacements of the dam to be

compared with previous GNSS results. Different strategies have been evaluated for the case study, mainly located in a vegetated area.

The techniques are based on the traditional PS technique introduced by Ferretti et al. (2001), but aims to introduce many innovations to find the best suitable strategies for extra-urban areas monitoring. Indeed, the PS-InSAR technique is a powerful tool to monitor and provide the deformation over time of structures and infrastructures, that are generally located in urban areas (Bakon et al., 2016). The technique is based on the detection of natural targets characterized by high reflectivity over time, not affected by temporal or spatial decorrelation; these are easily identified over buildings, bridges, dams. In vegetated areas the detection of natural targets become more difficult. To enlarge the number of PS on the study areas, mainly vegetated, different approaches need to be involved, e.g. based on the multi connections between the images of the dataset.

The aim of the work is the detection of horizontal displacements (both reversible and irreversible components) to be compared with previous findings from GNSS analysis. In this study both linear and non-linear components of displacements have been reached. The linear component is generally considered the non-reversible part of the displacements, strongly connected to the stability of the structure (Milillo et al., 2016); the non-linear displacements (generally characterized by sinusoidal behavior), are mainly generated by external seasonal loads (e.g., the thermal dilation and the hydrostatic pressure). The software

allows the estimation of both displacements components, performing two different strategies.

The linear trend estimation is the standard procedure for the deformations evaluation, generally adopted with the traditional InSAR technique. The non-linear displacements are estimated using an innovative approach based on a non-parametric model. Both components have been evaluated using two Multi-Baseline Construction methods. The first is the star graph, generally used for PS-InSAR technique, based on single baselines connecting one image taken as reference (master) and the others (slaves); the second is the full graph, involving all available connections between the images (n), using the spatial coherence as weight.

Preliminary the dataset was co-registered to the master image, centrally located in the normal and temporal baseline span. The process allows aligning a pair of SAR images (S-1A in this case), so the same area can be detected by corresponding pixels within the two scenes.

In the first case (n-1) connections are available, excluding the connection master-master (Lanari et al., 2004), while, the full graph involves (n!/2(n-2)!) connections, representing all available connections between the images. Another graph connection has been preliminary tested on few images, called Minimum Spanning Tree (MST) (Perissin et al., 2007). The latter maximizes the average coherence to obtain the best interferograms, and achieve smaller temporal baselines.

After the co-registration, the reflectivity map, defined as the temporal average of the available dataset, and the amplitude stability

index (ASI) were calculated. The aim of the averaging processing is suppressing the noise, enhancing all targets which kept stable reflectivity over time. Also, statistics were recorded, as the temporal standard deviation and the ratio of the mean and the standard deviation matrix (https://www.sarproz.com/software-manual/).

Then, a preliminary geocoding of the dataset need to be assessed, thus the globally available DEM from the Shuttle Radar Topography Mission (SRTM) automatically downloaded from the software was used and a Ground Control Point (GCP) was selected (Perissin, 2009-2017). Indeed, although several authors analysed the influence of external DEM on PS-InSAR and SBAS processing (Bayer et al., 2017), many authors (*e.g.* Ferretti et al. 2001) agree that the processing steps involved for the InSAR technique allow correcting the phase caused by the DEM error. Also, according to Du et al., (2017), it was found that the influences of external DEMs on the evaluated mean deformation rate are not relevant, the standard deviations difference found for the Sentinel images (C-band) is 0.30 mm/year.

The interferograms formation was mandatory for Multi-Baseline Construction (MBC) methods. It represents the final product of the existing correlation between the corresponding pixels within the two images (master-slave). If a correlation exists, the interferometric phase is able to detect the changing distance between two recorded signals from the sensor to the targets with sub-millimetre precision.

A Goldstein model filter has been applied and the phase were unwrapped using the sparse least square method. The interferograms are processed after choosing the graph connection between the images and

represent complex images with contents related to the phase and the amplitude. The first, called interferometric phase, is calculated as difference between two images (e.g., master-slave in case of the star graph), the second represents the calculated coherence.

The spatial coherence map is another product, representing the average coherence of the set of the interferograms previously generated. Then, the coherence of all available interferograms has been estimated, to generate the minimum best set of interferograms maximizing the average coherence, used for the MST graph.

The Atmosphere Phase Screen (APS) has been estimated using the inverted residuals approach, using as input the reflectivity map as parameter for the sparse points selection. The threshold for the parameter was set to 1.8 and the choice of reflectivity map as input parameter allowed selecting PS candidate on the left bank and the dam itself, excluding sparse points falling in the reservoir characterized by values of normalized average amplitude less than the fixed threshold. The atmospheric delay need to be correctly estimated and minimized to assess a higher accuracy. Indeed, the water vapour is the main cause of radar signals delay. Many instruments are able to provide water vapour maps and reducing the effects of atmospheric delays in InSAR processing (e.g. GPS, spectrometers) and also several models and studies have been involved in the atmospheric delay correction (Li et al., 2006). The Inverted residual approach was used instead the Inverted parameter approach, also available in SARProZ, because the latter forces the solution even though it returns higher values of coherence. Also external

services, as the Generic Atmospheric Correction Online Service for InSAR – GACOS (http://cegresearch.ncl.ac.uk/v2/gacos/) are available online, but currently they are not supported in SARProZ, although an import of external APS delay maps could be implemented in the open source code of the software. The sparse points involved for the APS analysis have been connected using the Delaunay graph, making the relative observations and the model (Kampes, 2006).

For the evaluation of the displacements time series, from the interferometric phase analysis, two different strategies have been used involving both the linear and non-linear components of dam displacements, determined by using both the star and the full connections graphs between the available images.

In particular, the PS-InSAR technique has been involved for the estimation of the linear trend of displacements of selected PS. The non-linear displacements have been obtained using a non-parametric model implemented in the software. Both analysis have been performed for both the estimation of the APS and the multi-image sparse points (MISP). Using the star graph, no weights have been used but the external DEM has been removed. Also the preliminary generation of interferograms is not necessary using the single-baseline connections. On the contrary, using the multi-master approach, the coherence has been used as weight for the phase processing. Then, the two different approaches have been established for both linear and-linear displacements determination during the APS estimation and MISP processing for the whole dataset. The preliminary test based on few images and different connection graphs

(Star, MST and Full) has been performed only for the linear trend estimation, using the ASI as parameter for the sparse points selection, with a fixed threshold (0.8). The use of the three connection graphs has been used to preliminary test the accuracy of InSAR results using few images over the dam itself and extra-urban areas. In this case, with only 7 images, the results obtained with the star graph look in agreement with GNSS measurements than other multi baseline construction methods involved (Pipitone et al., 2018). Indeed, despite the technique is very suitable for the detection of displacements over urban areas (Dixon et al., 2006; Ng et al., 2012) with lots of natural PS, other studies involved different InSAR strategies, *e.g.* full graph connections (Vaka et al. 2017), to increase the number of suitable points for the analyses also in extra-urban areas (Perissin et al., 2007; Hooper et al., 2007).

Using the whole dataset over one year (20 images), the length of the temporal filter of the non-parametric model has been set equal to 3. The analysis was also performed after the processing of the connections using the Delaunay graph, with the determination of a reference point to be selected with high temporal coherence. The interferometric phase of all points will be referred to the reference point chosen in a stable area and the estimation will be relative to it.

In this work the objective is the determination of the horizontal components of displacements to be compared with GNSS analysis. Thus, the height estimation and the vertical components will not be discussed.

Also, using the whole dataset, the displacements have been evaluated as the average of selected PS displacements close to the dam crest, directed along the LOS of the sensor. The main steps of the methods

involved in the InSAR analysis have been summarized below (Figure 3.3).

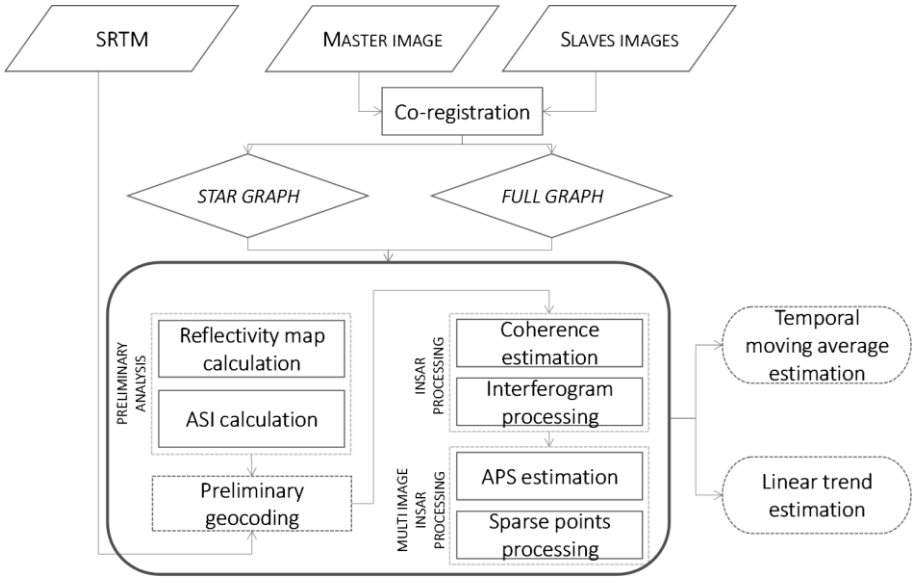

Figure 3. 3 Flowchart of the main steps involved for InSAR analyis

3.2 Reservoir water surface and level detection

Water levels are considered one of the main causes involved in the deformation process of dams. Generally, traditional hydraulic instruments are installed close to the dam and the values of the parameters are manually recorded by the dam operators. In this work, we are looking for a complete monitoring system from satellite. Thus, the water levels have been investigated using different satellite techniques involving several strategies.

The techniques involved for the estimation were based on the radiometric classification, a visual comparison between the satellite imagery and the existing contour lines, and OBIA. The first is considered a standard procedure for water surface mapping and in this case study is based on the application of unsupervised classification. The visual matching is an innovative technique, based on the visual interpretation of the reservoir shoreline, according to the shape of the artificial lake and the existing contour lines. The OBIA techniques include two different analysis, based on the comparison between classified images and reference objects, according to their geometric characteristics. The reference objects are the contour lines extracted from the LIDAR DEM. The strategies used for the analysis are described in the following paragraphs.

The dataset was acquired since GNSS monitoring period (2011) and it made up of different optical and SAR images with different geometric and spectral resolutions. Preliminary, to assess the suitable resolution of optical images for water levels evaluation, evaluating the loss of accuracy at different resolutions, three different high resolution images have been selected from Google Earth at their maximum resolution, involving three different reservoir extents. Pixels of high spatial resolution images have been aggregated at different geometric resolutions (R_G) to evaluate the loss accuracy, using lower resolutions, obtained from multiples of the original one. The loss of accuracy (%) has been quantified as:

$$\Delta S = \frac{(S - S_i)}{S_i}\ 100\ (\%) \qquad \text{(Eq. 3.7)}$$

Once verified the suitable resolutions for the analysis, different techniques for the reservoir water levels estimation have been assessed for both optical and SAR images.

The first two analysed methods were based on the visual matching between the highest resolution images and the contour lines from the dam project, and on the radiometric classification and post-classification processing (Figure 3.4) The software involved for the analysis were ERDAS Imagine and Research Systems, Inc. (RSI) ENVI 4.3.

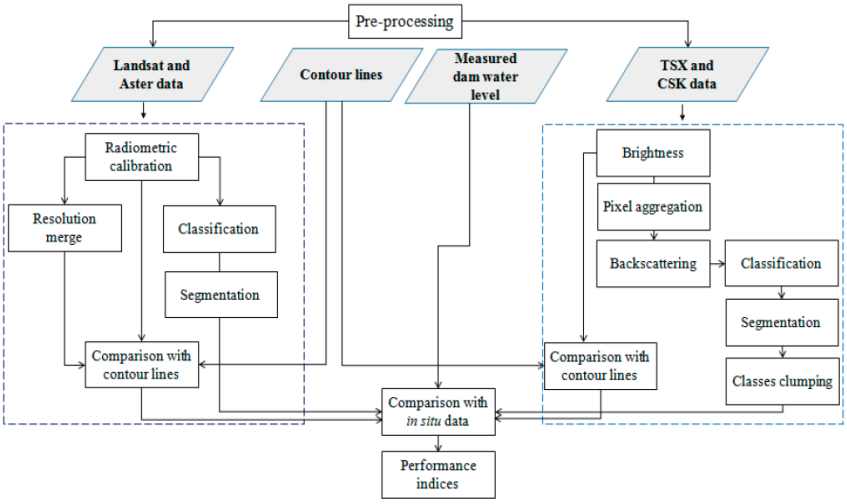

Figure 3. 4 Flowchart of the classification and visual matching techniques applied on both optical and SAR dataset (Pipitone et al., 2018, Remote Sensing)

The other two techniques involved in the water surface and level estimation are based on different algorithms implemented within Quantum GIS software (v. 2.18.7).

3.2.1 Visual matching

Visual matching is a technique based on the interpretation of the closest contour lines to the reservoir shoreline. The images are characterized by different geometric and spectral resolutions, thus the identification of the highest resolutions and the best suitable combination of bands need to be correctly identified for the discrimination between land and water pixels within the scene.

The interpretation of the reservoir edge became difficult over mixed pixels and depends also on the different slopes on the left and right banks. Therefore, the two slopes have been considered in the estimation, assuming the water levels inversely proportional to the slopes. Preliminary, the accuracy of the technique has been tested evaluating the range of variability of the estimations (ΔH), based on different geometric resolutions of the available images and the different bank slopes. The final estimate of the water level (H_e) using the visual matching technique will consider the weighted average between the water levels estimates for the two banks obtained from the comparison with the contour lines, within a Geographic Information System (GIS) software (Quantum GIS v. 2.18.7). The water levels estimated by visual matching will be compared to those in situ measured (H_m).

Optical data processing

The optical images used for the analysis were LS5, LS7, LS8 and ASTER. The images were preliminary calibrated in spectral radiance

(Thome et al., 1997), using the Markham and Barker equation (1986) and then in reflectance (Epema, 1990).

LS7 and LS8 images are characterized by MS, TIR and PAN bands. The latter has a higher spatial resolution than multispectral. Thus, the MS and the PAN bands were combined applying the Resolution Merge (RM) based on the Principal Component (PC) analysis (Welch and Ehlers, 1987). The final product, indeed, preserve the highest spectral content of MS bands and the highest spatial resolution of the PAN band (15 m). The PC method allows increasing the spatial information of the reservoir shoreline, preserving the radiometric content, with low distortions.

LS5 and ASTER images are characterized by 30-60 m and 15 m resolutions, respectively. The bands used for the identification of the water bound are the most suitable for the analysis. In particular, ASTER images the available bands were used (VNIR), for LS5, LS7 and LS8 the SWIR and NIR bands have been selected.

SAR data processing

For the visual interpretation of the reservoir bounds, using SAR data, TSX and CSK imagery have been used with their original highest spatial resolution and only grey-scale band.

The determination of water levels, also in this case, was based on the identification of the closest contour line to the boundary of the reservoir. The high resolutions of the images (1.25 m for CSK and 2.5 and 8.25 m for TSX, Stripmap and ScanSAR, respectively) allows better recognition of the shape of reservoir. Anyway, the analysis considered also in this case the different contributes from the two bank slopes.

3.2.2 Classification

The other technique, based on the radiometric content allows determining the water surface extent using an automatised algorithm based on the unsupervised classification. The algorithm involved in this study is the k-means, based on an iterative clustering algorithm. The processing requires the knowledge of some parameters, as the number of classes, change threshold and the fixed number of iterations. In this study the number of classes is three (water, bare and vegetated soils), the threshold was fixed at 1% with maximum number of iterations set to 100. The clustering of pixels, to be associated to one of the three classes, iteratively continues until the maximum number of iterations is reached or the threshold overcame. Also the selection of an appropriate area of study is required to achieve best results from the application of the method. In particular, after preliminary analysis of the images during the emptying and filling periods, the area strictly including the reservoir at its maximum water level has been selected.

Then, to improve the results from the unsupervised classification, the segmentation of the classes has been applied on the whole dataset (optical and SAR). This technique, implemented in ERDAS Imagine, transforms the resulting image from classification into regions belonging to the same class. The application of the method requires the minimum number of pixels to be selected for the identification of a region (segment) and the neighbouring pixels to be used for the connectivity of segments. In this case study, 1000 are the population selected for the

segmentation and 4 are the neighbouring pixels, except for two CSK images for which the number of pixels has been set equal to 8.
The results of this process are the water surface extent estimation. Then, using the evaluated specific relationship between Area-Volume and Level for the monitored site the water levels are determined. Finally, the estimated water levels are compared with those measured *in situ* (H_m).

Optical data processing

The k-means algorithm has been applied on VNIR bands for ASTER images and SWIR bands for Landsat images, except for LS7. Indeed, the LS7 images are characterized by missing scan lines, with no data information within the scenes, due to the failure of Scan Line Corrector (SLC). The width of the missing scan lines changes within the scene, becoming maximum along the edge of the acquisition and minimum in the centre. The use of LS7 images allows increasing the dataset with a larger time span of acquisition, during the period 2011-2013. The filling of the missing scan lines is mandatory for the application of the classification method and identification of the reservoir extent.

For this purpose, the “replace bad values” method implemented within ENVI software was applied. The method is based on the use of the Delaunay triangulation connecting surrounding pixel values. After filling, the unsupervised classification was also applied to SWIR bands of LS7 images.

SAR data processing

The SAR images used for the analysis were TSX and CSK involved in both classification and visual matching methods and S-1A images acquired in Single Look Complex (SLC) format involved in OBIA methods and for the displacements estimation *via* interferometry. All images were preliminary radiometric calibrated. In particular for TSX and CSK the standard procedures from Airbus and Defence Space (https://spacedata.copernicus.eu/documents/12833/14537/TerraSAR-X_RadiometricCalculations) and E-Geos (http://www.e-geos.it/products/pdf/COSMO-SkyMed-Image_Calibration.pdf) have been adopted, based on the brightness and backscattering evaluation, using the ERDAS software. Pixels were aggregated using multiple of the original resolution between the two separate steps (brightness and backscattering determination). Indeed, using the pixel resampling, the speckle noise, characterizing the SAR images is reduced. The output consider different contributes of averaged pixels, considering the area involved.

Classification for SAR data

The SAR images used for the classification were preliminary aggregated at lower spatial resolution to reduce the effect of speckle noise within the scene, producing the reduction of the performances.

Many problems occurred for SAR images, due to the high resolution of the images in the processing, caused by residual speckle within the scene, and the surface roughness over water surfaces. By using the pixel

aggregation most of the images were performed for the analysis, reducing the effects of the speckle in the scenes. The aggregation allows the computation of the average of all pixel values able to determine the output pixel. Using a multiple of the original geometric resolution, the resulting pixel after aggregation will correspond with the straight average. Indeed, according to Capodici et al., (2017), the simple spatial averaging technique was considered more suitable for the analysis, despite several filters are proposed in literature.

The original spatial resolution of the SAR images was 2.50 m for CSK, 1.25 m for TSX Stripmap and 8.25 m for TSX ScanSAR images. Preliminary the influence of loss of spatial resolution on the accuracy for the water surface estimation has been evaluated and the more suitable pixel size was 5.00 m for both TSX Stripmap and CSK data. The TSX ScanSAR image has been considered with its original resolution (8.25 m) close to the best aggregation value. However, from the analysis, residual speckle reduced the classification performance and also, a relation between the surface roughness and the wind direction and speed has been found for CSK images. The roughness produced an underestimation of the water surface extent. Indeed, due to the wind action on the reservoir the water surface seems brighter than usually, in normal conditions. The phenomenon is probably caused by the waves generation over the reservoir after the wind action. Indeed, even small, the waves modify the signal transmitted by the sensor and returned from the water surface. The wind directions and speeds occurred in the two hours antecedent the acquisitions of SAR images, recorded by the station located 2 km far away from the monitored site, in the north direction, have been analysed

for all CSK and TSX images. Two images characterized by brighter water surface and surface roughness were also characterized by high wind speed (> 1.5 m s^{-1}) and wind direction along the look direction. The post-classification techniques allowed improving the recognition of the surface extent, reducing the loss of accuracy due to these factors.

Indeed, the class clumping technique, applied after the segmentation has been used to add spatial coherence to the results, characterized by holes or residual speckle within the area. The kernel has a specific size of 3 x 3.

3.2.3 OBIA

Optical and SAR data processing

The analysis based on the geometric comparison between the processed images and the reference objects has been performed on an ideal case, on optical images (influenced by shadows, clouds, roughness within the scene or clear images) and SAR images. The S-1A images have been preliminary radiometric calibrated using SNAP software.

The processing allows determining the calibrated images to be used for the water level estimation, using the following steps:

TOPSAR split: the sub-swaths of the S-1A images can be selected, including the polarization (VV in this case study). In particular, the images including the study area, are acquired in both ascending and descending orbits. In the first case, the reservoir is in the sub-swath IW2,

while in descending orbits the reservoir is detected in IW1 or IW3, depending on the acquisition dates;

- Application of precise orbits;
- radiometric calibration: the backscattering is in decibel;
- TOPSAR deburst;
- Multi-looking application with Range 4 and Azimuth 1;
- Terrain Correction using the more high quality product for automatic downloaded DEM (SRTM 1sec HGT).

These steps are mandatory for the analysis of water surface and level by using S-1A images.

Once converted the dataset into reflectance for optical images and backscattering for SAR images, the OBIA methods have been performed on the whole dataset using the same strategies. In particular, two different methods have been analysed, both implemented within QGIS, (v.2.18.7). The first technique uses the Shape (S), Theme (T), Edge (E), Position (P) (STEP) similarity metrics, by using a plugin implemented within the software (Lizarazo, 2014); the other is an independent GIS technique based on the evaluation of the distances between the classified images and the reference objects. These techniques have been tested on different images to overcome the limits of the classification techniques. Indeed, many disadvantages occur when images are partly characterized by shadows, clouds, surface roughness or missing scan lines (LS7 ETM+ SLC-Off images). The aim is finding the best strategy to detect the water surface extent by using the comparison between “objects” or polygons characterized by different geometries. The reference objects are

identified with the contour lines extracted from the original Digital Terrain Model (DTM), in both analyses.

The analysis of OBIA techniques has been performed on an ideal case, using as classified image and reference the same objects (the contour lines), on optical images characterized by shadows, clouds and clear sky, and, finally, on S-1A SAR images.

STEP algorithms

In particular, the similarity metrics involved in the STEP algorithms are discussed and summarized below (Lizarazo, 2014). The indices range between 0 and 1. The maximum value corresponds to the perfect match between the classified and the reference objects.

The S index involves the perimeters of the objects, through the evaluation of a Normalized Perimeter Index (NPI) for both classified (c) and reference (r) images:

$$S = \left(\frac{NPI_c}{NPI_r}\right)^k \quad \text{(Eq. 3.8)}$$

k is a power exponent that can be 1 or -1 depending on the ratio value. It is negative when the ratio is positive, positive otherwise.

The T index involves the area (A) of the compared objects, evaluating a point set intersection (int) with the classified objects:

$$T = \frac{A_{int}}{A_r} \quad \text{(Eq. 3.9)}$$

The E metric determines the matching between the classified and reference objects boundaries, involving the length (l) of the boundary of the point set intersection with the classified images and the perimeter (p) of the reference objects:

$$E = \left(\frac{l_{int}}{p_r}\right)^k \quad \text{(Eq. 3.10)}$$

This specific index, considers also a buffer zone of the boundary, assuming a variable distance (ε) which corresponds to the maximum error. In our case study ε was ranging between 0 and half of the geometric resolution.

The last index, P, involves the distances (d) between the centroids (cent) of classified and reference objects trough the Euclidian distance calculation and the diameter of a circle. It is assumed that the area of the latter object corresponds to the sum of both classified and reference objects:

$$P = 1 - \frac{d_{cent}}{d_{cac}} \quad \text{(Eq. 3.11)}$$

As discussed below, the classified images need to be processed before applying the OBIA techniques. The discussion of the classification processing is discussed in paragraph 3.2.2, for both SAR and optical images. Preliminary, the available contour lines extracted

from DTM have been used, ranging between 292 m and 300 m, with intervals of 1 m.

Distance method

For the application of the distance method, some independent plugins implemented within Quantum GIS software have been used. In particular, the reference objects (polygons) have been preliminary converted into a raster layer of distances selecting as raster cells size the DEM resolution (2 m) obtained from the DTM, by using the *r.grow.distance* tool. Then, the classified images were converted into vectorial files and the nodes information were extracted from the latter using the *point sampling* plugin. The tool preserves the sampling points and the attributes of the reference objects (distance cells). To evaluate the accuracy of this techniques, some statistics have been performed (as the mean, 5^{th} (P_{005}) and 95^{th} (P_{095}) percentiles).

Chapter 4

Results and Discussion

4.1 Dam displacements evaluation

4.1.1 GNSS data processing

The displacements time series of three receivers located on the top of the dam have been analysed over approximately 2 years (April 2011-May 2013). The coordinates of the receivers location (X, Y, Z) have been obtained using the static survey from the CORS of Agrigento, far away from the monitored site, and obtained in the ITRF system (epoch 2008). The time series was not continuously monitored and many gaps occurred because of no-data acquisition or post-processing failures. A continuous time series without gaps covers an overall period of ~1 year.

The time series are reported in Figures 4.1, 4.2 and 4.3, the time is expressed in Modified Julian Day (MJD).

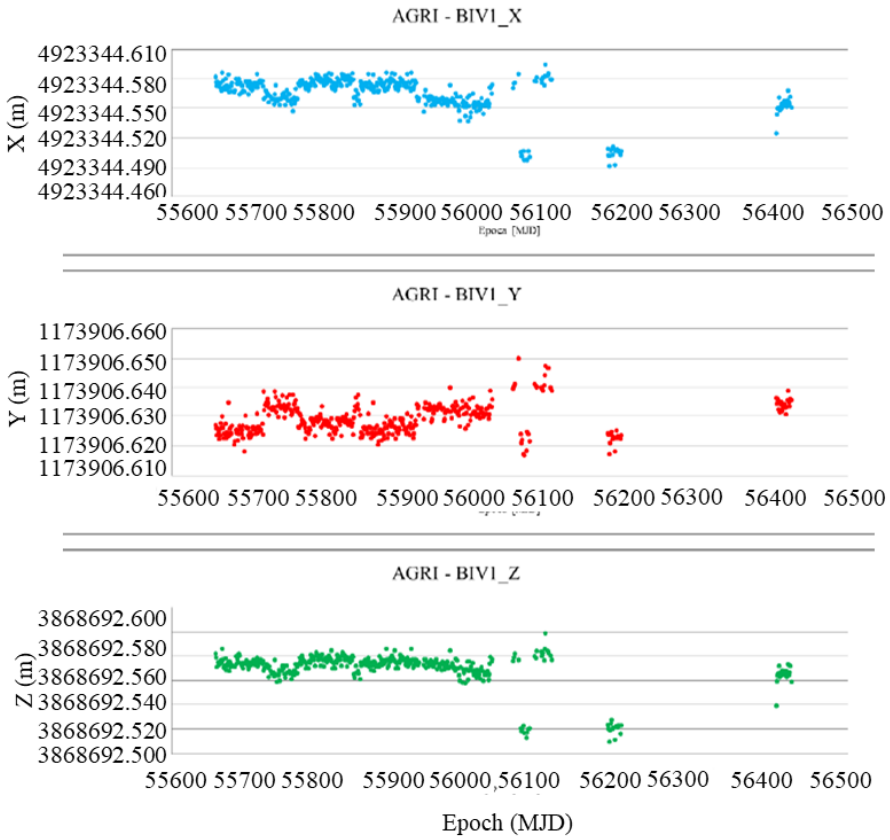

Figure 4. 1 Coordinates time series of the receiver located on the right hydraulic side (X, Y, Z; from top to the bottom)in the geocentric system.

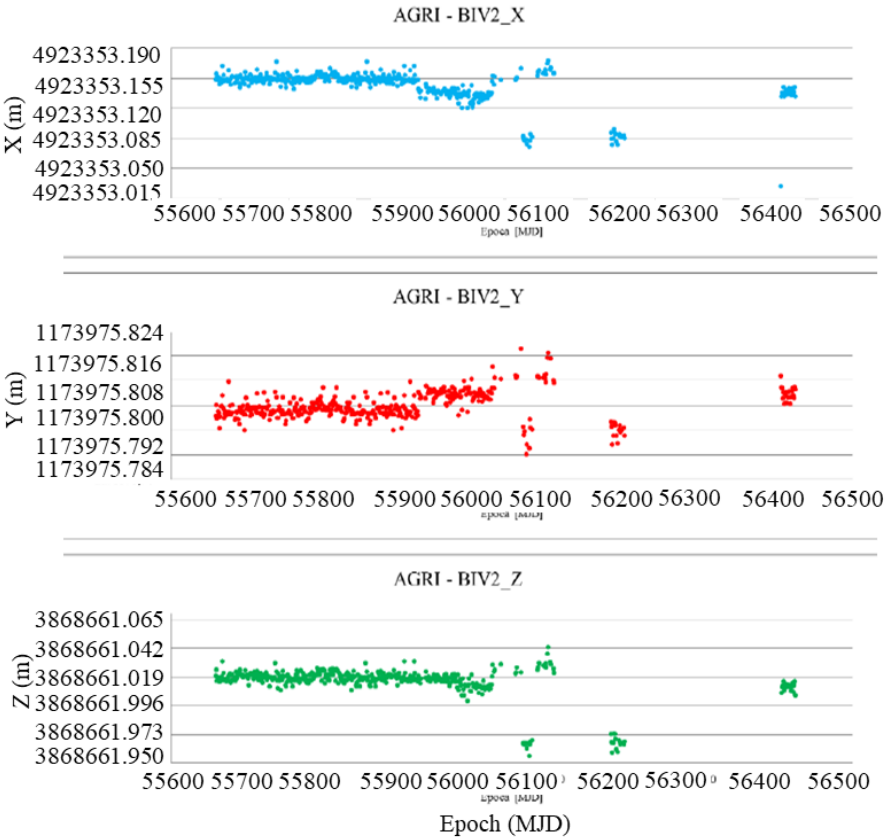

Figure 4. 2 Coordinates time series of the receiver located in the mid-section (X, Y, Z, from top to the bottom)in the geocentric system.

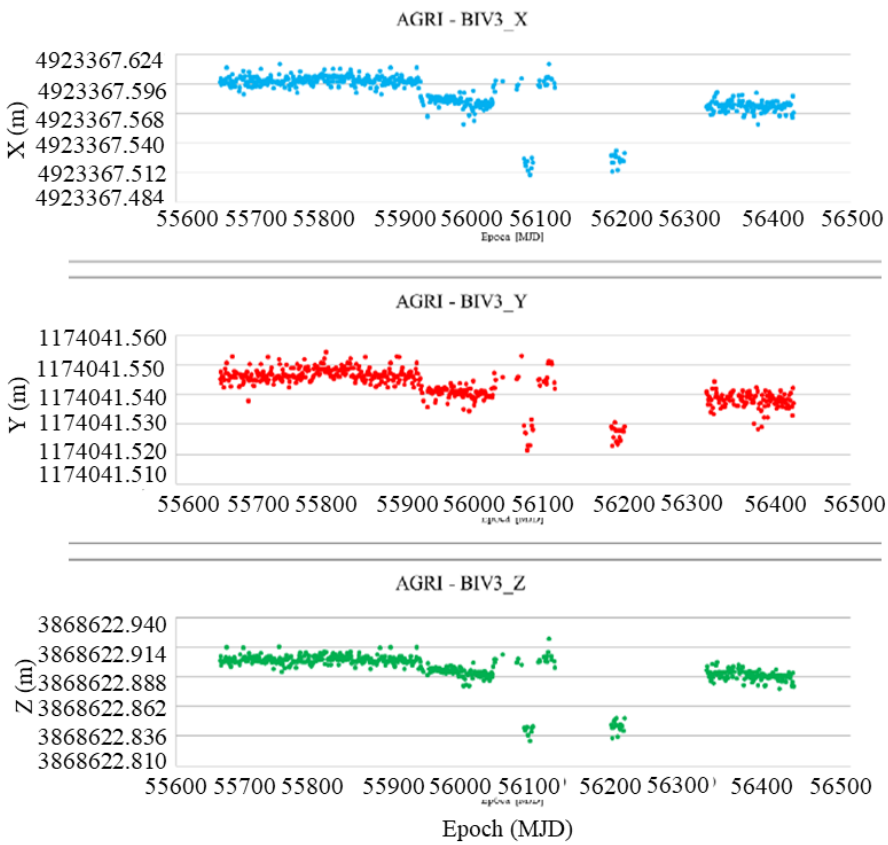

Figure 4. 3 Coordinates time series of the receiver located on the left hydraulic side (X, Y, Z, from top to the bottom)in the geocentric system).

The coordinates of the receivers were then converted into a local system and the displacements have been evaluated. Only the planimetric components have been evaluated because the horizontal accuracy is the most suitable for dam displacements monitoring. Indeed, the achieved planimetric accuracy was better than the vertical one and the precision of the latter is one order of magnitude less than other geodetic techniques, traditionally involved for monitoring, as spirit levelling.

The planimetric components of displacements were obtained along the upstream-downstream and tangential directions. Then, the results along the upstream-downstream direction, have been processed using different temporal moving average, with different size window. Best results have been obtained using a moving averaging period of approximately two months, successively compared with results obtained by using different models, involving physical parameters, as hydraulic loads and temperature, and time effects. The comparison aims to determine the influence of environmental causes on the dam displacements and highlight the trend of the latter (Figure 4.4).

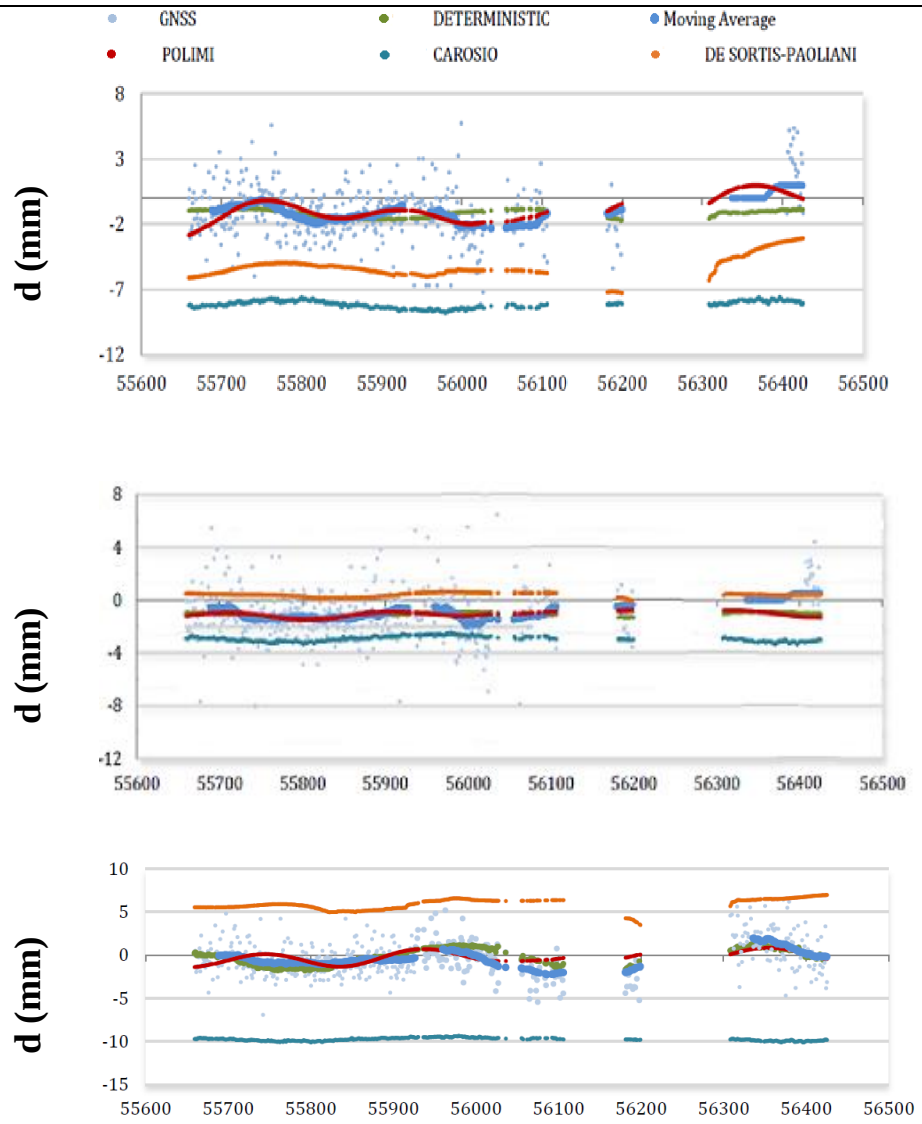

Figure 4. 4 Comparison between displacements (d) obtained via GNSS and existing models, referred to: the receiver located on the right hydraulic side (on the top), on the central section (in the middle) and on the left hydraulic site (on the bottom).(Dardanelli and Pipitone, 2017, Periodica Polytechnica)

From results the best fitting models for the three sections are the deterministic model and the sinusoidal one (called Polimi in Figure 4.4) by Barzaghi et al. (2012). Obviously the results need to be analysed in the first period where no gaps occurred (~1 year). For all sections the other two models, by Carosio and Dupraz, (1993) and De Sortis and Paoliani, (2007) are not able to describe the behaviour of the dam, this is more relevant for the displacements time series of the two receivers located on the left and right banks. For the receiver located in the central section of the dam, the time series showed a good convergence of results between the other two models and the moving average displacements, with an average difference of 0.2 mm between those. These preliminary results were encouraging because they showed that a relation between physical parameters and dam displacements exists, but also the long term trend of displacements emphasize a sinusoidal behaviour of displacements, generally related to oscillating forces, as water levels and temperature. Of course, the embankment dam's behaviour is more difficult to be interpret than concrete structures, because of the composing material involving during the emptying and filling periods. Anyway, significant relations and a sinusoidal trend for the displacements time series were highlighted during the analysis of these preliminary results.

According to these, only the central section has been analysed in future studies for monitoring dam displacements along the orthogonal section to the dam itself. Indeed, also several studies, showed that for both the concrete and earth dams, the most relevant horizontal component of displacements occurred in the mid-section, orthogonal to

the dam (Behr et al., 1998, Tasci, 2008, Yigit et al., 2016, Kalkan, 2014, Yavasoglu et al., 2018, Radhakrishnan, 2014).

The orthogonal component of displacement of the central section has been evaluated only during the first period, without gaps occurring in the time series, due to missing data acquisition or failure of data processing. The period analysed was approximately 1 year (April 2011 – March 2012), covering the whole emptying and filling phases of the hydrological cycle. Both linear and non-linear components of displacements have been investigated during the monitoring period. From the analysis of the ~2 months moving average during the monitored period, the variability of displacements ranged between ± 2 mm (vertical orange bars in Figure 4.5) and a non-linear behaviour emerged. The linear trend of GNSS data highlighted an estimated velocity of approximately -1 mm y^{-1}.

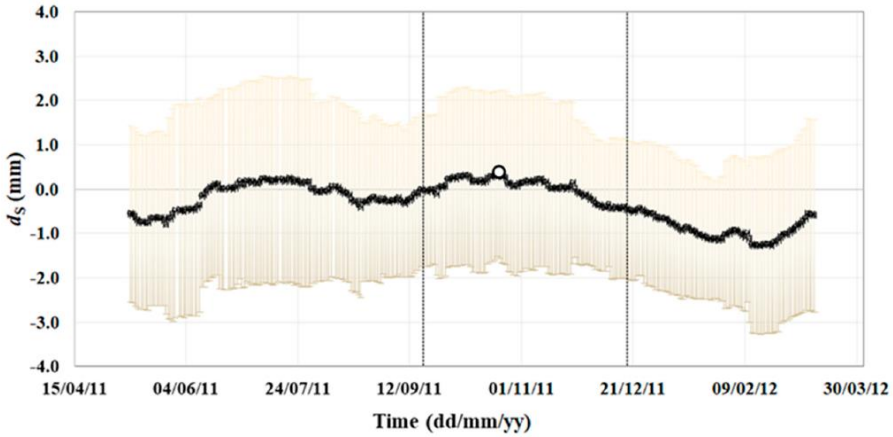

Figure 4. 5 Temporal moving average with 2 months window of GNSS displacements along the orthogonal section in the middle section of the dam over approximately one year. The two black vertical lines separate the different emptying

period, stationary minimum water level and filling period during the monitoring. (Pipitone et al., 2018, Remote Sensing)

Three different periods are considered during the monitoring process, represented in Figure 4.5: the first is the emptying phase of the reservoir, until 17 September 2011, then a period with stationary minimum water level was following and finally, the filling phase of the reservoir, starting from 17 December 2011. From the analysis of the moving average, two maximum and a minimum displacements occurred in different periods. Therefore, the comparison between the moving averaged displacements and the water levels measured *in situ* has been evaluated.

Comparison between GNSS displacements and water levels

The comparison between the variables showed that a maximum displacement occurred when the minimum water level is reached and the water level is stationary (20 October 2011). But, apparently the water level by itself, is not able to describe the behaviour of the displacements time series. Indeed, another maximum displacement is recorded via GNSS during the emptying period and a minimum displacement during the filling period of the reservoir (Figure 4.6)

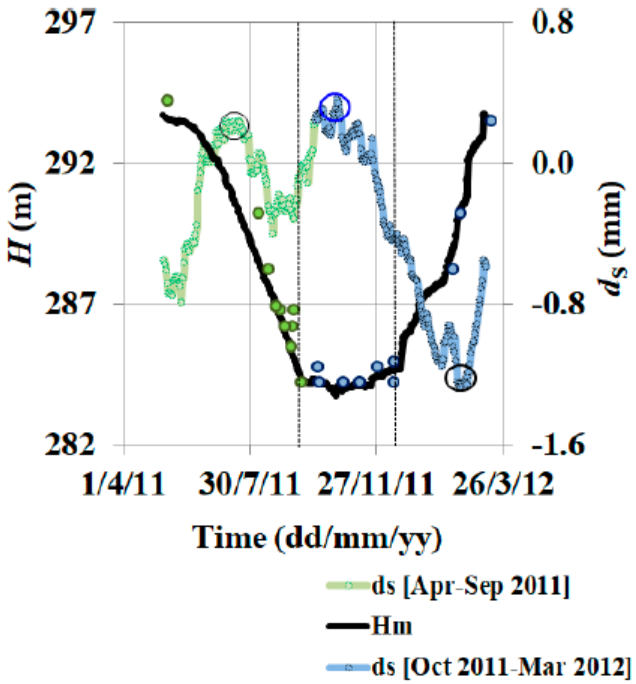

Figure 4. 6 Comparison between displacements time series during the emptying (in green) and filling (in blue) periods (on the y-secondary axis) and water levels measured in situ (in black, on the primary y-axis) (Pipitone et al., 2018, Remote Sensing).

Thus, another variable was included in the monitoring process to better understand and explain the behaviour of the structure. The parameter involved is the daily average air temperature, recorded *in situ* by the dam supervisor. The relationship between the water levels, the daily average air temperature and the dam displacements is better explained in the following figure (Figure 4.7).

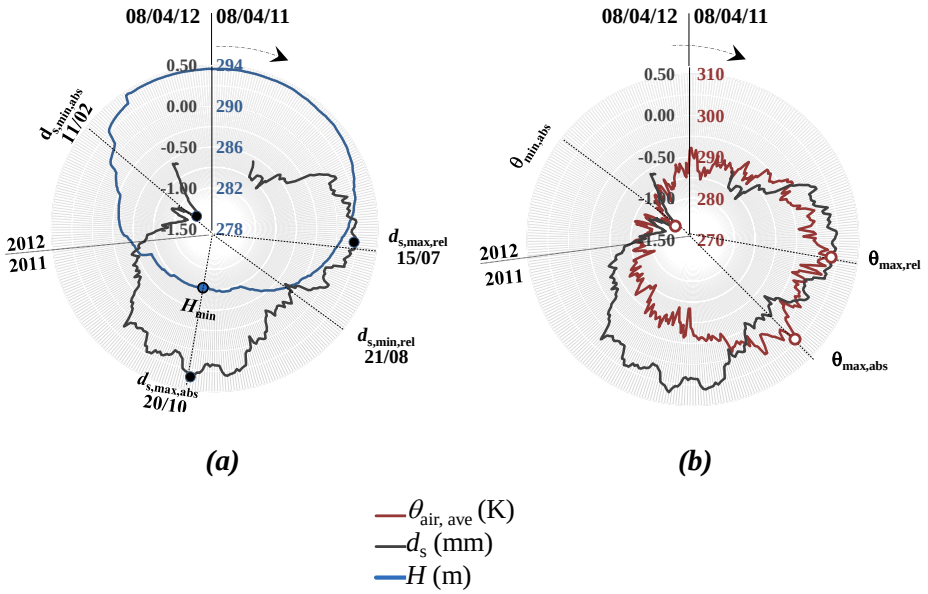

Figure 4. 7 Comparison between: (a) water levels (in blue) and dam displacements (in black), (modified from Pipitone et al., 2018, HIC 2018. 13th International Conference on Hydroinformatics), (b) daily average air temperature (in red) and dam displacements (in black).

The absolute maximum displacement is found when the water level is minimum (on the 20 October 2011), and another relative maximum displacement has been recorded on the 15 July 2011, during the emptying period, when the average daily air temperature reached its relative maximum value (30.5°). Also, two minimum displacements recorded during the emptying period (21 August 2011) and the filling period (11 February 2012) occurred when the absolute maximum and the minimum values of temperature were reached, respectively (32° for the maximum daily averaged air temperature, recorded during the emptying period, approximately close to the date of the maximum GNSS displacement

recording date and 2.5° for minimum daily averaged air temperature, during the filling period).

Figure 4.8 shows the relation between the measured water levels and the orthogonal dam displacements occurred during the emptying (green dots) and filling (blue dots) periods. The red line over imposed to the data represents the polynomial interpolating relation describing the non-linear behaviour of the body dam, probably due to the oscillating force but also the arrangement of the material composing the dam itself during the deformation process.

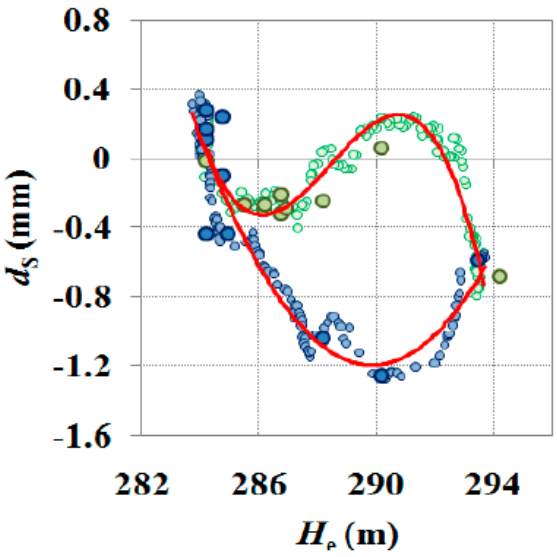

Figure 4. 8 Relation between measured water levels (x-axis) and orthogonal dam displacements (y-axis) during the emptying (green circles) and filling periods (blue circles) (Pipitone et al., 2018, Remote Sensing).

These results highlighted the existing relation between the dam displacements and external loads, as the water levels and the air and water temperatures. Also, they confirmed the previous findings obtained by using deterministic and sinusoidal models to describe the long-term behaviour of the dam. The relation between the cause-response of the dam is, of course, not easy to be determined, but, future works will investigate the deformation process as a whole, to assess the influence of the acting loads on the dam over a more larger period and involving the characteristics of the material used for the structure construction.

4.1.2 InSAR data processing

The dam displacements have been estimated also using another satellite technique, based on a multi-temporal InSAR analysis, based on the identification of PS within the images, from the spatial and temporal combination of the available dataset. The use of different strategies highlighted the capability of InSAR to detect both linear and non-linear displacements, according to GNSS analysis. Indeed, the use of MBC methods and different connections graph allows estimating the best strategy to be used for extra-urban areas monitoring. The use of different processing, involving the different graphs showed that both linear and non-linear terms of displacements can be detected by using InSAR technique. The results from InSAR analysis have been described below and a comparison with previous findings has been also evaluated.

Preliminary analysis for MBC methods

For a preliminary evaluation of MBC methods, a small spatial and temporal subset has been set. The study area involved the dam itself and the surrounding area and few images (only 7) have been used for this purpose.

The three MBC methods involving the star graph connection between the images (one master is taken as reference and all slaves are connected to it by single baselines), the full graph (connecting all available images) and the MST graph, using only the connections highly coherent from the interferograms analysis are reported in Figure 4.9.

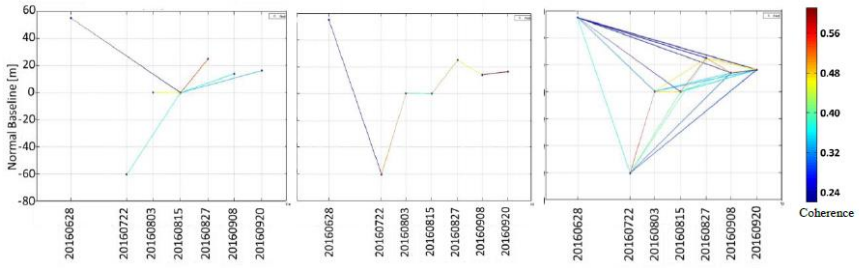

Figure 4. 9 Star, MST and full graph connections (on the left, central and right panels, respectively) after interferograms formations and full coherence estimation (Pipitone et al., 2018, Proceedings of SPIE Remote Sensing Conference).

The MST graph shows n connections, involving smaller temporal baselines than star graph connections. Indeed, the connections are between subsequent images acquired with a time span of 12 days, except for the first image, acquired 24 days before next one. The full graph shows all available connections between pairs of images (22 in this case)

and also in this case, the most coherent are those with smaller temporal baselines.

The reflectivity map represents the first result after the co-registration process between a master image, taken as reference (15 August 2016 in this case study) and all available images. The map shows the normalized average amplitude of multi-images analysis. In particular, in this case, the map shows medium-high values of average amplitude over the dam (main structure) and the hydraulic left side bank. Because the area is mainly vegetated, the represented values of amplitude are not homogenously distributed along the scene. The values representing the water reservoir are very low and the surface looks darker than the surrounding area (Figure 4.10).

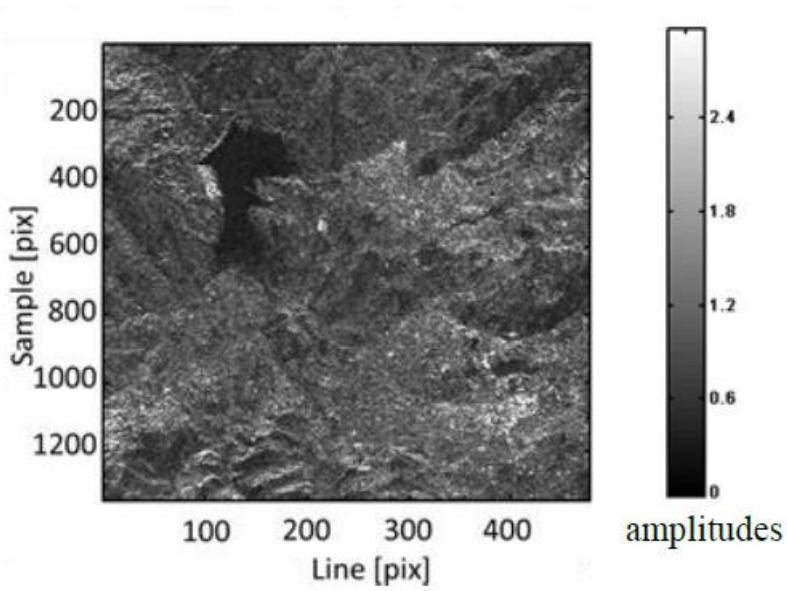

Figure 4. 10 Reflectivity map of the study area in SAR coordinates. (Pipitone et al., 2018, Proceedings of SPIE Remote Sensing Conference).

Then, after preliminary InSAR processing, the interferograms have been generated.

Figure 4.11 shows all available interferograms from the full graph connections analysis. Those characterized by small temporal baseline, also involved in the processing using the MST graph connection, look cleaner than those characterized by high temporal baseline, mostly noisy. The dam is identified in the upper left side of the interferograms.

The APS and MISP estimation have been performed using the same strategies for all MBC methods. Only for MST and full graph, the coherence has been used to weight the corresponding interferometric phase. The estimated results related to the choice of a reference point located close to the dam and characterized by high temporal coherence, have been geocoded and analysed in terms of distribution, number and expected behaviour.

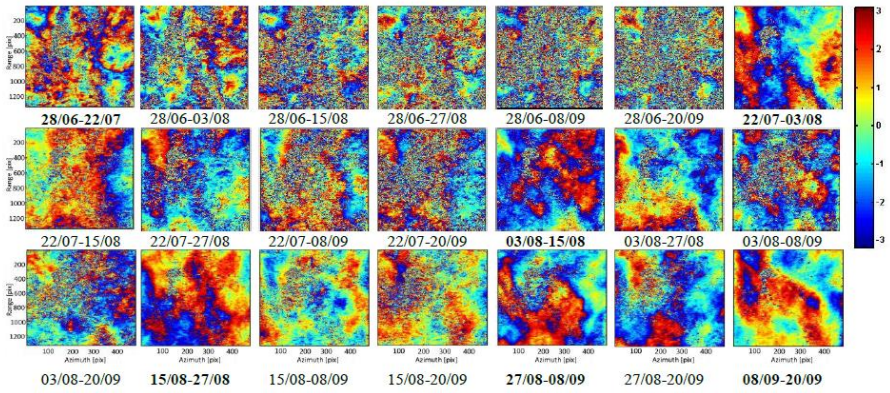

Figure 4. 11 Interferograms generated after preliminary InSAR processing using the full graph connection method. (Pipitone et al., 2018, Proceedings of SPIE Remote Sensing Conference).

The analysis, involving more interferograms and different connections showed different PS behaviour, especially on the dam. Best results have been retrieved using the star graph, in this case. Indeed, the use of more redundant connections and consequent interferograms provided a decreasing number of PS on the dam and also the coherence of selected PS after MST and full graph connection processing looks lower. The use of the ASI parameter for the selection of PS within the scene even though the high threshold selected for the analysis (0.8), was not able to suppress points filling in the reservoir, probably with a consequent loss of accuracy of the techniques (Figure 4.12).

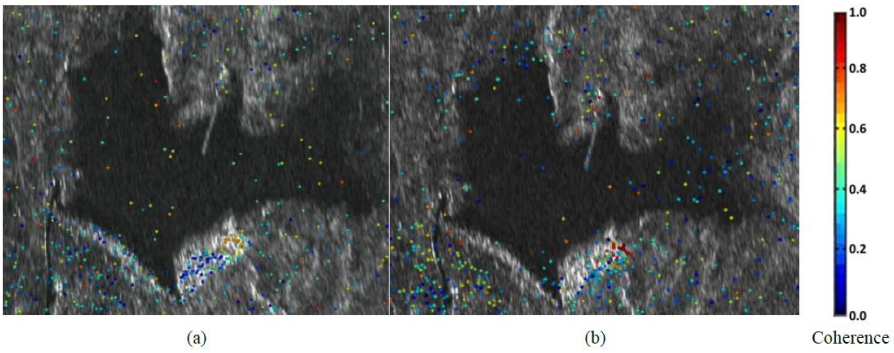

Figure 4. 12 Sparse points detected over the dam and the surrounding area characterized by different coherence, for the MST analysis (on the left) and full analysis (on the right panel). (Pipitone et al., 2018, Proceedings of SPIE Remote Sensing Conference).

Unexpectedly, best results has been found using the star graph connection between the images, for this case study. The technique applied over the dam was able to identify many points on the structure

characterized by high spatial and temporal coherence (higher than 0.8), especially on the left bank (Figure 4.13). Also, the results in terms of displacements along the LOS of the sensor were qualitative compared to those obtained via GNSS in different years.

In particular, the direction of the projected LOS displacements along the orthogonal section of the dam (June – September 2016) agree with the direction of the GNSS displacements recorded during the emptying and filling periods, from April 2011 to March 2012.

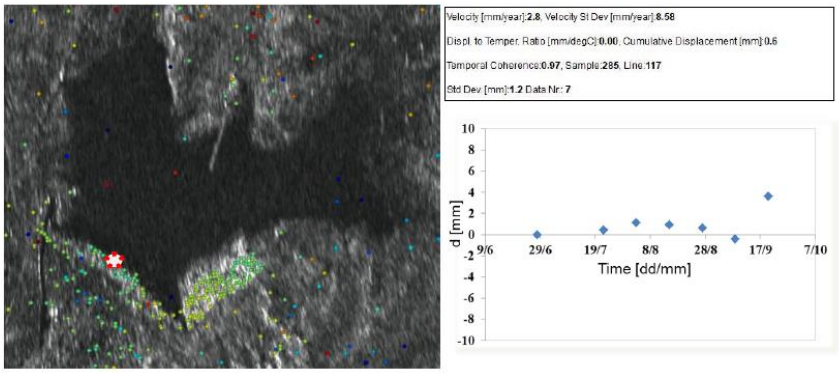

Figure 4. 13 Analysis of distribution of PS, in terms of deformation trend over the dam and the surrounding area, characterized by high spatial and temporal coherence over time. On the right panel the displacement time series of a selected point (on the left panel, with red circle). (Pipitone et al., 2018, Proceedings of SPIE Remote Sensing Conference).

InSAR analysis for the Castello dam displacement evaluation

Based on the preliminary results, the InSAR technique, involving the star and the full graph connections has been used to detect the global behaviour, in terms of displacements, over one year (January 2015 –

January 2016). The strategies involved are essentially the same of those discussed in the previous paragraph, but also many innovations have been added in order to improve the analysis.

In particular, a small area has been selected also in this case, but larger than the other selected in the preliminary evaluation. Indeed, 860 samples, 1120 lines have been considered, avoiding significant differences in terms of computational time using the star and the full graphs.

The parameter selected for the APS and MISP analysis for the sparse points selection has been identified with the reflectivity map, using a threshold of 1.8. As a consequence, all selected points are located outside from the reservoir.

The evaluation of the displacements has been performed using two different strategies, considering the results from GNSS analysis. In particular, the comparison refers to the velocity estimation between the different techniques.

The coherence of the connections between the pairs of images, after the full coherence estimation is reported in Figure 4.14 for the two connections graph (star and full, respectively on the left and right panels). In this case, 20 connections are available for the star graph (19 excluding the master-master connection) and 190 for the full graph. Figure 4.15 shows the reflectivity map generated for the study area.

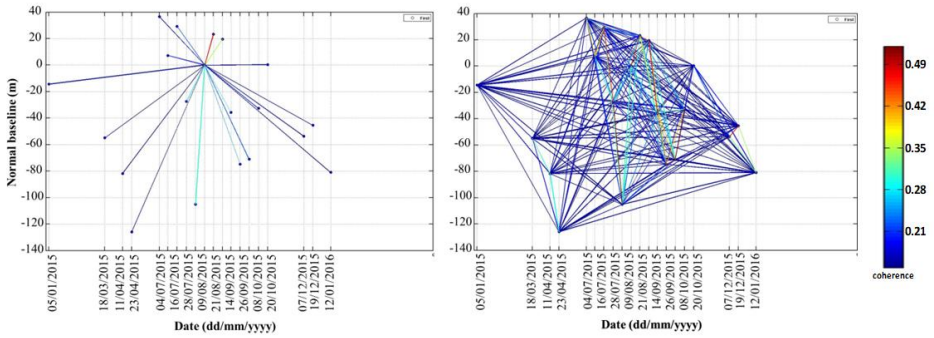

Figure 4. 14 Star and full graph connections (on the left and right panels, respectively) after interferograms formations and full coherence estimation.

Figure 4. 15 Reflectivity map of the study area superimposed on Google Earth image

Results, after APS and MISP processing are qualitative similar to those previously found. In particular many PS are identified over the dam, especially on the left hydraulic side, due to the high backscattering signal from the material covering the bank. However, in this case, no points have been identified within the reservoir, according to the high threshold selected for the reflectivity map (Figure 4.16).

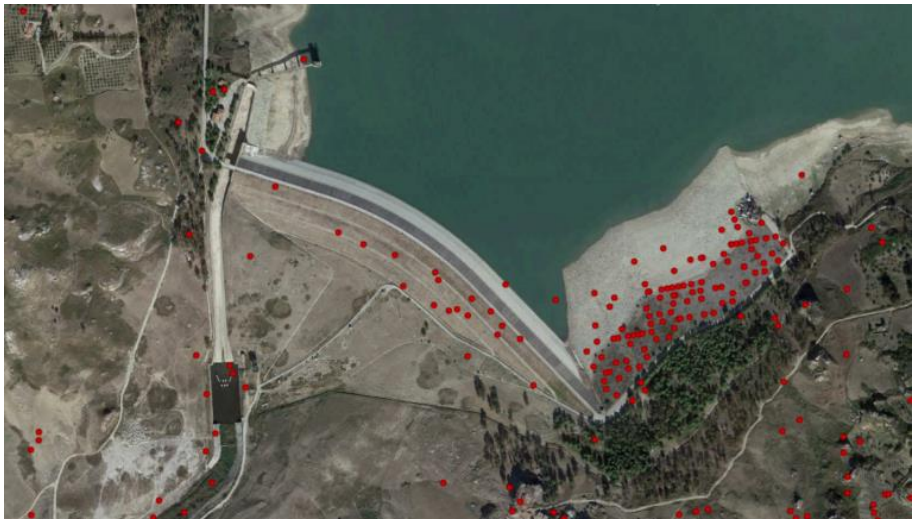

Figure 4. 16 Selected PS with high coherence (> 0.7) located over the dam

Using the star graph connection, the linear trend estimation, *via* the traditional PS-InSAR technique and global displacements (including both linear and non-linear components) using a temporal moving average have been shown in Figure 4.17, along the LOS of sensors. The LOS displacements have been estimated using the average values of selected PS close to the dam crest .

According to the first traditional strategy, the velocity of the time series has been computed and compared to the GNSS velocity. The resulting value from InSAR analysis is -4.05 mm y^{-1} (on the left panel). The estimated velocity using the non-parametric model, with a 3 samples temporal weighted moving average, showed a higher value of the velocity (-8.91 mm y^{-1}), but the polynomial model fits better the time series, with a determination coefficient $r^2 = 0.8$ (on the right panel).

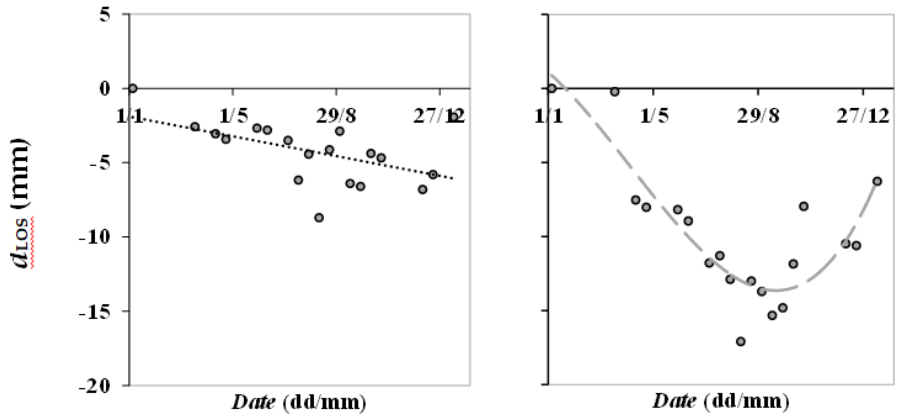

Figure 4. 17 LOS displacements time series of selected PS located on the dam obtained from linear trend estimation (on the left panel) and non-parametric model (on the right panel), involving the star-graph connection.

Using the full graph connection, the same strategies have been involved to find both the linear and no-linear components of LOS displacements time series of selected PS on the dam (Figure 4.18). The differences consist in the use of redundant connections and the coherence as weight.

In this case, the resulting average velocity found using the linear trend estimation is -0.62 mm y^{-1}, comparable with GNSS velocity

estimation (~ -1 mm y^{-1}), while using the non-parametric model, the resulting average velocity is -7.45 mm y^{-1}. However, as for the star graph connections, using the temporal moving average, a polynomial model fits better the time series (r^2 = 0.81)

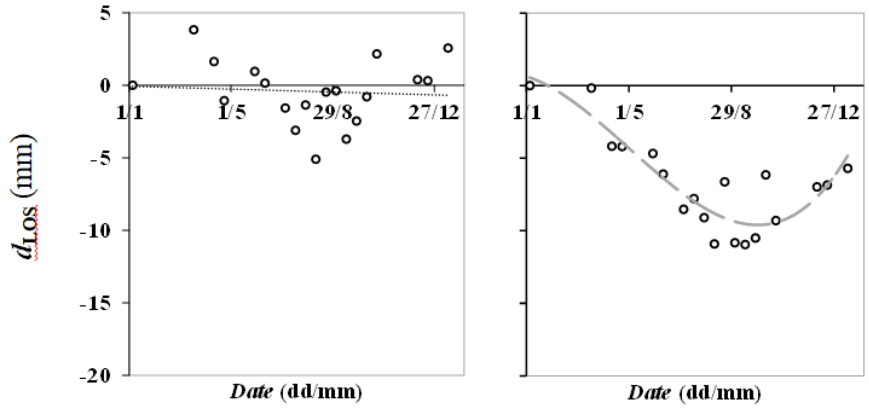

Figure 4. 18 LOS displacements time series of selected PS located on the dam obtained from linear trend estimation (on the left panel) and non-parametric model (on the right panel), involving the full-graph connection.

Finally, the linear trend estimation, using the full graph connection allows a better estimation of the yearly average velocity of selected PS located close to the dam crest, according to the results obtained via GNSS. The use of a temporal moving average doesn't allow estimating the linear component of displacements (far from GNSS estimation) but the polynomial models fit with high determination coefficient the time series. In particular, the full graph shows a low improvements of results, in terms of r^2 and shorter variability range of LOS displacements.

4.2 Reservoir water surface and level detection

Water surface and levels have been retrieved using, also in this case, several strategies, involving a consistent optical and SAR dataset. The objective is the construction of a monitoring project design involving all variables influencing the dam behaviour (causes, e. g. water levels fluctuations and temperature and response, e.g. deformations and in particular displacements). The first two techniques involved in the water level identification process were the classification technique and the visual matching. The first allows estimating the water surface and then, using the specific relation Surface-Volume-Level the water levels evaluation, the other allows obtaining directly the water levels and it is based on the operator subjectivity for the estimation.

The performances of the two methods were statistically analysed and from results both techniques were able to detect the water levels, but depending on the dataset involved, the classification method could be influenced by several factors (e.g., presence of clouds, shadows, missing scan lines, surface roughness). Table 4.1 shows the main statistical indicator (the slope, m, the intercept, q, the Pearson coefficient, r and the standard error, S.E.) found for each type of image and method (visual matching, M, and classification, C). The numbers in the brackets represent the number of images involved after the image processing. As reported in this table the total number of image decrease more after classification processing.

Table 4. 1 Statistical performances indicators for the different techniques involved (visual matching and classification) using different optical and SAR images. Best and worst results are highlighted in black and blue bold respectively. (Pipitone et al., 2018, Remote Sensing)

	SAR		*ASTER*		*LS8*		*LS5*		*LS7*		*All Data*	
	M	*C*	*M*	*C*	*M*	*C*	*M*	*C*	*M*	*C*	*M*	*C*
	(8)	*(8)*	*(8)*	*(6)*	*(9)*	*(8)*	*(6)*	*(5)*	*(21)*	*(10)*	*(52)*	*(37)*
m (−)	**0.98**	0.78	0. 96	0.92	1.04	1.08	1.37	1.27	0.95	**1.02**	**1.02**	0.96
q (m)	**5.06**	62.41	12.78	22.91	−10.07	−25.28	−107.13	−77.98	13.43	−7.73	−5.99	10.68
r (−)	**1.00**	**0.99**	**1.00**	0.98	0.95	**1.00**	0.78	0.96	0.98	**1.00**	0.98	0.98
S.E.(m)	0.38	0.58	0.30	0.81	0.61	**0.14**	1.83	0.65	0.86	**0.21**	0.92	0.70

The performances of visual matching and classification techniques are based on the determination of the Pearson correlation coefficient (r), compared to the critical value (r_{crit}) with a fixed significance level (p) for two-tailed test. The results in terms of estimated water levels were compared to the water levels measured *in situ* to analyse the most suitable method for water levels detection, highlighting the advantages and pointing out also the limits of the techniques.

4.2.1 Visual matching

The visual matching depends on the operator ability to distinguish the water bound from the land. The estimation of the water levels depend also on the different slopes on the left and right banks. Indeed, the final value is estimated as the weighted average, considering the values inversely proportional to the slopes (0.65-0.66 for the left bank and 0.34-0.35 for the right bank).

A preliminary analysis allowed estimating the variability range of water levels at different increasing geometric resolutions, for the left and

right banks (ΔH_L and ΔH_R, respectively), corresponding to the horizontal shift equal to the geometric resolution (Table 4.2).

Table 4. 2 Variability range of water levels for different slopes. (Pipitone et al., 2018, Remote Sensing)

R_G (m)	ΔH_L (m)	ΔH_R (m)
1.25	0.11	0.20
2.50	0.23	0.41
5.00	0.45	0.81
8.25	0.75	1.34
15.00	1.36	2.44
30.00	2.73	4.88
60.00	5.45	9.77

Using the whole dataset (52/58 optical and SAR images), a strong correlation has been found comparing the estimated and the measured water levels (higher than 0.9) (Figure 4.19). The advantages of this technique are the direct interpretation of the water levels from existing contour lines, the use of a consistent optical dataset, including images with clouds, shadows, missing scan lines, at their highest resolution, which usually are not suitable for other techniques (e.g., classification method). The limits of the method are the subjectivity of the operator, the accuracy of georeferencing, and the low spatial resolutions of optical images.

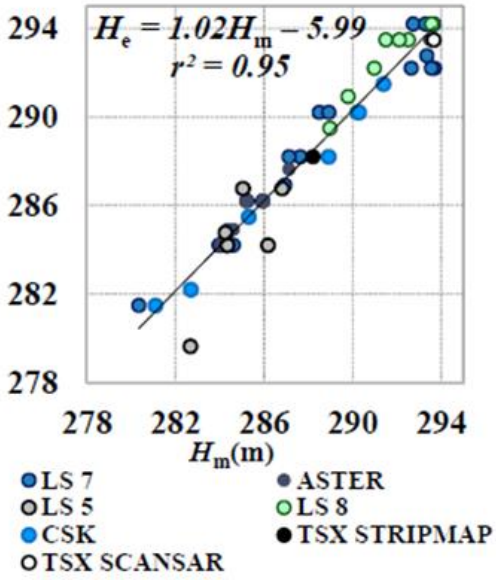

Figure 4. 19 Comparison between measured water levels (x-axis) and water levels estimated via visual matching (y-axis) using all optical and SAR images. (Pipitone et al., 2018, Remote Sensing)

The advantages and the limits of the technique are also reported separately for optical and SAR images in the following paragraphs.

Optical data processing

The optical dataset includes ASTER, LS5, LS7 and LS8 images. The results from visual matching processing are discussed below, by comparing with measured water levels.

For all available images the most suitable band combination has been evaluated, corresponding to the NIR, SWIR bands. Only for ASTER images the available band combinations is the VNIR and the geometric resolution is 15 m. The Pearson coefficient (1.00) for ASTER images was higher than r_{crit} (0.54) with a significance level at 1% and

S.E. 0.30 m. The determination coefficient is ~1.00 (Figure 4.20, left panel).

For LS 5 images, the geometric resolution and the available band combination is not uniform; indeed, two image have a geometric resolution of 60 m and the bands used for the analysis were VNIR also in this case. Worst results have been found for these images. Indeed, the r^2 is the minimum reached for the visual matching analysis (0.61). Also, the Pearson coefficient (0.78) was approximately the same of r_{crit} (0.76) with a significance level at 5% and S.E. 1.83 m (Figure 4.20, right panel).

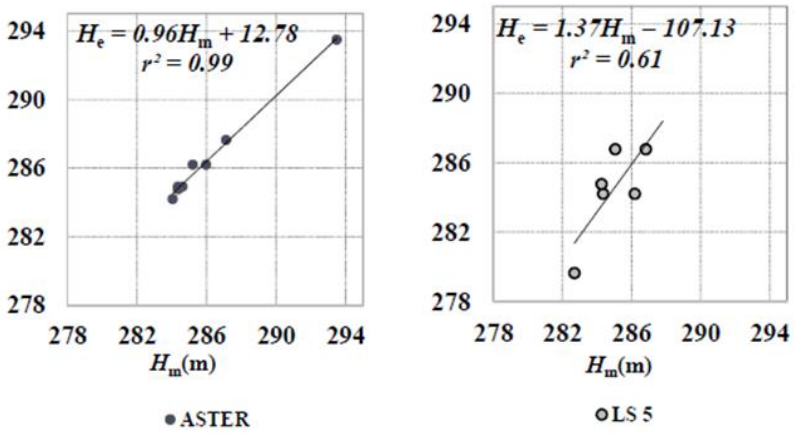

Figure 4. 20 Comparison between measured water levels (x-axis) and water levels estimated via visual matching (y-axis) using ASTER images (on the left panel) and LS5 images (on the right panel). (Pipitone et al., 2018, Remote Sensing)

The geometric resolution of multi spectral bands of LS7 and LS8 images (30 m) was preliminary improved using the Resolution Merge technique, involving the panchromatic band with highest resolution (15 m). the most suitable band combination for the boundary of the reservoir

is the NIR, SWIR for both LS7 and LS8 images. The combination of the two solutions (highest resolution and best band combination) allows obtaining high performances. Indeed, for LS8, $r^2 = 0.90$, the r value was higher than r_{crit} (0.95 > 0.77) with p = 0.01 and S. E. = 0.61 m (Figure 4.21, left panel).

For LS7 many problems occurred when the gaps covered the left and/or the right banks. Indeed, in this case, the water levels estimation didn't give any results or the estimate considered only the results from one bank. 21/26 LS7 images were used for the analysis, showing a strong correlation with measured data (r^2 =0.9). Also, the Pearson coefficient (0.98) was higher than r_{crit} (0.54), with a significance level at 1 % and S. E. = 0.86 m (Figure 4.21, right panel).

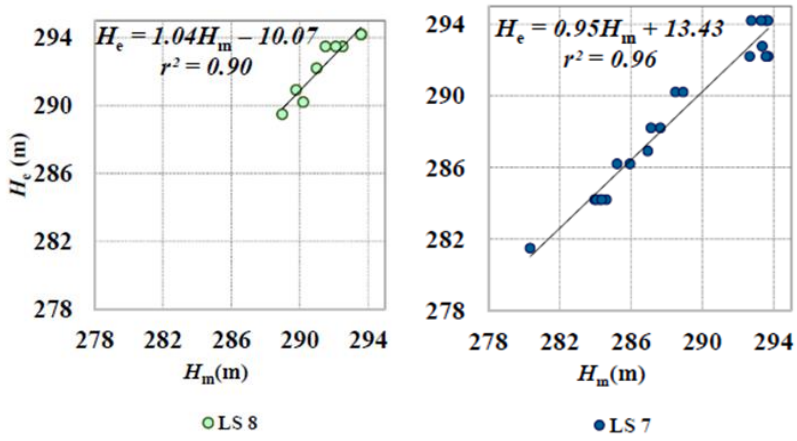

Figure 4. 21 Comparison between measured water levels (x-axis) and water levels estimated via visual matching (y-axis) using LS8 images (on the left panel) and LS7 images (on the right panel). (Pipitone et al., 2018, Remote Sensing)

SAR data processing

To analyse the capability of visual matching for SAR data , the only available band was used to identify the reservoir bound. Also, the spatial resolution was the maximum achieving, corresponding to 1.25 m for CSK, 2.5 m for TSX Stripmap and 8.25 m for TSX ScanSAR. Best results have been found for SAR dataset, probably due to the high spatial resolution and consequent higher accuracy in the determination of the water shoreline.

The determination coefficient, in this case, is the highest value reached from the analysis (0.99); the Pearson coefficient (1.00) was higher than r_{crit} (0.87) with p = 0.01 and S. E. =0.38 m (Figure 4.22).

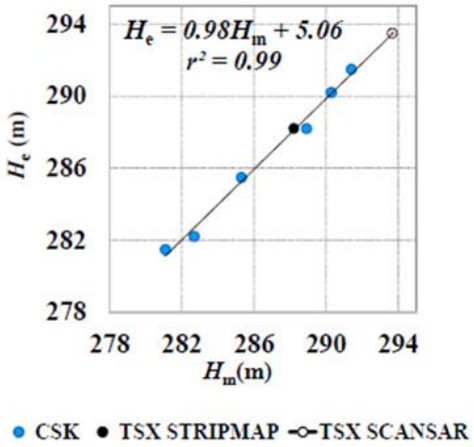

Figure 4. 22 Comparison between measured water levels (x-axis) and water levels estimated via visual matching (y-axis) using SAR dataset. (Pipitone et al., 2018, Remote Sensing)

4.2.2 Classification

The classification method is based on the analysis of the radiometric content and aims to determine the water surface extent and consequently the water levels by using the relation Surface-Volume-Level for the monitored reservoir. The method, based on the unsupervised classification process, could be easily automatised, but many limits occur when the images are affected by clouds, shadows, gaps within the scene (e.g. for LS7 ETM+ SLC-Off images), surface roughness. Indeed, in these cases, the method is not able to retrieve with high accuracy the extent of the reservoir and the estimation of the water levels fail. Also the geometric resolution can influence the estimation processing with consequent loss of accuracy.

Therefore, a preliminary analysis has been conducted over three different reservoirs with different surface extent, using decreasing spatial resolutions, aimed to determine the loss of accuracy in the surfaces evaluation. The surface associated to the highest resolution was taken as reference and then the variation between the estimated surface and the reference was evaluated. The surfaces have been estimated after pixel aggregation, unsupervised classification and segmentation (Figure 4.23).

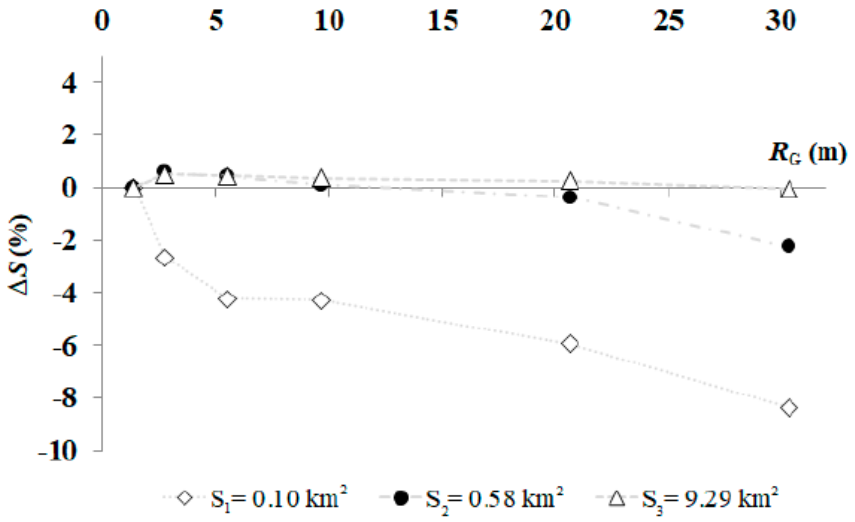

Figure 4. 23 Differences in terms of surface between the estimation from classification method and the reference surface, at decreasing resolutions. (Pipitone et al., 2018, Remote Sensing)

The analysis points out that the differences are consistent for large extents of reservoirs (S_3 = 9.29 km^2), they are negligible for small lakes (S_1 and S_2).The surface extent of Castello dam varies from 0.72 and 1.62 km^2 during the emptying and filling periods, respectively. Considering the surface extent S_2 the resolution of Landsat images (30 m) is considered suitable for the water levels detection using the classification technique with a loss of accuracy lower than 2%.

As the visual matching, also the classification method was applied on the whole dataset and advantages and limits were separately discussed in the following paragraphs. Considering the whole dataset, after applying the unsupervised classification and the segmentation methods on the whole dataset and the clumping classes only on SAR data, the

results have been analysed using the same statistical indicators reported in the paragraph 4.2.

A strong correlation has been found between the evaluated and the measured water levels, considering the whole dataset. Indeed, the r^2 value was higher than visual matching (0.97), the S. E. = 0.70 m at p = 4.3 x 10^{-27} (Figure 4.24). However, the number of images involved are much more less than the others involved in the visual matching (37/58 images, corresponding to less than 70% of the dataset.

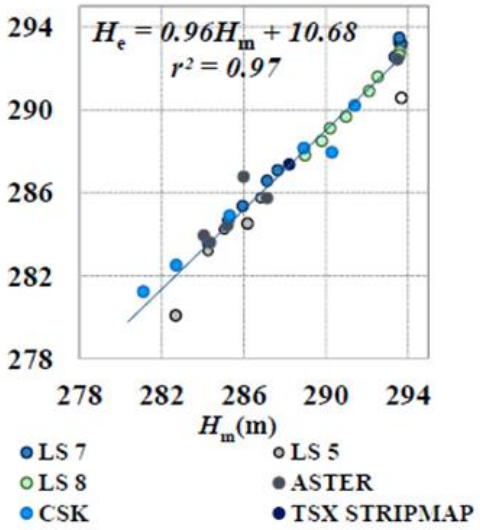

Figure 4. 24 Comparison between measured water levels (x-axis) and water levels estimated via classification (y-axis) using all optical and SAR images. (Pipitone et al., 2018, Remote Sensing)

Indeed, although the classification method obtained high values of statistical indicators, and it represent a technique to be easier automatized, the presence of clouds, shadows, gaps within the scene

influence the final accuracy and many images need to be discarded. Also, the application of the segmentation, which generally allows excluding the pixels wrongly classified as water class, but not connected to the reservoir, in many cases, produces an over or underestimation of the water surface. The first case is typical for images characterized by clouds, shadows or missing scan lines within the scenes (optical images, generally discarded), while an underestimation occurs for example for SAR images characterized by surface roughness (Figure 4.25).

The reduction of included and excluded pixels classified as water class has been estimated and reported in Table 4.3.

Table 4. 3 Reduction of included and excluded pixels classified as water levels after segmentation and clumping classes at different geometric resolutions, including the standard deviation (Pipitone et al., 2018, Remote Sensing)

	SAR		ASTER	LS8	LS5	LS7
R_G	Stripmap 5.00	Scansar 8.25	15.00	30.00	30.00	30.00
Segmentation	-36.2 ± 16.9	-2.5	-2.9 ± 1.9	-1.1 ± 1.5	-0.5 ± 0.8	-0.2 ± 0.3
Clump	4.8 ± 4.8	0.8				

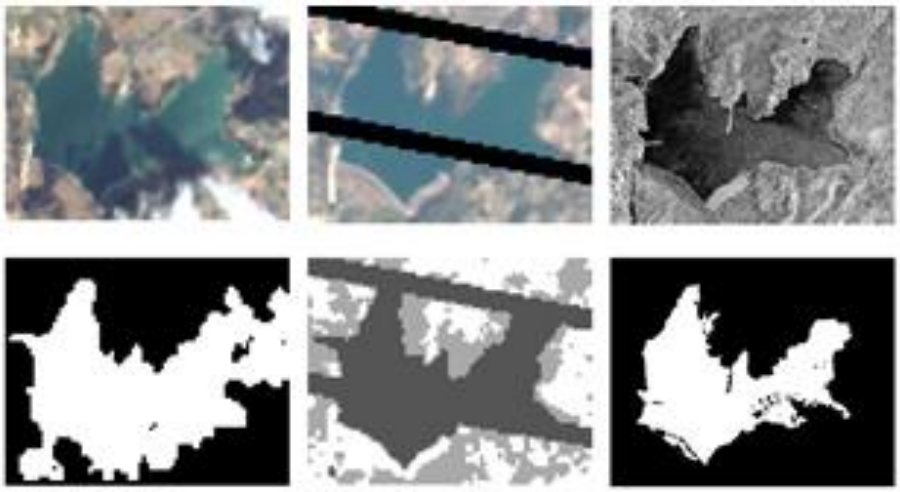

Figure 4. 25 Results from classification over cloudy, shadowed optical images (LS8 on the left panel and LS7 on the central panel) and surface roughness of CSK image. (Pipitone et al., 2017, Proceedings of SPIE Remote Sensing Conference).

Optical data processing

The classification of optical images can be influenced by the cloudiness, shadows and gaps characterizing for example LS7 data. These problems reduce the dataset availability and many images need to be discarded during the process.

Analysing the ASTER and LS5 images (Figure 4.26) the results in terms of r^2 showed a strong correlation between the estimated and measured water levels (0.95 and 0.93, respectively). However, two images for both ASTER and LS5 have been discarded because characterized by clouds and large missing scan lines, respectively.

For LS5 images worst performances have been obtained, the Pearson coefficient is 0.96 and S. E. = 0.65.

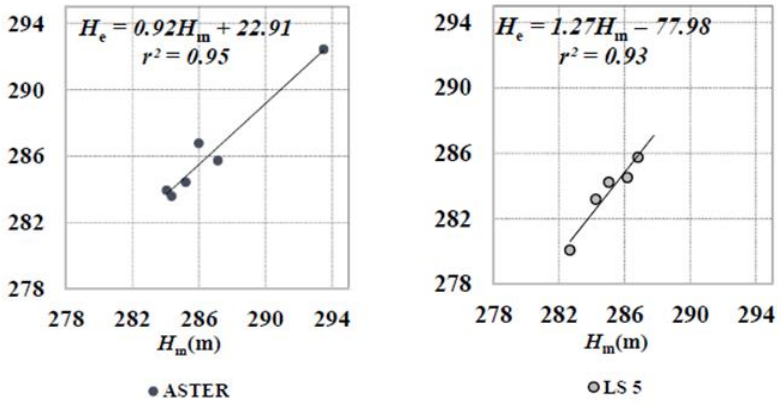

Figure 4. 26 Comparison between measured water levels (x-axis) and water levels estimated via classification (y-axis) using ASTER images (on the left panel) and LS5 images (on the right panel. (Pipitone et al., 2018, Remote Sensing)

Despite the possibility to enhance the geometric resolution of LS7 and LS8 images using the resolution merge, worst results have been obtained with the highest resolution. So, the classification was applied to the SWIR and NIR bands, with a spatial resolution of 30 m.

Many problems occurred also for LS7 ETM+ SLC-Off . Indeed, the presence of gaps of different sizes within the images required a preliminary filling of the missing lines especially within the reservoir, obtained with RBV method implemented in ENVI software. Two main scenes have been acquired for LS7 images, the 189/34 and 190/34. In the first scene the reservoir is located ~57 km from the left boundary and the gaps size is approximately 200 m, while in the scene 190/34 the reservoir is located ~8 km from the right boundary, with gaps size approximately equal to 400 m. Based on previous results (Dardanelli et al., 2014) the maximum underestimation of 10% is considered acceptable, with a ratio

between the width of unscanned rows (L_S) and the length of water body along the orthogonal direction to the missing scan line (L_L) less than 0.17. The missing scan lines within the reservoir for the scene 189/34 have a ratio lower than the fixed threshold and the results from RBV are considered acceptable, on the contrary the ratio in the scene 190/34 is higher than 0.2, thus all images from scene acquisition 190/34 (14 images) have been removed from the analysis because they are considered corrupted (Figure 4.27).

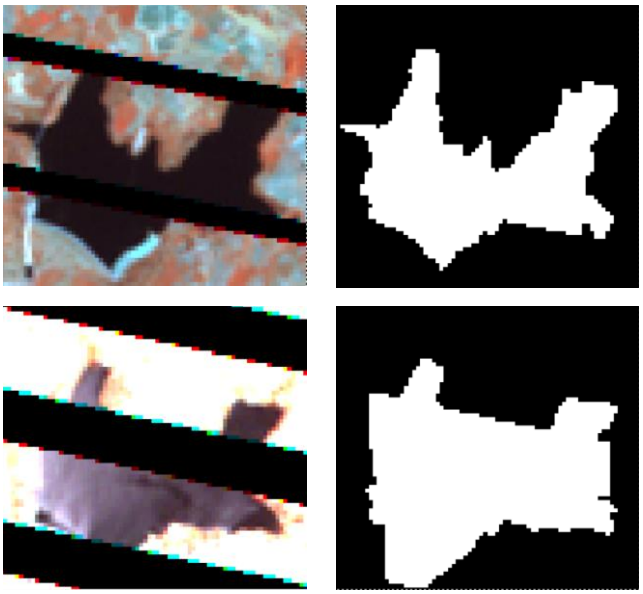

Figure 4. 27 Comparison between accepted (a) and removed (d) results after "replace bad value" analysis and classification, using SWIR and NIR bands, for scene 189 (a, date: 13/05/2011) and scene 190 (c, date: 06/07/2012).

Other two images from scene 189/34 have been removed from the analysis because characterized by cloudiness or gaps covering the reservoir boundary.

The results for LS7 and LS8 images are reported in Figure 4.28.

Very high performances have been obtained using these images; indeed the r^2 and r values are 1.00 for both LS7 and LS8 images and the lowest S. E. have been reached (0.14 m for LS8 and 0.21 for LS7).

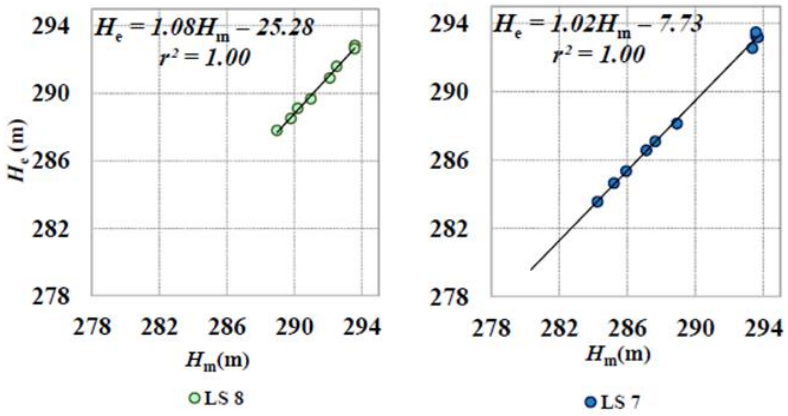

Figure 4. 28 Comparison between measured water levels (x-axis) and water levels estimated via classification (y-axis) using LS8 images (on the left panel) and LS7 images (on the right panel). (Pipitone et al., 2018, Remote Sensing)

SAR data processing

The steps involved for the estimation of the reservoir water surface using SAR images are similar to those used for optical images. Applying the segmentation process on the whole dataset, only for two CSK images,

characterized by surface roughness probably caused by the wind action, the setting parameter have been changed.

Comparing two different CSK image, the first acquired in still conditions and the other in windy conditions, the advantages and the limits of segmentation and clumping are evident (Figure 4.29). Indeed, in the first case, both techniques are able to define the water surface extent, even though a small part of the reservoir is excluded because of a bridge crossing the artificial lake. In windy conditions, the segmentation is able to remove many pixels wrongly classified as water but disconnected to the water reservoir, but not all. Also the clumping applied on the segmented image couldn't remove the misclassified pixels.

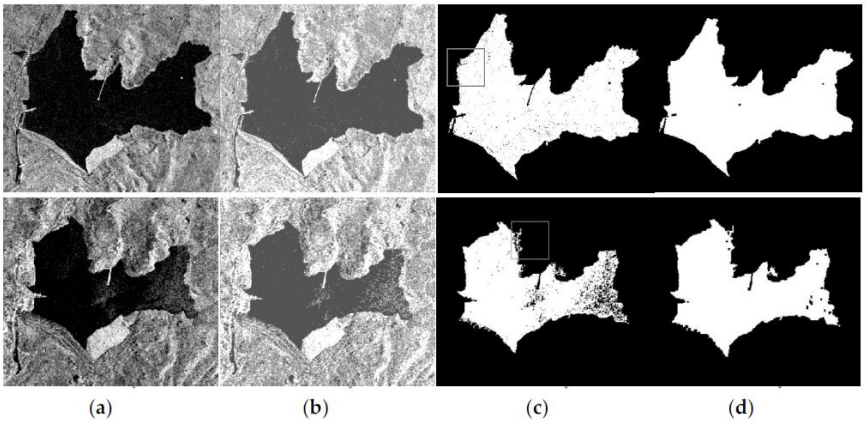

Figure 4. 29 Comparison between two CSK images acquired on the 8 February 2012, in still conditions (upper panels) and on 10 September 2012 in windy conditions. The images represent the backscattering (a), the unsupervised classified image (b), the segmented image (c) and the clumped image (d). (Pipitone et al., 2018, Remote Sensing)

Results from SAR data analysis showed high performances also in this case, even though many factors, as wind action or residual speckle can influence the results, with an overall underestimation. For TSX and CSK data, after pixel aggregation, unsupervised classification and post-classification techniques the results showed a high Pearson coefficient (0.98), r = 0.99 and S.E. =0.58 m (Figure 4.30)

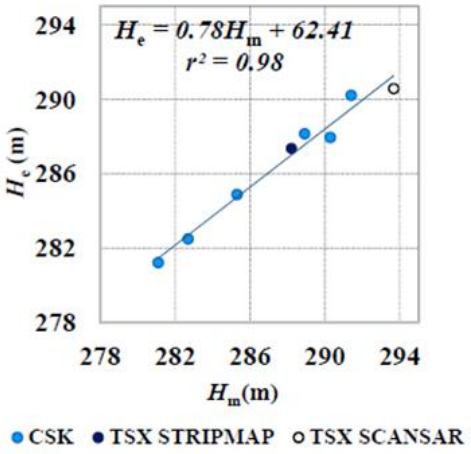

Figure 4. 30 Comparison between measured water levels (x-axis) and water levels estimated via classification (y-axis) using SAR images (on the right panel). (Pipitone et al., 2018, Remote Sensing)

4.2.3 OBIA

Optical and SAR data processing

Both visual matching and classification methods were able to detect the water surface and levels of the Castello reservoir, with high performances (Table 4.1). However, both exhibited limits occurred

depending on the dataset and the algorithms involved. Using the unsupervised classification, for example, the water surface extent could be overestimated (if clouds, shadow, missing scan lines, for LS7 images, are within the scenes) or underestimated (if the SAR image is characterized by surface roughness do to the wind action). As reported in 4.2.2.1 the original dataset (58 images) was drastically reduced, because of these factors (37 images).

To overcome these limits, two different techniques have been applied, the STEP algorithm implemented in QGIS software and an independent GIS technique based on the evaluation of distances between two pairs of images. Both techniques used reference objects and classified images applying the OBIA.

STEP algorithm

The reference objects, used for this analysis, are the contour lines from the available DEM, with resolution of 2 m. These present a variability range between 292 and 300 m and the distance between each line is 1 m in the first analysis, 0.5 m in the other.

Preliminary the technique has been assessed for an ideal case, using the contour lines not only as reference but also as “classified” objects. The classified object , used in this test, is the contour line with height 295.0 m a.g.l. The references are all available contour lines. The aim is the evaluation of similarity metrics for water levels detection. According to the equation for the edge index, also different values of the epsilon

distance (e) have been tested, from 0 to 1 (0.1, 0.5, 1). The maximum value was set equal to the distance between the contour lines.

Results for all similarity metrics, for the ideal case, are reported in Figure 4.31.

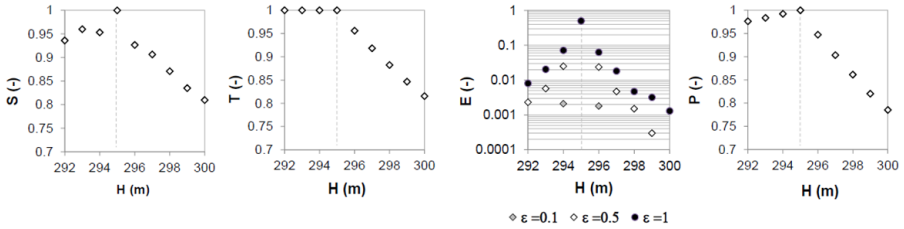

Figure 4. 31 Similarity metrics for the ideal case (contour lines used as reference and classified images). (Pipitone et al., 2017, Proceedings of SPIE Remote Sensing Conference).

From Figure 4.31 the performances of STEP algorithm are very high. Indeed, the maximum values of STEP metrics have been estimated when the classified object (contour line at 295.0 m a.g.l.) match with the same reference object (295.0 m a.g.l.). All STEP indices reached their maximum values with changing trend, except for the T metric, for which the maximum value has been reached for all contour lines with height less than the reference value.

According to these results, confirming the capability of the method to correctly identify the contour line corresponding to the classified object, the analysis was performed on different images. The images are characterized by failure of the classification with an overestimation or underestimation of the water surface. The aim is the determination of

water surface without any influence from external factors (e.g., clouds, shadows) with high accuracy.

However, the application of the method on these images was not satisfactory, because weather conditions influence the classification method and consequently the STEP method, with inaccurate results. Best results have been found for images acquired in still conditions.

This is the case of a Landsat 8 image on which the application of the method allowed achieving high performances (Figure 4.32).

Best results have been recorded using the E index, even though the values are still low and the epsilon distance need to be investigated. The E metric is able to identify the closest contour lines (293.5 and 294 m a.g.l.) to the measured water line for the classified image. Also the S metric correctly identifies the closest contour lines (293.0 and 293.5 m a.g.l.) to the measured water level. The other two indicators (T and P) were not able to univocally identify the reference contour line close to the classified image and also the trend is not univocally defined, as in the ideal case.

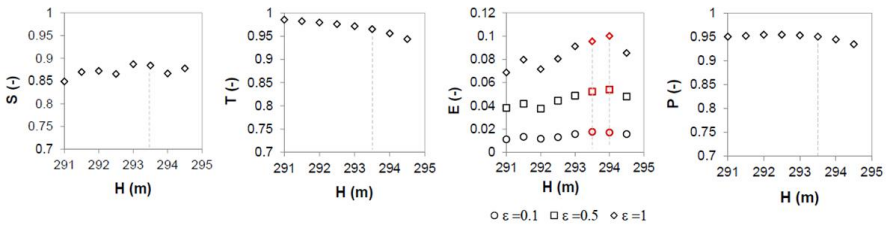

Figure 4. 32 Similarity metrics for LS8 image (characterized by measured water level 293.6 m). (Pipitone et al., 2017, Proceedings of SPIE Remote Sensing Conference).

Based on these results, the method has been applied also on SAR backscattering images, characterized by high resolution, but only the Edge metric has been evaluated. Indeed, from both ideal case and optical images analysis, the E index is the most suitable indicator to determine the closest contour lines with high accuracy. The epsilon distance has been also changed. Two different values have been tested (1.0 m and 14.0 m) corresponding to half of the DEM resolution and half of the pixel resolution (28.0 m) after aggregation.

The SAR dataset involved the S-1A images previously adopted for the displacements analysis *via* the InSAR technique. The application of the method on SAR images produced many discrepancies, compared to the previous analysed cases, but they even are comparable with the geometric resolution of the DEM.

The analysis has been preliminary performed over one year (November 2014 - November 2015), and the results are reported for three different measured water levels, corresponding to the minimum, an intermediate and a maximum water level, recorded on 06 November 2014, 09 August 2015 and 18 March 2015, respectively. The results are shown in Figure 4.33.

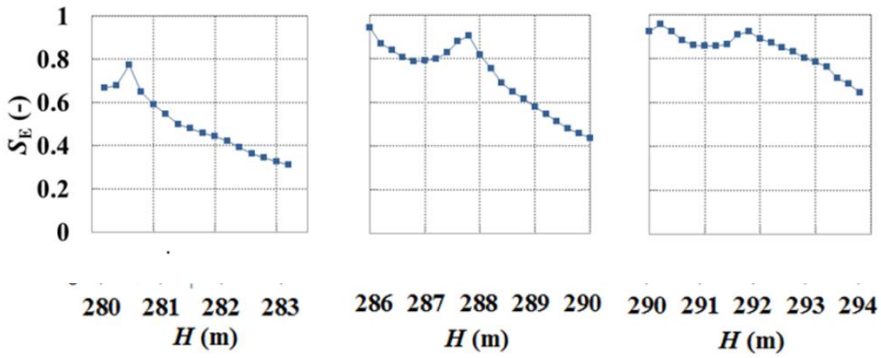

Figure 4. 33 E index evaluated for three different measured water levels with epsilon distance 14.0 m (minimum, intermediate and maximum in the left, central and right panels respectively)(Pipitone et al., 2018, HIC 2018. 13th International Conference on Hydroinformatics)

The use of different epsilon distance values showed that best results are achievable with $\varepsilon = 14.0$ m, except for minimum water levels, for which there are no differences using the two values (Table 4.4). Also from Figure 4.33 it is evident that for minimum water levels the method is able to recognize univocally the closest contour line (one peak), for the intermediate and maximum water levels many uncertainties occurred (two peaks). These uncertainties are due to the resolution of the DEM but also to the shape of the analysed reservoir, characterized by a bridge crossing it. The results after unsupervised classification for the reservoir during the filling periods are indeed, characterized by an underestimation of the water extent because part of the artificial lake (over the bridge) is separated from the main part and not considered during the analysis.

Table 4. 4 Comparison between measured water levels for the classified image and evaluated water level from STEP analysis using different epsilon distance values. (Pipitone et al., 2018, HIC 2018. 13th International Conference on Hydroinformatics)

Date	H_m (m)	HS_E (m) ε=1 m	HS_E (m) ε=14 m
06/11/2014	281.5	280.6	280.6
18/03/2015	293.7	291.2	291.8
09/08/2015	288.7	286.8	287.8

Distance method

The distance method consider the distances between the classified and the reference objects. Also in this case, three different cases have been evaluated: an ideal case (Figure 4.34), the application on LS8 image (Figure 4.35) and S-1A dataset (Figure 4.36). The reference objects are the contour lines from the available DEM, with resolution of 2 m, with a variability range between 292 and 300 m and the distance between the lines is 1 m.

The accuracy of the method has been evaluated through the mean value and other two statistical indicators (P_{095} and P_{005}), corresponding to the 95^{th} and 5^{th} percentiles, respectively.

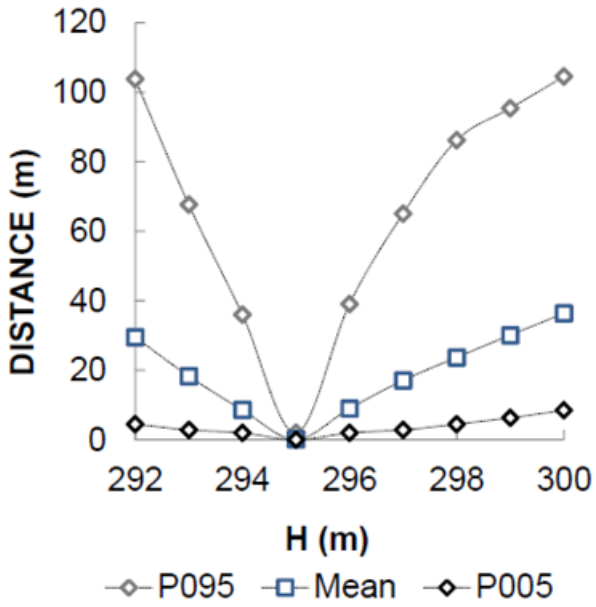

Figure 4. 34 Distance method for the ideal case (contour lines used as reference and classified images). (Pipitone et al., 2017, Proceedings of SPIE Remote Sensing Conference).

Results from the ideal case show values close to zero when the water levels associated to the classified and the reference objects correspond to each other (Figure 4.34).

Figure 4.35 shows the results for the LS8 image. In this case, the distance values are not close to zero, as in the previous case, but the minimum value of the mean distance is reached for the contour line characterized by height 294.0 m, close to the measured water level (293.6 m). Also the variability range for the two analysis is the same and the maximum value of the mean distance is approximately 40 m, according to the resolution of LS8 image (30 m).

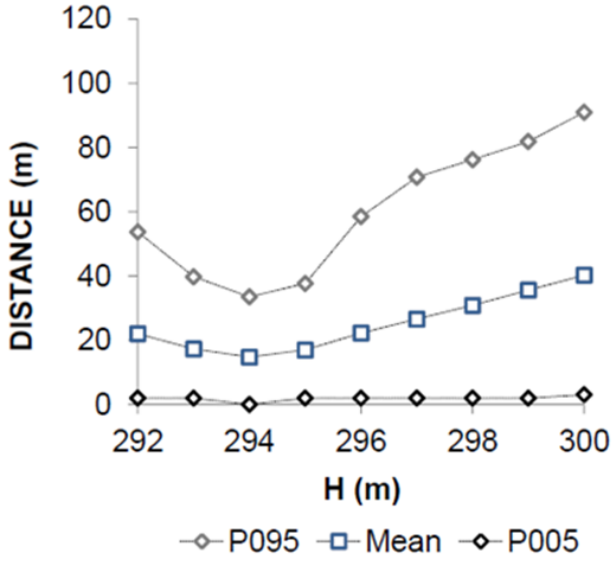

Figure 4. 35 Distance method for LS8 image (characterized by measured water level 293.6 m). (Pipitone et al., 2017, Proceedings of SPIE Remote Sensing Conference).

The method has been also preliminary tested on S-1A images (November 2014 - November 2015) at different water levels (Figure 4.36). Results from this analysis were comparable with those using the E metric, with ε = 1 m. Also in this case, the differences between the measured water levels and the estimated via distance method are quite small for minimum water levels, they become more relevant (~2 m) for intermediate and maximum water levels. The differences are comparable with the resolution of the DEM but an improvement has been found using the other technique with higher ε value (14 m).

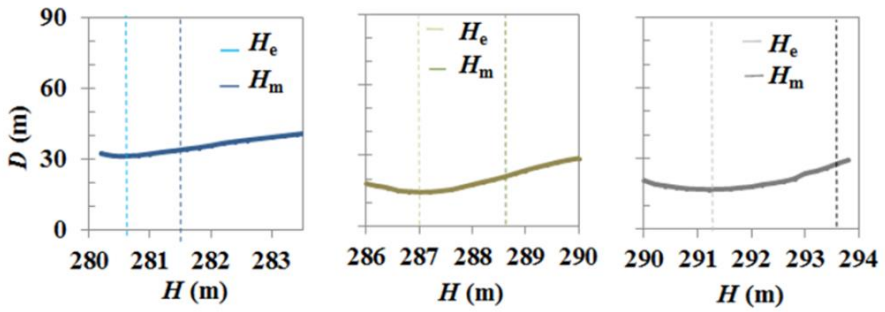

Figure 4. 36 Distance method for three different measured water levels with epsilon distance 14.0 m (minimum, intermediate and maximum in the left, central and right panels respectively). (Pipitone et al., 2018, HIC 2018. 13th International Conference on Hydroinformatics)

Then, more S-1A images have been included for the analysis (October 2014 - December 2016) to test the capabilities of the innovative technique. The results obtained from 60 Sentinel-1 images (from both ascending and descending obits) have been plotted and compared to the measured water levels (Figure 4.37).

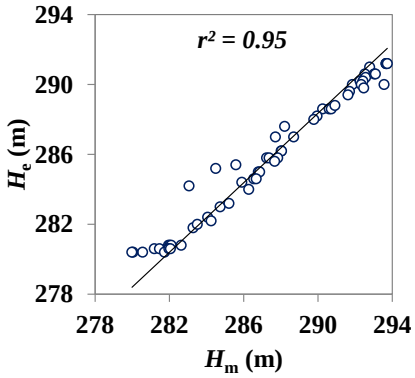

Figure 4. 37 Comparison between measured water levels (x-axis) and water levels estimated via *"distance method" (y-axis) using S-1A images.*

The same dataset has been also used to compute the reservoir water levels, using the classification method (Figure 4.38).

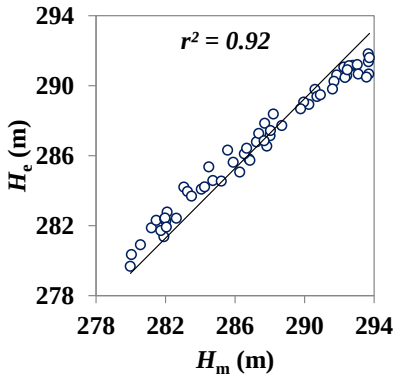

Figure 4. 38 Comparison between measured water levels (x-axis) and water levels estimated via *classification (y-axis) using S-1A images.*

Considering the consistent number of images involved for the analysis, a strong correlation has been found between the evaluated and the measured water levels, considering both the OBIA and the classification method. Indeed, the results show a high value of r2 coefficient for both analyses (higher than 0.9). In particular, using the distance method three possible outliers have been detected, corresponding to low measured water levels for three different dates, reported in Figure 4.39. However, the classification method applied on the same dataset didn't reveal the same problems for these images. Thus, the images were not removed from the analysis.

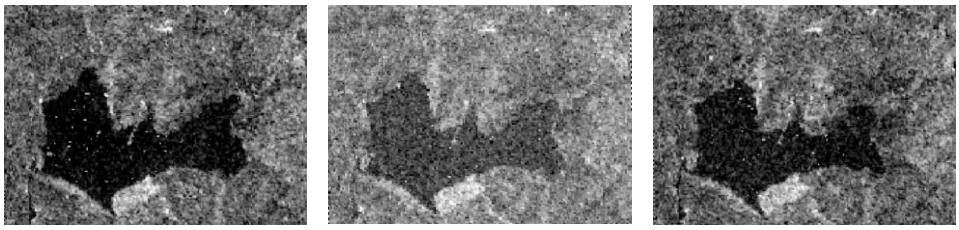

Figure 4. 39 S-1A images not well processed by using distance method, acquired on the 15 August 2016 (left panel), 27 August 2016 (central panel) and 8 September 2016 right panel). The corresponding measured water level for the three acquisitions are 285.58 m, 284.49 m and 283.06 m respectively.

The advantage of using both technique is that they are easily automatised, thus they are more suitable for monitoring. Also, results from both techniques confirmed their capabilities for estimating water surface and water levels, according to the values recorded *in situ*.

Conclusions

Structural health monitoring is important for maintaining and ensuring the functionality of strategic structures of social and economic importance. If a monitoring system is appropriately designed, it is possible evaluating the operational functions of these structures, in particular dams, operating in case of failures of potential deficiencies.

The instrumentations to be involved for structure monitoring must be properly chosen, and need to consider all aspects influencing the dam behaviour. Indeed, generally, geotechnical, structural and hydraulic parameters are involved in the deformation process and they are adequately monitored using traditional techniques (inclinometers, piezometers, assestimeters, geodetic instruments).

The aim of this research is the dam displacements monitoring using innovative satellite techniques, in particular GNSS and remote sensing. The latter technique demonstrated also to be able of detecting water levels, representing one of the external factors influencing the dam deformation process. The study area is the Castello dam, Agrigento (Italy).

The analysis points out the advantages and the limits of different techniques involved in the dam displacements estimation and water surface and levels detection. Also, the use of different dataset allows estimating the accuracy of the techniques involved, according to the characteristics of the satellite imagery.

The displacements have been analysed using both GNSS and InSAR techniques and preliminary, the use of existing models in literature allows estimating the influence of external loads on the dam and the long-term behaviour over one year of data. Indeed, the existing models are based on the concrete behaviour, a material with well-known characteristics, while there aren’t existing models for embankment or earth dams. Indeed, the behaviour of these structures is not easily determined and depends on the material filling the dam itself. Generally FEM analysis are able to describe the behaviour of these structures since their construction, but they require a deep knowledge of materials filling the dam.

The use of InSAR technique, more than GNSS, didn’t require any instruments installation on the dam or the surrounding area, reducing the materialization costs.

Also for both techniques, different strategies have been evaluated to determine both the reversible and irreversible components of displacements. Indeed, the first, is generally associated to the sinusoidal behaviour of the dam, the most important component is instead the linear term, caused by the structural "aging".

Preliminary results involving existing models able to describe the behaviour of concrete dams showed that those involving the physical parameters (e.g. hydrological, thermal effects) and sinusoidal behaviour, using the main frequency of the structure are suitable to describe the behaviour of the Castello dam. The GNSS displacements found on the top of the dam along upstream-downstream directions were in agreement with those obtained by using the two models. Best results have been found for the receiver located in the mid-section.

Based on these preliminary results and previous findings exploiting that the most relevant horizontal component of displacements occurred in the mid-section, orthogonal to the dam (Behr et al., 1998, Tasci, 2008, Yigit et al., 2016, Kalkan, 2014, Yavasoglu et al., 2018, Radhakrishnan, 2014), only the central section has been analysed for monitoring dam displacements along the orthogonal section to the dam itself.

The velocity estimated from the linear trend evaluation, during the monitoring period, was approximately -1 mm y^{-1}.

The analysis of the moving average displacements in the central section revealed the long-term dam behaviour over approximately one year (a whole hydrological cycle), from April 2011 to March 2012. The

sinusoidal behaviour is generally typical for non-linear displacements due to external oscillating forces (e.g., water levels, temperature).

From the comparison between the estimated dam displacements orthogonal to the dam and the measured water level a non-linear relation was obtained.

In particular the response of the dam to the water levels was different during the emptying and filling periods. Also, the influence of the air and water surface temperatures influenced the dam behaviour. Indeed, two maximum displacements have been recorded, the first corresponding to the minimum water level, the second to the maximum temperatures values; also the minimum displacement corresponds to the minimum temperatures values.

Results also demonstrated the capability of InSAR technique for dam displacements monitoring. Indeed, different analysis have been performed on the Sentinel-1 dataset aimed to detect the displacements of natural targets characterized by high backscattering signal (PS) on the dam. The analysis of the study area, mainly vegetated over extra urban areas, has been performed using different strategies involving the traditional PS-InSAR technique (Ferretti et al., 2001) and many innovations in the connection graphs using the Multi-Baseline Construction methods and the parameters estimation using the linear trend estimation and non-parametric models.

Results confirmed the capability of the technique for dam displacements estimation. Also the use of more redundant connections between the images allows obtaining higher accuracy. The irreversible

term of displacements has been evaluated using a linear trend estimation and the results showed comparable results (-0.62 mm y^{-1}) with those obtained via GNSS (-1 mm y^{-1}), in case of full connection graph.

The reversible component, generally associated to the external loads, especially for concrete dams, has been evaluated using the temporal moving average using three images as sample. In this case, indeed, the estimated velocity is not correctly estimated using both the different connection graphs, but the best fitting model has been obtained superimposing a polynomial interpolating curve (r^2 = 0.8 - 0.81 for the two connection graphs).

The analysis of water levels was also in this case based on different approaches, the unsupervised classification method, the visual matching of contour lines and OBIA. Good results have been preliminary obtained by using the first two techniques. Indeed, they were both able to determine the water levels, using different optical and SAR images with high accuracy (r^2 = 0.95 and r^2 = 0.97, for visual matching and classification, respectively).

Limits of the visual matching are in the operator capability to distinguish the water surface boundary from land. Also, the highest spatial resolutions and the most suitable band combinations need to be chosen to delimit the reservoir shoreline and determine the closest contour lines. The advantages reside in the possibility to use a consistent dataset, even affected by issues, as presence of clouds, shadows, missing scan lines…).

On the contrary, the unsupervised classification is an automatised process able to determine the water surface but, the issues of images are not easily solved and, generally, the corrupted images are discarded from the analysis.

For the proposed analysis, 52 images were used for visual matching and only 37 over 58 for classification.

To solve the limits of classification method, OBIA has been performed on different case studies: the ideal case using only the contour lines, optical images and SAR dataset.

The OBIA is based on the comparison of geometric characteristics between a reference object and a classified image. In the analysis, the reference objects have been identified with the existing contour lines delimiting the reservoir.

The STEP similarity metrics applied on an ideal case, showed the capability of the technique of identifying the perfect match between the reference and the classified objects. The indicators are characterized by different trends and a maximum is recorded, corresponding to the associated contour line. The same technique applied on optical images highlights the limits of the method itself. Indeed, it is not possible applying the technique over images characterized by overestimated surfaces, caused by the failure of classification technique. Indeed, the method is influenced by the quality of the classification results, the spatial resolution of images and the regularity of the reservoir shoreline.

Results from the application on LS8 images showed that only two indicators related to the shape (S) and edge (E) are suitable to detect with high accuracy the closest contour lines associated to the classified image.

Also, the parameter called epsilon distance influenced the performances of the edge indicator. Based on these preliminary results, the analysis performed on Sentinel-1A data considered only the edge index at different ε values, corresponding to half of the DEM resolution and half of the SAR geometric resolution after pixel aggregation.

The index was able to determine the closest contour lines associated to the classified image, especially for those characterized by minimum water level. The differences between the estimated and the measured water level are approximately 2 m, comparable with the DEM resolution and depending also by the irregularity of the shoreline and consequent failure of the classification procedure.

The other OBIA was based on the estimation of the distances between the reference contour lines and the nodes extracted from the classified images, previously vectorised. The comparison between the two groups of objects showed that for both the ideal case and optical LS8 images the distances were minimized. For the ideal case, values close to zero have been found and the maximum average distance (~40 m) was comparable with the resolution of the Landsat images.

The application of the method on the Sentinel-1A data revealed an agreement with the edge indicator, using an epsilon distance of 1 m; but a low improvement has been found using 14 m instead. The analysis of a more consistent dataset, including 60 images, and the comparison with measured water levels has shown a strong correlation (0.97) between evaluated and measured water levels. Also the results from the classification, mandatory for the application of the distance method, revealed that for SAR images, an overall underestimation of the water

surface is obtained. Results from the latter confirmed the high capability of the classification for the water surface estimation ($r^2 = 0.95$ comparing measured and evaluated water levels).

The best innovation in this study is the possibility to use the same dataset (Sentinel-1A) for dam displacements and water surface and levels determination.

Future works will exploit the use of InSAR techniques over a more consistent dataset, involving also the descending track acquisition to detect the planimetric displacements of the dam, not only along the LOS of sensors. Also, the comparison between GNSS and InSAR technique could be deepened analysed, involving the CORS located in the same area, evaluating the performances of both techniques for monitoring.

Bibliography

Acosta, L.E., Lacy, M.C., Ramos, M.I., Cano, J.P., Herrera, A.M., Aviles, M., Gil, A.J. (2018). Displacements study of an earth fill dam based on high precision geodetic monitoring and numerical modeling. Sensors, 18, 1369.

Alba, M., Bernardini, G., Giussani, A., Ricci, P., Roncoroni, F., Scaioni, M., Valgoi, P., Zhang, K. (2008). Measurement of dam deformations by terrestrial interferometric techniques. The International Archives of the Photogrammetry, Remote Sensing and Spatial Information Sciences, XXXVII, B1, 133–139.

Albright, R., Kaiser, L., Madsen, S., Policelli, F., Jasinski, M. (2011). Measuring reservoir heights via satellite altimetry products for global flood modelling. In: Forty Years of Earth

Observation…Understanding a Changing World, 14-17 November, Herndon, Virginia.

Alevizakou, E.G. and Pantazis, G. (2017). A comparative evaluation of various models for prediction of displacements. Applied Geomatics, 9(2), 93–103.

Alsdorf, D.E., Rodriguez, E., Lettenmaier, D.P. (2007). Measuring surface water from space. Reviews of Geophysics, 45, RG2002.

Altamimi, Z., Rebischung, P., Métivier, L., Collilieux, X. (2017). ITRF2014: A new release of the international terrestrial reference frame modeling nonlinear station motions. Journal of Geophysical Research: Solid Earth, 121, 6109–6131.

Armas, I., Gheorghe, M., Lendvai, A. M., Dimitru, P.D., Badescu, O., Calin, A. (2016). InSAR validation based on GNSS measurements in Bucharest. International Journal of Remote Sensing, 37:23, 5565-5580.

Avisse, N., Tilmant, A., Muller, M.F., Zhang, H. (2017). Monitoring small reservoirs' storage with satellite remote sensing in inaccessible areas. Hydrology and Earth System Sciences, 21, 6445–6459.

Bakon, M., Perissin, D., Lazecky, M., Papco, J. (2014). Infrastructure Non-Linear Deformation Monitoring Via Satellite Radar Interferometry. Procedia Technology, 16, 294-300.

Bakon, M., Papco, J., Perissin, D., Sousa, J.J., Lazecky, M. (2016). Multi-sensor InSAR deformation monitoring over urban area of Bratislava (Slovakia). Procedia Computer Science 100, 1127 – 1134.

Barzaghi, R., Pinto, L., Monaci, R. (2012). The Monitoring of Gravity Dams: Two Tests in Sardinia, Italy. In: FIG Working Week 2012, Rome, Italy, 6-10 May.

Bayer, B., Schmidt, D., Simoni, A. (2017). The Influence of External Digital Elevation Models on PS-InSAR and SBAS Results: Implications for the Analysis of Deformation Signals Caused by Slow Moving Landslides in the Northern Apennines (Italy). IEEE Transaction on Geosciences and Remote Sensing, 55(5), 2618-2631.

Behr, J.A., Hudnut, K.W., King, N.E. (1998). Monitoring Structural Deformation at Pacoima Dam, California Using Continuous GPS. In Proceedings of the Ion GPS, Nashville, TN, USA, 15–18 September, 59–68.

Bond, J., Kim, D., Fletcher, J. (2011). A Study of the Use of GPS Sensors for Structural Monitoring of the Mactaquac Dam. Available online: http://www.gemini-navsoft.com/GPS%20Structural%20Monitoring.pdf.

Busker. T., De Roo, A., Gelati, E., Schwatke, C., Adamovic, M., Bisselink, B., Pekel, J.F., Cottam, A. (2018). A global lake and reservoir volume analysis using a surface water dataset and satellite altimetry. Hydrology and Earth System Sciences Discussion, Manuscript under review for journal Hydrology and Earth System Sciences, 1-32.

Capodici, F., Maltese, A., Ciraolo, G., D'Urso, G., La Loggia, G. (2017). Power Sensitivity Analysis of Multi-Frequency, Multi-Polarized, Multi-Temporal SAR Data for Soil-Vegetation System Variables Characterization. Remote Sensing, 9, 677.

Carosio, A. and Dupraz, H. (1993). Mesures de deformation géodesiques et photogrammétriques pour la surveillance des ouvrages de retenue (Exploitation, precision et fiabilité). Wasser, Energie, Luft. N. 85/9.

Chen, Y.Q. (1983). Analysis of Deformation Surveys-A generalized Method. Technical Report, 94, Department of Geodesy and Geomatics Engineering, University of New Brunswick, Canada.

Chrzanowski, A., Chen, Y. Q., Szostak- Chrzanowski, A., Hayward, D.J., Thompson, G.A., Wroblewicz, Z. (1989). Integrated analysis of deformation surveys at Mactaquac. Int. Water Power Dam Construction, 8, 17–22.

Chrzanowski, A., Szostak, A., Steeves, R. (2011). Reliability and efficiency of dam deformation monitoring schemes. In Proceedings of the 2011 Annual Conference of Canadian Dam Association (CDA/ACB), Fredericton, NB, Canada, 15 October, Available online: http://www2.unb.ca/ccge/publications/downloads/CCGE_2011_CDA_Reliability.pdf

Corsetti, M., Fossati, F., Manunta, M., Marsella, M. (2018). Advanced SBAS-DInSAR Technique for Controlling Large Civil Infrastructures: An Application to the Genzano di Lucania Dam. Sensors, 18, 2371.

Cretaux, J.F., Biancamaria, S., Arsen, A., Bergé-Nguyen, M., Becker, M. (2015). Global surveys of reservoirs and lakes from satellites and regional application to the Syrdarya river basin. Environmental Research Letters, 10, 015002.

Crosetto, M., Montserrat, O., Cuevas-Gonzalez, M., Devanthery, N., Cripp, B. (2016). Persistent Scatterer Interferometry: A review. ISPRS Journal of Photogrammetry and Remote Sensing, 115, 78–89.

Dardanelli, G., La Loggia, G., Perfetti, N., Capodici, F., Puccio, L., Maltese, A. (2014). Monitoring displacements of an earthen dam using GNSS and remote sensing. In Proceeding of SPIE, 9239, 923928.

Dardanelli, G. and Pipitone C. (2017). Hydraulic models and finite elements for monitoring of an earth dam, by using GNSS techniques. Periodica Polytechnica Civil Engineering, 61(3), 421-433.

De Sortis, A. and Paoliani, P. (2007). Statistical analysis and structural identification in concrete dam monitoring. Engineering Structures, 29(1), 110-120.

Di Martire, D., Iglesias, R., Monells, D., Centolanza, G., Sica, S., Ramondini, M., Pagano, L., Mallorqui, J.J., Calcaterra, D. (2014). Comparison between Differential SAR interferometry and ground measurements data in the displacement monitoring of the earth-dam of Conza della Campania (Italy). Remote Sensing of Environment, 148, 58–69.

Di Pasquale, A., Nico, G., Pitullo, A., Prezioso, G. (2018). Monitoring Strategies of Earth Dams by Ground-Based Radar Interferometry: How to Extract Useful Information for Seismic Risk Assessment. Sensors, 18, 244.

Dixon, T.H., Amelung, F., Ferretti, A., Novali, F., Rocca, F., Dokka, R., Sella, G., Kim, S. W., Wdowinski, S., Whitman, D.(2006). Subsidence and flooding in New Orleans, Nature, 441, 587-588.

Drummond, P. (2010). Combining CORS Networks, Automated Observations and Processing, for Network RTK Integrity Analysis

and Deformation Monitoring. In Proceedings of the 15th FIG Congress Facing the Challenges, Sydney, Australia, 11–16 April.

Du, Y., Feng, G., Li, Z., Peng, X., Zhu, J., Ren, Z. (2017). Effects of External Digital Elevation Model Inaccuracy on StaMPS-PS Processing: A Case Study in Shenzhen, China. Remote Sensing, 9, 1115.

Duan, Z. and Bastiaanssen, W.G.M. (2013). Estimating water volume variations in lakes and reservoirs from four operational satellite altimetry databases and satellite imagery data. Remote Sensing of Environment, 134, 403-416.

Epema, G.F. (1990). Effect of moisture content on spectral reflectance in a playa area in Southern Tunisia. In Proceedings of the International Symposium Remote Sensing and Water Resources, Enschede, The Netherlands, 20–24 August; 301–308.

Famiglietti, J.S., Cazenave, A., Eickler, A., Reager, J.T., Rodell, M., Velicogna, I. (2015). Satellites provide the 'big picture. Science, 14, 684–685.

Ferretti, A., Prati, C., Rocca, F. (2001). Permanent Scatterers in SAR Interferometry. IEEE Transaction on Geoscience and Remote Sensing, 19(1), 8-20.

Ferretti, A., Monti-Guarnieri, A., Prati, C., Rocca, F. (2007). InSAR Principles: Guidelines for SAR Interferometry Processing and Interpretation, ESA TM-19: Noordwijk, The Netherlands.

Galan-Martin, D., Marchamalo-Sacristan, M., Martinez-Marin, R., Sanchez-Sobrino, J.A. (2013). Geomatics applied to dam safety DGPS

real time monitoring. International Journal of Civil Engineering, Transaction A: Civil Engineering, 11(2), 134-141.

Gao, H., Birkett, C., Lettenmaier, D.P. (2012). Global monitoring of large reservoir storage from satellite remote sensing. Water Resources Research, 48, W09504.

Gao, H. (2015). Satellite remote sensing of large lakes and reservoirs: from elevation and area to storage. WIREs Water, 2, 147-157.

Ghiglia, D.C. and Pritt, M.D. (1998). Two-dimensional Phase Unwrapping: Theory, Algorithms, and Software. Wiley, New York.

Gikas, V. and Sakellariou, M. (2008). Horizontal deflection analysis of a large earthen dam by means of geodetic and geotechnical methods. 13th FIG Symposium on Deformation Measurement and Analysis, 4th IAG Symposium on Geodesy for Geotechnical and Structural Engineering, LNEC, Lisbon, 12-15 May.

Gikas, V. and Sakellariou, M. (2008). Settlement analysis of the Mornos earth dam (Greece): Evidence from numerical modeling and geodetic monitoring. Engineering Structures, 30, 3074–3081.

Hanssen, R., 2001. Radar Interferometry. Kluwer Academic Publishers, Dordrecht, The Netherlands.

Herring, T.A. (1992). Modelling atmospheric delays in the analysis of space geodetic data. In: Refraction of transatmospheric signals in geodesy. Proceedings of the symposium. (de Munk, J. C., Spoelstra, T. A. Eds), 157-164. Netherlands Geodetic Commission Series, 36.

Hofmann-Wellenhof, B., Lichtenegger, H., Collins, J. (1992). GPS theory and practice. Springer-Verlag and Environment.

Hooper, A., Segall, P., Zebker, H. (2007). Persistent scatterer interferometric synthetic aperture radar for crustal deformation analysis, with application to Volcan Alcedo, Galapagos, Journal of Geophysical Research, 112, B07407.

ICOLD Constitution Statuts, July 2011. (https://www.icold-cigb.org/userfiles/files/CIGB/INSTITUTIONAL_FILES/Constitution2011.pdf).

Jiang, W., Liu, H., Liu, W., He, Y. (2012). CORS development for Xilongchi dam deformation monitoring. Geomatics and Information Science of Wuhan University, 37, 949–952.

Jiang, H., Feng, M., Zhu, Y., Lu, N. Huang, J., Xiao, T. (2014). An Automated Method for Extracting Rivers and Lakes from Landsat Imagery, Remote Sensing, 6, 5067-5089.

Kalkan, Y. (2014). Geodetic deformation monitoring of Ataturk Dam in Turkey. Arabian Journal of Geosciences, 7, 397–405.

Kampes, B.M. (2006). Radar Interferometry: Persistent Scatterer Technique. Remote Sensing and Digital Image Processing, 12, Springer.

Kaplan, G., Avdan, U. (2017). Object-based water body extraction model using Sentinel-2 satellite imagery, European Journal of Remote Sensing, 50(1), 137-143.

Klemas, V. and Pieterse, A. (2015). Using Remote Sensing to Map and Monitor Water Resources in Arid and Semiarid Regions. Advances in Watershed Science and Assessment, 33-60.

Klobuchar, J.A. (1996). Ionospheric effects on GPS.” In: Global Positioning System: Theory and Applications. Vol. I, Ch.12, 485-515. American Institute of Aeronautics and Astronauitcs Inc.

Koch, K.R. (1999) Parameter Estimation and Hypothesis Testing in Linear Models, Springer.

Lanari, R., Mora, O., Manunta, M., Mallorquí, J.J., Berardino, P., Sansosti, E. (2004). A small-baseline approach for investigating deformations on full-resolution differential SAR interferograms. Geosci. Remote Sens. IEEE Trans. 42(7), 1377–1386.

Lazecky, M., Bakon, M., Sousa, J.J., Perissin, D., Hlavacova, I., Patricio, G., Papco, J., Rapant, P., Real, N. (2015). Potential of Multi-Temporal InSAR Techniques for Structural Health Monitoring. In Proceeding of Fringe 2015, Frascati, Italy.

Lazecky, M., Perissin, D., Zhiying, W., Ling., L., Yuxiao, Q. (2015). Observing dam’s movements with spaceborne SAR interferometry. In Engineering Geology for Society and Territory—Volume 5; Lollino, G., Manconi, A., Guzzetti, F., Culshaw, M., Bobrowsky, P., Luino, F., Eds.; Springer International Publishing: Cham, Switzerland, 131–136.

Li, Z.H., Fielding, E.J., Cross, P., Muller, J.P.(2006). Interferometric synthetic aperture radar atmospheric correction: GPS topography-dependent turbulence model, Journal of Geophysical Research, 111.

Lier, E., Ekström, I., Larsen, Y, Lauknes, T.R. (2015). Verification of Remote Sensing in Dam Surveillance – results of the Scandinavian InSAR pilot. In Hydropower ’15, Stavanger, Norway, 15-16 June.

Liu, J. (2010). Progress in deformation monitoring for dams, bridges and power lines. Annals of GIS, 16, 81–90.

Lizarazo, I. (2014). Accuracy assessment of object-based image classification: another STEP. International Journal of Remote Sensing, 35(16), 6135-6156.

Luzi, G., Crosetto, M.; Monserrat, O. (2010) Advanced techniques for dam monitoring. In Proceedings of the 2nd International Congress on Dam Maintenance and Rehabilitation, Zaragoza, Spain, 23–25 November, 1103–1108.

Magome, J., Ishidarira, H., Takeuchi, K. (2003). Method for satellite monitoring of water storage in reservoirs for efficient regional water management. Water Resources Systems — Hydrological Risk, Management and Development (Proceedings of symposium HS02b held during IUOG2003 at Sapporo, July 2003).

Markham, B.L. and Barker, J.L. (1986). Landsat MSS and TM post-calibration dynamic ranges, exoatmospheric reflectances and at-satellite temperatures. Earth Observation Satellite Co., Lanham, MD, Landsat Technical Note 1.

Mazzanti, P., Perissin, D., Rocca, A. (2015). Structural health Monitoring of Dams by Advanced Satellite SAR Interferometry: Investigation of Past Processes and Future Monitoring Perspectives. In 7th International Conference on Structural Health Monitoring of Intelligent Infrastructure, Torino, Italy.

Milillo, P., Perissin, D., Lundgren, P., Serio, C. (2015). Cosmo-skymed very short repeat-pass SAR interferometry over rural areas: The VAL D'agri and potenza test cases in Basilicata, Italy. IEEE International Geoscience and Remote Sensing Symposium (IGARSS), 26-31 July, Milan, Italy.

Milillo, P., Perissin, D., Salzer, T., J., Lundgren, P., Lacava, G., Milillo, G., Serio, C. (2016). Monitoring dam structural health from space: Insights from novel InSAR techniques and multi-parametric modeling applied to the Pertusillo dam Basilicata, Italy. International Journal of Applied Earth Observation and Geoinformation, 52, 221–229.

Milillo, P, Bürgmann, R., Lundgren, P., Salzer, J., Perissin, D., Fielding, E., Biondi, F., Milillo, G. (2016). Space geodetic monitoring of engineered structures: The ongoing destabilization of the Mosul dam, Iraq. Scientific reports, 6, 37408.

Milillo, P., Porcu, C.M., Lundgren, P., Soccodato, F., Salzer, J., Fielding, E., Burgmann, R., Milillo, G., Perissin, D., Biondi, F. (2017). The ongoing destabilization of the Mosul dam as observed by Synthetic Aperture Radar Interferometry. In IEEE International Geoscience and Remote Sensing Symposium (IGARSS), 23-28 July, Fort Worth, Texas, USA.

Montillet, J.P., Walter, M.S., Timothy, I.M., Rex, M.F., Schrock, G. (2016). Critical infrastructure monitoring with global navigation satellite systems. Journal of Surveying Engineering, 142(4), 04016014.

Mura, J.C., Gama, F.F., Paradella, W.R., Negrao, P., Carneiro, S., Oliveira, C.G., Brandao, W.S. (2018). Monitoring the Vulnerability of the Dam and Dikes in Germano Iron Mining Area after the Collapse of the Tailings Dam of Fundão (Mariana-MG, Brazil) Using DInSAR Techniques with TerraSAR-X Data. Remote Sensing, 10(10), 1507.

Mustafa, Y.T. and Noori, M.J. (2013). Satellite remote sensing and geographic information systems (GIS) to assess changes in the water

level in the Duhok dam. International Journal of Water Resources and Environmental Engineering, 5(6), 351-359.

Ng, A. H. M., Ge, L., Li, X., Zhang, K. (2012). Monitoring ground deformation in Beijing, China with persistent scatterer SAR interferometry, Journal of Geodesy 86 (6), 375-392.

Ni, S., Chen, J., Wilson, C.R., Hu, X. (2017). Long-TermWater Storage Changes of Lake Volta from GRACE and Satellite Altimetry and Connections with Regional Climate. Remote Sensing, 9, 842.

Nico, G., Di Pasquale, A., Corsetti, M., Di Nunzio, G., Pitullo, A., Lollino, P. (2015). Use of an Advanced SAR Monitoring Technique to Monitor Old Embankment Dams. In: G. Lollino et al. (eds.), Engineering Geology for Society and Territory – Volume 6, 731-737.

Niell, A.E. (1996). Global mapping functions for the atmosphere delay at radio wavelengths. Journal of Geophysical Research, 101(B2), 3227-3246.

Oro, S.R., Mafioleti, T.R., Chaves Neto, A., Garcia, S.R.P., Neumann Junior, C. (2016). Study of the influence of temperature and water level of the reservoir about the displacement of a concrete dam. International Journal of Applied Mechanics and Engineering, 21(1), 107-120.

Peng, D., Guo, S., Liu, P., Liu, T. (2006). Reservoir Storage Curve Estimation Based on Remote Sensing Data. Journal of Hydrologic Engineering, 11, 2, 165-172.

Perissin, D., Piantanida, R., Piccagli, D., Rocca, F. (2007). Landslide in Dossena (BG): Comparison between interferometric techniques, Biogeosar, 9, 1–7.

Perissin D., Ferretti A., Piantanida R., Piccagli D., Prati C., Rocca F., Rucci A., de Zan F. (2007b). Repeat-pass SAR interferometry with partially coherent targets", Fringe, Frascati (Italy), 26-30 November.

Perissin, D. SARPROZ Manual, Copyright (c). http://www.sarproz.com/software-manual/ (2009-2017).

Pipitone, C., Maltese, A., Dardanelli, G., Capodici, F., Lo Brutto, M., La Loggia, G. (2017). Detection of a reservoir water level using shape similarity metrics. In Proceeding of SPIE 10421, 104211L.

Pipitone, C., Maltese, A., Dardanelli, G., Lo Brutto, M., La Loggia, G. (2018). Monitoring Water Surface and Level of a Reservoir Using Different Remote Sensing Approaches and Comparison with Dam Displacements Evaluated via GNSS. Remote Sensing 10(1), 71.

Pipitone, C., Cigna, F., Dardanelli, G., La Loggia, G., Maltese, A., Muller, J. (2018). Reservoir monitoring using satellite SAR and GNSS: a case study in southern Italy. In: Goffredo La Loggia, Gabriele Freni, Valeria Puleo and Mauro De Marchis (editors). HIC 2018. 13th International Conference on Hydroinformatics, 3, 1682-1691.

Pipitone, C., Maltese, A., Dardanelli, G., Capodici, F., Muller, J., La Loggia, G. (2018). Evaluation of different InSAR multi-baseline construction methods over a dam in southern Italy. Proc. SPIE 10783, Remote Sensing for Agriculture, Ecosystems, and Hydrology XX, Berlin, Germany, 10 October 2018, 107831A.

Pytharouli, S.I. and Stiros, S.C. (2005). Ladon dam (Greece) deformation and reservoir level fluctuations: evidence for a causative relationship

from the spectral analysis of a geodetic monitoring record. Engineering Structures, 27(3), 361–370.

Pytharouli, S.I. and Stiros, S.C. (2009). Investigation of the parameters controlling the crest settlement of a major earthfill dam based on the threshold correlation analysis. Journal of Applied Geodesy, 3(1), 55-62.

Qiu, Z., Yue, J., Wang, X., Yue, S. (2016). Deformation monitoring of large structures by ground-based SAR interferometry. Boletim de Ciências Geodésicas, sec. Artigos, Curitiba, 22(1), 35-53.

Radhakrishnan, N. (2014). Application of GPS in structural deformation monitoring: A case study on Konya dam. Journal of Geomatics, 8(1), 48-54.

Roque, D., Perissin, D., Falcao, A.P., Fonseca, A.M., Henriques, M.J., Franco, J. (2015). Dams regional safety warning using time-series InSAR techniques. In 2nd International Dam World Conference, Portugal, Lisbon, 21-24 April.

Ruiz-Armenteros, A.M., Lazecky, M., Hlacova, I., Bakon, M., Delgado, J.M., Sousa, J.J., Lamas-Fernandez, F., Marchamalo, M., Caro-Cuenca, M., Papco, J., Perissin, D. (2018). Deformation monitoring of dam infrastructures via spaceborne MT-InSAR. The case of La Viñuela (Málaga, southern Spain). Procedia Computer Science, 138, 346-353.

Rutledge, D.R., Meyerholtz, S.Z., Brown, N.E., Baldwin, C.S. (2006). Dam stability: Assessing the performance of a GPS monitoring system. GPS World, 17, 26–33.

Saastamoinen, J. (1972). Atmospheric correction for the troposphere and stratosphere in radio ranging of satellites. In: The Use of Artificial Satellites for Geodesy. (Henriksen, S. W., Mancini, A., Chovitz, B. H. (Eds)), 247-251. Geophyscal Monograph Series, 15. AGU, Washington DC.

Sacerdote, F., Cazzaniga, N.E., Tornatore, V. (2010). Some considerations on significance analysis for deformation detection via frequentist and Bayesian tests. Journal of Geodesy, 84, 233–242.

Scaioni, M., Marsella, M., Crosetto, M., Tornatore, V., Wang, J. (2018). Geodetic and Remote-Sensing Sensors for Dam Deformation Monitoring. Sensors, 18, 3682.

Schwiderski, E. W. (1980). On charting global ocean tides. Reviews of Geophysics. 18 (1), 243-268.

Shengnan, N., Chen, J., Wilson, C. R., Hu, X. (2017). Long-Term Water Storage Changes of Lake Volta from GRACE and Satellite Altimetry and Connections with Regional Climate. Remote Sensing, 9(8), 842.

Shimizu, N. (2015). Rock Displacement Monitoring using Satellite Technologies-GPS and InSAR. In Proceedings of the ISRM VietRock International Workshop, Hanoi, Vietnam, 12–13 March.

Singh, A., Kumar, U., Seitz, F. (2015). Remote Sensing of Storage Fluctuations of Poorly Gauged Reservoirs and State Space Model (SSM)-Based Estimation. Remote Sensing, 7, 17113–17134.

Siyahi, B. and Arslan, H. (2008). Earthquake induced deformation of earth dams. Bulletin of Engineering Geology and the Environment 67(3), 397-403.

Solander, K.C., Reager, J.T., Famiglietti, J.S. (2016). How well will the Surface Water and Ocean Topography (SWOT) mission observe global reservoirs?. Water Resources Research, 52, 2123–2140.

Sousa, J.J., Hlavacova, I, Bakon, M., Lazecky, M., Patricio, G., Guimaraes, P., Ruiz, A.M., Bastos, L., Sousa, A., Bento, R.. (2014). Potential of Multi-Temporal InSAR Techniques for Bridges and Dams Monitoring. Procedia Technology, 16, 834-841.

Sousa, J.J., Lazecky, M., Hlavacova, I., Bakon, M., Patricio, G, Perissin, D. (2015). Satellite SAR interferometry for monitoring dam deformations in Portugal. Second International Dam World Conference, Portugal, 21–24 April.

Sousa, J.J., Ruiz, A. M., Bakon, M., Lazecky, M., Hlavacova, I., Patricio, G, Delgado, J.M., Perissin, D. (2016). Potential of C-band SAR Interferometry for Dam Monitoring. Procedia Computer Science, 100, 1103-1114.

Szostak-Chrzanowski, A. (2006). Interdisciplinary approach to deformation analysis in engineering, mining, and geosciences projects by combining monitoring surveys with deterministic modelling-Part I. Technical Sciences, 9,147-172.

Szostak-Chrzanowski, A. and Massiera, M. (2004). Modelling of deformations during construction of a large earth dam in the La Grande Complex, Canada. Technical Sciences, 7, 109-122.

Talich., M. (2016). The Deformation Monitoring of Dams by the Ground-Based InSAR Technique - Case Study of Concrete Hydropower Dam Orlík. International Journal of Advances in Agricultural & Environmental Engg. (IJAAEE) 3(1), 192-197.

Tarsisius Aris, S., Kabul Basah, S., Fakrurazzi, D., Adin, S., Adhi, D., Susilo, A. (2012). Design and installation for Dam Monitoring Using Multi sensors: A Case Study at Sermo Dam, Yogyakarta Province, Indonesia. In FIG Working Week 2012, Knowing to manage the territory, protect the environment, evaluate the cultural heritage, Rome, Italy, 6-10 May.

Tasci, L. (2008). Dam deformation measurements with GPS. Geodesy and Cartography, 34(4), 116-121.

Teunissen, P.J.G. (1995). The least-squares ambiguity decorrelation adjustment: a method for fast GPS integer ambiguity estimation. Journal of Geodesy, 70, 65-82.

Thome, K., Markham, B. Barker, J., Slater, P., Biggar, S.F. (1997). Radiometric Calibration of Landsat. Photogrammetric Engineering and Remote Sensing, 63(7), 853-858.

Tomas, R., Cano, M., Garcia-Barba, J., Vicente, F., Herrera, G., Lopez-Sanchez, J. M., Mallorqui, J. J. (2013). Monitoring an earthfill dam using differential SAR interferometry: La Pedrera dam, Alicante, Spain. Engineering Geology, 157, 21–32.

Vaka, D.S., Sharma, S., Rao, Ys. (2017). Comparison of HH and VV Polarizations for Deformation Estimation using Persistent Scatterer Interferometry. In the 38th Asian Conference on Remote Sensing, October 23 –27 , New Delhi, India.

Vörösmarty, C., Birkett, C., Dingman, L., Lettenmaier, D.P., Kim, Y., Rodrigues, E., Emmitt, G.D. (1999). NASA post 2002 Land Surface Hydrology Mission Component for Surface Water Monitoring,

HYDRA-SAT, Report from the NASA Post 2002 LSHP Planning Workshop, USA.

Wang, T., Perissin, D., Rocca, F., Ming-Sheng, L. (2011). Three Gorges Dam stability monitoring with time-series InSAR image analysis. Science China Earth Sciences, 54, 720-732.

Welch, R. and Ehlers, W. (1987). Merging Multiresolution SPOT HRV and Landsat TM Data. Photogrammetric Engineering and Remote Sensing, 53, 301–303.

Whitaker, C., Duffy, M.A., Chrzanowski, A. (1998). Design of a continuous monitoring scheme for the eastside reservoir in Southern California. In Proceedings of the International Federation of Surveyors (FIG) XXI International Congress, Brighton, UK, 19–25 July, 329–344.

Xue, H., Liao, J., Zhao, L. (2018). A Modified Empirical Retracker for Lake Level Estimation Using Cryosat-2 SARin Data. Water, 10, 1584.

Yang, G., He, X., Chen, Y. (2010). Integrated GPS and pseudolite positioning for deformation monitoring. Survey Review, 42, 72–81.

Yavasoglu, H.H., Kalkan, Y., Tiryakioglu, I., Yigit, C.O., Ozbey, V., Alkan, M.N. (2018). Monitoring the deformation and strain analysis on the Ataturk Dam, Turkey. Geomatics, Natural Hazards and Risk, 9(1), 94-107.

Ye, Z., Liu, H., Chen, Y., Shu, S., Wu, Q., Wang, S. (2017). Analysis of water level variation of lakes and reservoirs in Xinjiang, China using ICESat laser altimetry data (2003±2009). PLoS ONE, 12(9), e0183800.

Yigit, C.O., Alcay, S., Ceylan, A. (2016). Displacement response of a concrete arch dam to seasonal temperature fluctuations and reservoir level rise during the first filling period: evidence from geodetic data, Geomatics, Natural Hazards and Risk, 7(4), 1489-1505.

Zebker, H.A., Rosen, P.A., Hensley, S., (1997). Atmospheric effects in interferometric synthetic aperture radar surface deformation and topographic maps. Journal of Geophysical Research: Solid Earth (1978–2012),102(B4), 7547–7563.

Zhang, J., Xu, K., Yang, Y., Qi, L., Hayashi, S., Watanabe, M. (2006). Measuring water storage fluctuations in lake Dongting, China, by Topex/Poseidon satellite altimetry. Environmental Monitoring and Assessment, 115(1-3), 23-37.

Zou, J., Thi Bui, K.T, Xiao, Y., Van Doan, C. (2018). Dam deformation analysis based on BPNN merging models. Geo-spatial Information Science, 21(2), 149-157.